BIOMIMETIC MENISCUS SCAFFOLD FROM ELECTROSPUN POLY(LACTIC ACID)/SILK FIBROIN

SIRIPANYO PROMNIL

A Thesis Submitted in Partial Fulfillment of the Requirements for the

Degree of Master of Engineering in Materials Engineering

Suranaree University of Technology

Academic Year 2021

โครงร่างเลี้ยงเซลล์จำลองหมอนรองกระดูกข้อเข่าจากกระบวนการอิเล็กโตรสปินนิงด้วยพอลิแลคติกแอซิดและไหมไฟโบรอิน

นางสาวสิริปัญโญ พรหมนิล

วิทยานิพนธ์นี้เป็นส่วนหนึ่งของการศึกษาหลักสูตรปริญญาวิศวกรรมศาสตรมหาบัณฑิต
สาขาวิชาวิศวกรรมวัสดุ
มหาวิทยาลัยเทคโนโลยีสุรนารี
ปีการศึกษา 2564

BIOMIMETIC MENISCUS SCAFFOLD FROM ELECTROSPUN

POLY(LACTIC ACID)/SILK FIBROIN

Suranaree University of Technology has approved this thesis submitted in partial fulfillment of the requirements for a Master's Degree.

Thesis Examining Committee

....
(Asst. Prof. Dr. Nitinat Suppakarn)

Chairperson

....
(Assoc. Prof. Dr. Yupaporn Ruksakulpiwat)

Member (Thesis Advisor)

....
(Assoc. Prof. Dr. Chaiwat Ruksakulpiwat)

Member (Thesis Co-advisor)

....
(Asst. Prof. Dr. Piya-on Numpaisal)

Member (Thesis Co-advisor)

....
(Assoc. Prof. Dr. Ittipol Jangchud)

Member

....
(Assoc. Prof. Dr. Pranee Chumsamrong)

Member

....
(Asst. Prof. Dr. Tatiya Trongsatitkul)

Member

....
(Assoc. Prof. Dr. Chatchai Jothityangkoon)

Vice Rector for Academic Affairs and

Quality Assurance

....
(Assoc. Prof. Dr. Pornsiri Jongkol)

Dean of Institute of Engineering

สิริปัญโญ พรหมนิล : โครงร่างเลี้ยงเซลล์จำลองหมอนรองกระดูกข้อเข่าจากกระบวนการ
อิเล็กโตรสปินนิงด้วยพอลิแลคติกแอซิดและไหมไฟโบรอิน (BIOMIMETIC MENISCUS
SCAFFOLD FROM ELECTROSPUN POLY(LACTIC ACID)/SILK FIBROIN)
อาจารย์ที่ปรึกษา : รองศาสตราจารย์ ดร.ยุพาพร รักสกุลพิวัฒน์ , 89 หน้า.

คำสำคัญ : พอลิแลคติกแอซิด ไหมไฟโบรอิน อิเล็กโตรสปินนิง วิศวกรรมเนื้อเยื่อ

        จุดมุ่งหมายในการศึกษานี้คือ ต้องการที่จะพัฒนาโครงร่างเลี้ยงเซลล์จำลองหมอนรองกระดูก
ข้อเข่าจากกระบวนการอิเล็กโตรสปินนิงโดยใช้วัสดุคือพอลิแลคติกแอซิดและไหมไฟโบรอิน และ
ต้องการที่จะศึกษาความสามารถของวัสดุในการที่จะนำไปใช้งานเป็นโครงร่างเลี้ยงเซลล์สำหรับหมอน
รองกระดูกข้อเข่า

        พอลิแลคติกแอดซิดเป็นพอลิเมอร์สังเคราะห์ที่ถูกนำมาใช้งานอย่างแพร่หลายในด้านวัสดุ
ทางการแพทย์ เนื่องจากเป็นวัสดุที่มีสมบัติทางกลที่ดี ทนทานต่อการเปลี่ยนแปลงรูปร่าง สามารถย่อย
สลายได้ แต่มีข้อด้อยคือขาดสมบัติด้านการยึดติดกับเซลล์ ส่วนไฟโบรอินเป็นโปรตีนที่ได้จากเส้นใย
ไหมซึ่งจัดเป็นวัสดุที่น่าสนใจ เนื่องจากมีความสามารถในการปรับปรุงการยึดเกาะของเซลล์ ใน
งานวิจัยนี้จึงต้องการนำไฟโบรอินมาผสมกับพอลิแลคติกแอซิดเพื่อปรับปรุงสมบัติของวัสดุให้มีความ
เข้ากันได้กับสภาพแวดล้อมทางชีวภาพในร่างกาย และส่งเสริมการยึดเกาะของเซลล์ซึ่งเป็นสมบัติที่
สำคัญที่โครงร่างเลี้ยงเซลล์ควรมี โดยไหมไฟโบรอินที่นำมาใช้ในการศึกษานั้นจะเตรียมมาจากรังไหม
ของหนอนไหม (Bombyx mori) จากนั้นนำไปผ่านกระบวนการสกัด แล้วทำให้เป็นผงโดยใช้
กระบวนการทำแห้งแบบแช่เยือกแข็ง ในส่วนของพอลิแลคติกแอซิดจะศึกษาเกรดทางการค้าจำนวน
2 ชนิด ซึ่งมีค่าน้ำหนักโมเลกุลที่แตกต่างกัน และเกรดทางการแพทย์ 1 ชนิด โดยพอลิแลคติกแอซิด
จะถูกนำไปขึ้นรูปชิ้นงานด้วยกระบวนการอิเล็กโตรสปินนิงที่ความเข้มข้นต่างกัน เพื่อศึกษาผลกระทบ
ของน้ำหนักโมเลกุลและความเข้มข้นของพอลิแลคติกแอซิดที่มีต่อสมบัติทางกายภาพของเส้นใย ซึ่ง
พอลิเมอร์มีที่น้ำหนักโมเลกุลและความเข้มข้นที่ให้ลักษณะสัณฐานวิทยาของเส้นใยที่เหมาะสม จะถูก
นำไปผสมกับไหมไฟโบรอินที่ความเข้มข้น 12 % (w/v) ที่สัดส่วนต่างกัน (PLA75:SF25, PLA50:SF50
และ PLA25:SF75) เพื่อศึกษาผลกระทบของปริมาณไฟโบรอินที่ส่งผลต่อสมบัติทางกายภาพและ
สมบัติความเข้ากันได้ทางชีวภาพของเส้นใยพอลิแลคติกแอซิดเมื่อผสมกับไหมไฟโบรอิน

        จากการศึกษาความหนืดของสารละลายพอลิแลคติกแอซิดที่มีน้ำหนักโมเลกุลและความ
เข้มข้นต่างกันเพื่อนำไปขึ้นรูปโดยผ่านกระบวนการอิเล็กโตรสปินนิงพบว่า ความหนืดของสารละลาย

พอลิเมอร์และน้ำหนักโมเลกุลเป็นสองปัจจัยสำคัญในกระบวนการขึ้นรูปด้วยวิธีนี้ ซึ่งจะส่งผลต่อ
ลักษณะและขนาดของเส้นใยที่ได้ออกมา นอกจากนี้ยังได้ทำการศึกษาความแตกต่างของคุณสมบัติ
ของโครงร่างเลี้ยงเซลล์ที่ทำจากพอลิแลคติกแอซิดเกรดทางการค้ากับเกรดทางการแพทย์ โดยได้ทำ
การทดสอบสมบัติทางกล สมบัติทางความร้อน ความสามารถในการเปียกผิวของวัสดุ สมบัติความเป็น
พิษต่อเซลล์ และการแสดงออกของยีน

　　　จากการศึกษาพอลิแลคติกแอซิดเกรดทางการแพทย์มีสมบัติทางกล สมบัติการย่อยสลาย
และสมบัติด้านการส่งเสริมการเจริญเติบโตของเซลล์ดีกว่าเกรดทางการค้าที่ใช้โดยทั่วไป ดังนั้นในวัสดุ
ที่นำมาเพื่อทำโครงสร้างเลี้ยงเซลล์จึงควรเป็นเกรดทางการแพทย์ ส่วนโครงร่างเลี้ยงเซลล์ที่ทำจาก
วัสดุคอมโพสิตระหว่างพอลิแลคติกและไหมไฟโบรอิน พบว่าเมื่อเพิ่มปริมาณสัดส่วนของไหมไฟโบรอิน
จะส่งผลให้มีสมบัติด้านการย่อยสลายและความชอบน้ำที่ดีขึ้นเมื่อเปรียบเทียบกับโครงร่างเลี้ยงเซลล์ที่
ผลิตจากพอลิแลคติกแอซิดเพียงอย่างเดียว ดังนั้นเมื่อศึกษาคุณสมบัติต่าง ๆ แล้วพบว่าโครงสร้างเลี้ยง
เซลล์ที่ผลิตจากกระบวนการอิเล็กโตรสปินนิงโดยใช้สารละลายพอลิแลคติกแอซิดเกรดทางการแพทย์
ผสมกับสารละลายไหมไฟโบรอินที่อัตราส่วน 50 ต่อ 50 มีความสามารถในการพัฒนาเพื่อใช้เป็นวัสดุ
สำหรับโครงร่างเลี้ยงเซลล์สำหรับรักษาหมอนรองกระดูกข้อเข่าที่เกิดการบาดเจ็บได้

สาขาวิชาวิศวกรรมพอลิเมอร์　　　　　　　　ลายมือชื่อนักศึกษา ....
ปีการศึกษา 2564　　　　　　　　　　　　　ลายมือชื่ออาจารย์ที่ปรึกษา ....
　　　　　　　　　　　　　　　　　　　　　ลายมือชื่ออาจารย์ที่ปรึกษาร่วม ....
　　　　　　　　　　　　　　　　　　　　　ลายมือชื่ออาจารย์ที่ปรึกษาร่วม ....

SIRIPANYO PROMNIL : BIOMIMETIC MENISCUS SCAFFOLD FROM ELECTROSPUN POLY(LACTIC ACID)/SILK FIBROIN THESIS ADVISOR : ASSOC. PROF. YUPAPORN RUKSAKULPIWAT, Ph.D., 89 PP.

Keyword: Poly(lactic acid) Silk fibroin Electrospinning Tissue Engineering

The aim of this present research is to develop biomimetic meniscus scaffold using electrospun poly (lactic acid) (PLA)/silk fibroin (SF) and explore their potential use for scaffold augmented suture.

Poly(lactic acid) (PLA) is one of the most widely used synthesis polymers in the biomedical field because it has good mechanical properties such as high strength and high stiffness. However, it has poor cell adhesion and slowly degrades in in vitro surroundings. Silk fibroin (SF) is a good candidate to improve the cell adhesion and degradability of electrospun PLA. SF powder was prepared from silk cocoon of Bombyx mori silkworm by degumming and freeze-drying method. Two commercial grade PLA were fabricated by using electrospinning process at different concentration (10%, 15% and 20 % w/v). This is to study the effect of PLA molecular weight and the effect of PLA concentration on physical properties of electrospun PLA. The suitable PLA solution that provides suitable morphology was chosen for mixing with 12 % (w/v) SF solution at different ratios (PLA75:SF25, PLA50:SF50 and PLA25:SF75). The effect of SF content on the physical properties and biocompatibility of electrospun PLA/SF was studied.

Related factors including solution viscosity and SF content were investigated in order to create a PLA/SF scaffold that offered both biological and mechanical capabilities. The solution viscosity considerably varied when PLA concentration and molecular weight were altered. It was clarified how solution viscosity affected fiber formation and fiber shape. Additionally, research was done on both commercial (L-lactide, D-lactide PLA) and medical grade PLA (pure PLLA). Electrospun PLA and PLA/SF based nanofibrous scaffolds were studied for their mechanical, thermal, biodegradable, wettability, cell viability, and gene expression characteristics.

The findings showed that for the regeneration of meniscus tissue, medical grade PLA electrospun scaffolds exhibited superior mechanical properties, degradability, and cellular induction. However, due to its toxicity, the commercial, non-medical grade PLA employed in this study was not suggested for use in medical applications. The in vitro degradability and hydrophilicity of PLA-based scaffolds were enhanced by the addition of SF. Based on cell survival, gene expression, surface wettability, and in vitro degradation, the PLAmed50:SF50 scaffold has the potential to be developed as a meniscus tissue engineering scaffold.

School of <u>Polymer Engineering</u>

Academic Year 2021

Student's Signature ....

Advisor's Signature ....

Co-advisor's Signature ....

Co-advisor's Signature ....

ACKNOWLEDGEMENT

TABLE OF CONTENTS

TABLE OF CONTENTS (Continued)

TABLE OF CONTENTS (Continued)

TABLE OF CONTENTS (Continued)

LIST OF TABLES

LIST OF FIGURES

Figure   **Page**

LIST OF FIGURES (Continued)

CHAPTER 1

INTRODUCTION

1.1 Background

Meniscus is an crescent-shaped structure of knee joint, which functioning in load transfer, stress reduction, joints lubrication and stability (Myers, Sgaglione, & Goodwillie, 2014). Meniscus tear is the most frequent knee injury, regardless of age (Sari, Gunaydin, & dinçel, 2018). Meniscus injury often leads to osteoarthritis (OA) and meniscus degeneration due to the breakdown and weakening of the meniscal structure (Englund, Guermazi, & Lohmander, 2009). Loss of meniscus tissue permanently changes knee biomechanics and homeostasis. Apparently, the vascular supply of the problem zone directly affects how well the meniscus can be healed. The tear in the vascularized zone is more likely to heal, whereas the injury in the avascular zone has poor healing potential (de Caro, Perdisa, Dhollander, Verdonk, & Verdonk, 2020). Therefore, repair or regeneration of the menisci can help the patients to relieve the pain, regain function and prevent the risk of OA.

Nowadays, there are many techniques to improve the healing potential of the meniscus, especially tissue engineering scaffolds. Using cells and biomaterial scaffolds, tissue engineering is now becoming a novel approach for meniscus regeneration. Scaffold is an important cue that serves as a cell shelter and cell delivery for tissue regeneration. The structural support for cell adhesion and subsequent tissue formation is provided by scaffolds, which are typically made up of polymeric biomaterials (Chan & Leong, 2008). A greater part of biomaterial research for tissue engineering and regenerative medicine is focused on designing and producing the scaffold (Reddy, Ponnamma, Choudhary, & Sadasivuni, 2021). In general, polymeric materials can be

categorized as either synthetic, natural, or a mix of the two. Synthetic polymers such as polycaprolactone (PCL), polylactic acid (PLA), and poly(vinyl alcohol) (PVA) are commonly used to make scaffolds (Coluccino et al., 2018; Haider et al., 2020; Hirano et al., 2021). Natural polymeric materials like proteins, polysaccharides, lipids, and polynucleotides. are also investigated (Panjapheree, Kamonmattayakul, & Meesane, 2018; Warnecke et al., 2018). Moreover, a composite scaffold is created from synthetic and natural polymers, which combines the advantages of each substance while promoting the regeneration of functional tissues with desired functions. A scaffold not only acts as a cell carrier but can also provide strength for the tissue construct. Scaffolds must have biological qualities compatible with cell viability and proliferation and material properties similar to the native meniscus in order to offer mechanical support (Ahmed et al., 2015).

Scaffolds that enable the rapid expansion of three-dimensional tissues can be created using the latest methods for the production of biomaterials, many of which have functional vascular systems that are similar to those found in living organisms. There are several processes for fabricating scaffolds. For many years, extracellular matrix (ECM)-like fibrous scaffolds have been created via electrospinning. It is possible to create artificial functional tissues using electrospun fibrous scaffolds, could provide fibrous structures with connecting pores at the nano- and microscale that resemble genuine ECM in tissues. There are also various methods for creating three-dimensional fiber scaffolds that are stacked in hierarchical configurations for tissue engineering (Baek et al., 2015).

Frequently utilized in tissue engineering, polylactic acid (PLA) has been a well material. Due to their biodegradability, PLA and its copolymers are utilized in implants and many other devices. Producing PLA and lactide copolymers from renewable resources is feasible; they are biodegradable and environmentally safe and humans. PLA provides strong mechanical resistance that is appropriate for making bone tissue engineering scaffolds, but both bioactivity and cell affinities are inadequate. Therefore, a composite scaffold can serve to overcome these shortcomings.

The composite fiber membranes made of PLA, silk fibroin, and gelatin may offer favorable conditions for cell growth and proliferation (Yin Gui-Bo, 2009). A naturally occurring protein called silk fibroin (SF) is very biocompatible, barely immunogenic, non-toxic, non-carcinogenic, and biodegradable. Due to its remarkable intrinsic characteristics, biocompatibility, biodegradability, and mechanical strength, the SF has recently attracted a lot of attention as a material for tissue engineering scaffolds.

Therefore, the objective of the current study is to create electrospun poly (lactic acid)/silk fibroin scaffold imitate meniscus fibers and assess their potential application as meniscus tissue engineering scaffold.

1.2   Research objectives

The main purpose of this research is to develop scaffold mimic meniscus fibers using electrospinning poly(lactic acid)/ silk fibroin and explore their potential use for meniscus tissue engineering scaffolds and study the materials factors as followed.

1.2.1   To study the effect of molecular weight of PLA on mechanical properties of electrospun PLA scaffolds.

1.2.2   To study the effect of PLA concentration on physical properties of electrospun PLA scaffolds.

1.2.3   To study the effect of SF content on physical properties and cell proliferation of electrospun PLA/SF scaffolds.

1.2.4   To study the potential use of electrospun PLA/SF for meniscus tissue engineering scaffolds.

1.3   Scope and limitation of the study

Two commercial non-medical grades of PLA with different molecular weights (55000 and 150000 g/mol) and one medical grade of PLA (200000 g/mol) were fabricated by using electrospinning process at different concentrations (10%, 15% and 20 % w/v) for the commercial grades. While, the medical grade PLA was prepared at

6% (w/v) concentration. Commercial non-medical grade PLA with suitable molecular weight and concentration that provides optimum suitable morphology was chosen for mixing with 12 % (w/v) concentration of SF at different ratios (PLA75:SF25, PLA50:SF50 and PLA25:SF75). SF powder was prepared form cocoons of Bombyx mori silkworm by degumming and freeze-drying method. Electrospinning was used to fabricate PLA/SF samples.

Electrospun PLA/SF morphology was observed by field emission scanning electron microscopy. Mechanical properties of electrospun PLA/SF were determined by universal testing machine. Biocompatibility of electrospun PLA/SF was characterized by human chondrocyte cells culturing for observing the cell viability. Degradation of electrospun PLA/SF was studied by immersing in PBS solution. The percentages of weight loss were calculated. The possibility to be use as mimic meniscus scaffold were evaluated.
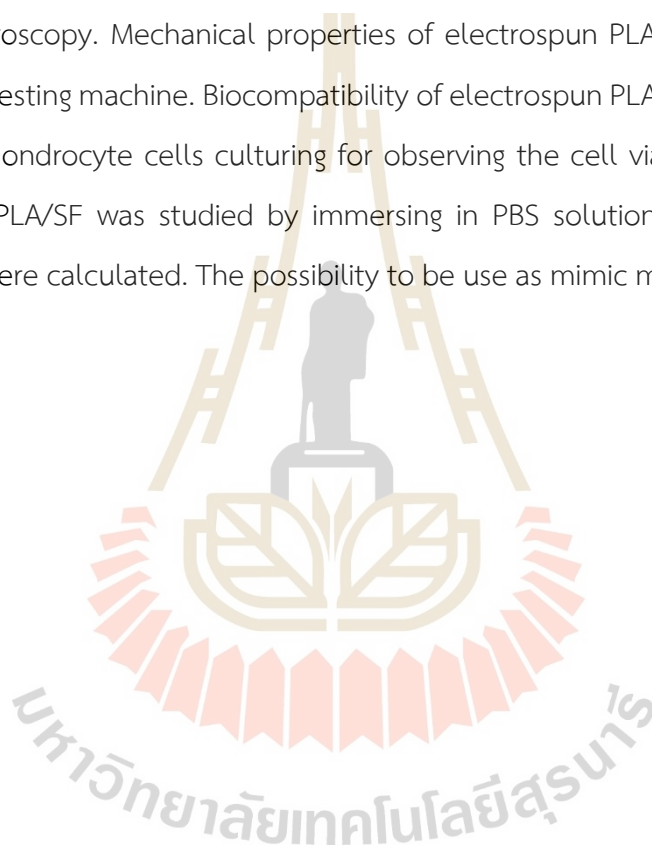
CHAPTER 2
LITERATURE REVIEWS

2.1   Meniscus

2.1.1   Meniscus anatomy and cellular components

The knee is the big hinge joint in the body and is sensitive to injury from trauma, inflammation, infection, and degenerative changes. The joint line lives between the femoral and tibial joint. The menisci are crescent-shaped wedges of glossy white fibrocartilages which located on the medial and lateral aspects of the knee joint (Fox, Bedi, & Rodeo, 2012; Vadodaria, Kulkarni, Santhini, & Vasudevan, 2019). The tibial plateau is more thoroughly covered by the lateral menisci (80-90% lateral) in comparison to medial menisci (50-70% medial) (Ridley, McCarthy, Bollier, Wolf, & Amendola, 2017).
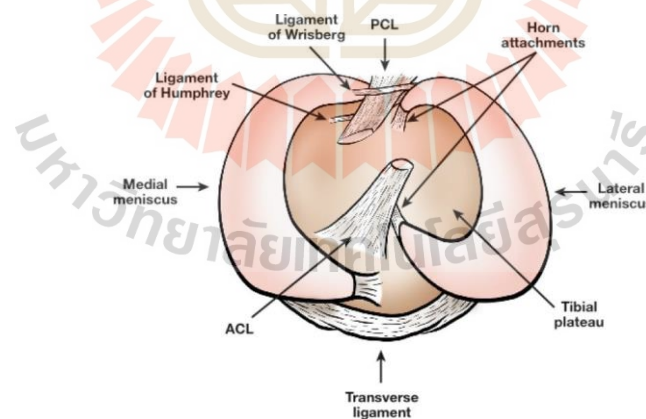
Figure 2.1 The superior view of meniscus anatomy (Makris, Hadidi, & Athanasiou, 2011)

Human meniscus is composed of approximately 70% water and 30% organic matter. The water content provides cushion and lubrication effect as well as in transferring nutrients. Normally, dry matter composed of mainly collagen (75%), Glycosaminoglycans (GAGs) (17%), DNA (2%), elastin (less than 1%), adhesive glycoproteins (less than 1%) in meniscus matrix. The above proportions could vary depending on age, injuries, and other pathological conditions (Makris et al., 2011).

The red-red zone (outer zone), red-white zone (middle zone), and white-white zone are the three zones that make up the meniscus (inner zone). Vascularization and healing capacity separate the zones. The meniscus's periphery is known as the red-red zone. It heals quickly and has high vascularization. The white-white zone is largely avascular and has a low chance of healing, whereas the red-white zone is the middle third with reduced vascularization. Different meniscus area capacity for self-healing varies directly with the presence of blood vessels. (de Caro et al., 2020). As a result, in the majority of instances involving meniscus lesions, meniscus repair is required.
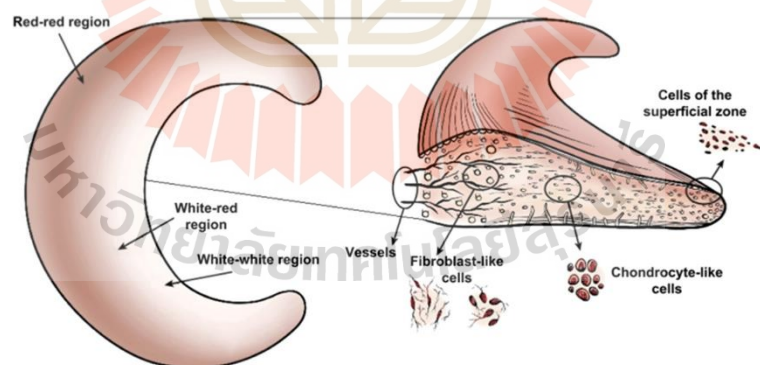
Figure 2.2 Variations in the meniscus' vascularization and cell population
(Makris et al., 2011)

Chondrocyte-like cells embedded in collagen type II and glycosaminoglycans can be found in the inner zone of the meniscus (GAGs). The outer

zone has significant collagen type I deposition and a greater number of elongated fibroblast-like cells than the inner zone (H. Li et al., 2021). As seen in Figure 2.3, the collagen fibers within the menisci are organized into three distinct layers. The bulk of the fibers are oriented circumferentially and are found in the intermediate layer, where they provide resistance to hoop stresses. This layer is sandwiched between two surface layers that include shorter fibers that function as links and are organized radially. These fibers provide structural stiffness against compressive forces, prevent longitudinal splitting, and provide resistance to shear stresses. (Bryceland, Powell, & Nunn, 2017).
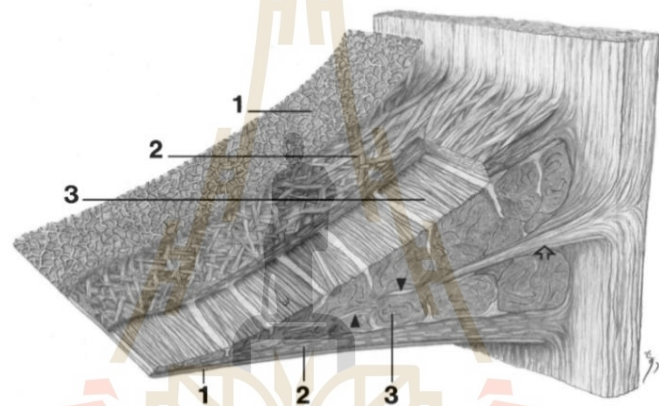
Figure 2.3 Pattern of collagen fiber within meniscus. Random fibers (1), Radial fiber (2), Circumferential fibers (3) (W. Petersen & Tillmann, 1998).

2.1.2 Meniscus mechanical properties

The meniscus serves a variety of functions, such as distributing loads, absorbing shock, and transmitting force across the knee joint. They also provide joint congruity and stability as well as providing nutrition and joint lubrication (Myers et al., 2014). The meniscus withstands many different forces such as shear, tension, and compression. Highly orientated collagen fibers play a significant role in creating the meniscus' unique mechanical characteristics. The meniscus has an aggregate modulus of 100–150 kPa and can withstand axial compression. The tissue's tensile modulus

varies in the circumferential and radial directions; it is between 100 and 300 MPa circumferentially and ten times less radially. And last, the meniscus has a shear modulus at about 120 kPa. (Makris et al., 2011).
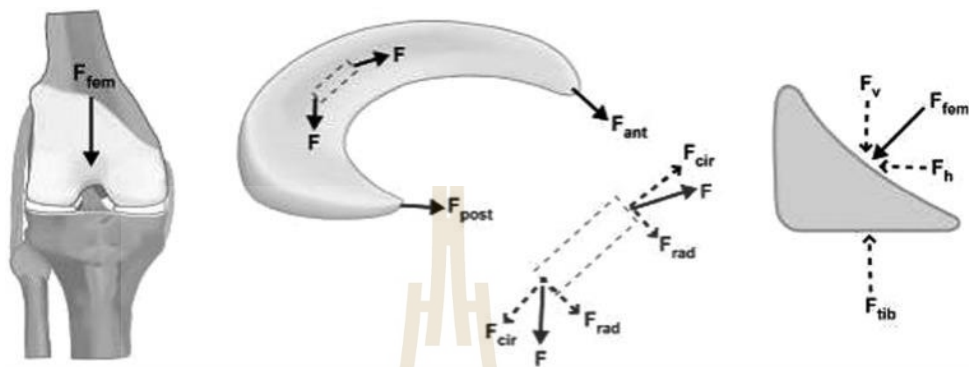
Figure 2.4 Forces operating on the meniscus during loading are illustrated in a free body diagram (Fox et al., 2012)

2.2   Meniscus repair

Meniscus tends to damage during excessive physical activities, over twisting or bending of the knee joint due to sports, accidents, brittleness in aged people, or any other reason (Vadodaria et al., 2019). The healing capacity of the meniscus after injury is basically controlled by the tear site and tear pattern (H. Li et al., 2021). Meniscal repair prevents the joint from increased loading and reduces the development of OA (Spalding, Damasena, & Lawton, 2020).

Arthroscopic meniscectomy is one of the most common methods in orthopedic surgery which remove torn meniscus. Partial meniscus removal is a procedure that causes abnormal biomechanical changes (Jeong, Lee, & Ko, 2012). Total meniscectomy can lead to osteoarthritis due to cartilage degeneration. Loss of the medial meniscus led to a decrease in contact areas of approximately 75% and an increase in the peak contact pressures of approximately 235% (McDermott & Amis, 2006).

An arthroscopic repair technique for meniscal tear using a needle and suture can be delivered via inside-out, outside-in, or all-inside techniques (Spalding et al.,

2020; Z. Wang et al., 2019). There are several variables that have been discovered as affecting meniscal repair success (joint stability, associated ACL reconstruction, age, tear shape, methods of stimulating healing) (Wolf Petersen, Karpinski, Bierke, Müller Rath, & Häner, 2022). Meniscal allograft transplantation (MAT) is one option which may help to restore knee function even further, but the risks associated with disease transmission, immunological rejection, and non-matching donors outweigh this benefit (H. Li et al., 2021).

Tissue engineering and scaffold-based regenerative medicine technologies have emerged as one of the most promising methods for treating meniscal injury in a clinical context. Meniscal scaffolds are an alternative that might be less invasive.

2.3   Meniscus tissue engineering

A damaged meniscus (some section) might be completely replaced with a tissue-engineered construct, or the damage could be repaired via tissue engineering. Based on a combination of cells, growth factors, and scaffolds, tissue engineering (Buma, Ramrattan, van Tienen, & Veth, 2004).
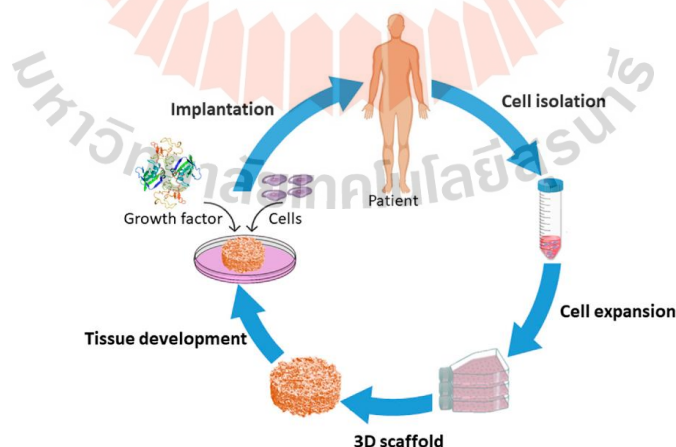
Figure 2.5 Schematic of the scaffold-based tissue engineering approach (Asadian et al., 2020).

2.3.1 Cell

To create in vitro engineered tissue, cells must be used to transfer into the matrix to create a matrix similar to that of native tissue. The primary cells collected from the patient and utilized in combination with scaffolds to create tissue for re-implantation have been the main source of improvements in this field. (Trivedi, Gupta, Bey, & Kirmani, 2016). For repairing damaged or severely injured tissues in patients, there are three main cell therapy approaches: (1) implanting isolated cells, (2) implanting a construct made of cells and scaffolds, and (3) in situ tissue regeneration by native cells (Murphy, O'Brien, Little, & Schindeler, 2013).

2.3.2 Bioactive molecules

Cellular behavior is strongly influenced by biochemical and biophysical cues from the extra cellular matrix. The biomimetic tissue engineering strategy of incorporating bioactive molecules (both soluble and insoluble) aims to stimulate and accelerate the healing process (Dang, Saunders, Niu, Fan, & Ma, 2018). Bioactive molecules include many soluble molecules such as growth factors, cytokines, hormones, DNA, siRNAs, angiogenic factors, and immunosuppressive drugs that interact with cells to regulate their activity. (Kurtis Kasper & Mikos, 2013).

2.3.3 Scaffold

A scaffold is a type of cell accommodation that generates an environment that encourages cell proliferation and tissue differentiation by delivering nutrients and growth factors. A scaffold should resemble the structure and chemical content of extracellular matrix (ECM) and be biodegradable, biocompatible, mechanically resistant, and durable (Gautam & Ambwani, 2019). Tissue engineering makes considerable use of scaffold-based three-dimensional (3D) extracellular matrices to support, arrange, and distribute therapeutic cells. A microenvironment with cell-cell interactions and manifestations of many cellular processes is created by the 3D scaffolds (Talukdar, Nguyen, Chen, Sah, & Kundu, 2011). Scaffolds for tissue engineering are commonly produced of biodegradable polymeric materials, which comes under the types of synthetic or natural polymers.

2.3.3.1 Natural scaffolds

Natural biodegradable polymeric biomaterials commonly include proteins (collagen, fibrin, silk, etc.) and polysaccharides (hyaluronic acid derivatives, starch, alginate, chitin/chitosan, etc.) (Song et al., 2018). The biological features of natural polymers have proven better suited to the normal environment of tissues, encouraging favorable cellular responses, biocompatibility, and degradability (Pina et al., 2019). Natural polymers have the disadvantage of having limited control over the structural or architectural characteristics of the scaffold, such as fiber diameter, alignment, or porosity (Jenkins & Little, 2019).

2.3.3.2 Synthetic scaffolds

Polyester (PLA and PGA), Polycaprolactone (PCL) and Poly (vinyl alcohol) (PVA) have found widespread application in medical application especially tissue engineering scaffold owing to their mechanical properties and biodegradability (Roy et al., 2018). The major shortcoming of synthetic scaffold is lacking of bioactivities which offers less conducive environment for cell proliferation but it generally can be produced reliably and reproducibly with minimal batch-to-batch variation.(Kesireddy & Kasper, 2016)

2.4 Silk Fibroin

Silk is a protein polymer found in the glands of arthropods as silkworms, spiders, and mites; some of these creatures have the ability to spin silk into fibers during metamorphosis. However, the greatest amount of research on silk sources has focused on silkworms (Figure 2.6) (DeBari, King, Altgold, & Abbott, 2021). Silk has two main proteins; silk fibroin (70-80 wt.%) and sericin (20-30 wt.%). The SF fibers undergo a degumming process to remove sericin, which is typically performed under boiling, alkaline conditions (Dou & Zuo, 2015). Silk fibroin (SF) is a natural protein, well known for its excellent biocompatibility, biodegradability and the versatility of structural re-adjustments.
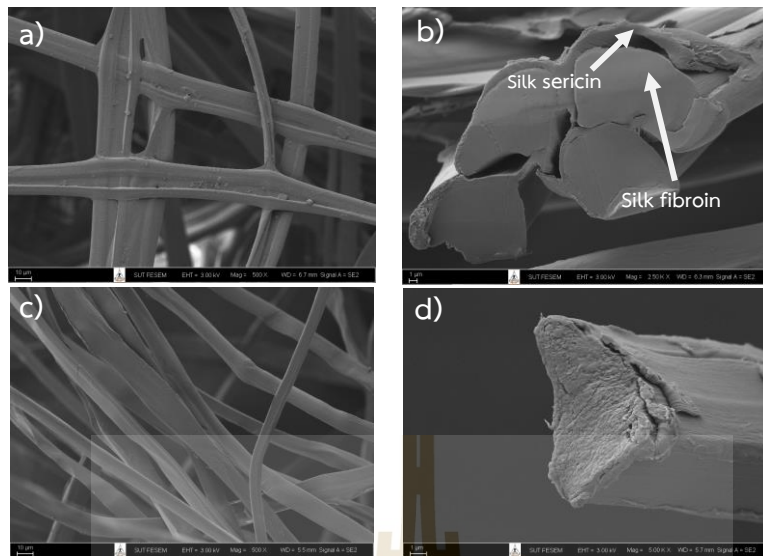
Figure 2.6 SEM images of (a) silk cocoon, (b) silk fiber (c) degummed silk fiber and (d) cross-section of degummed silk fiber.
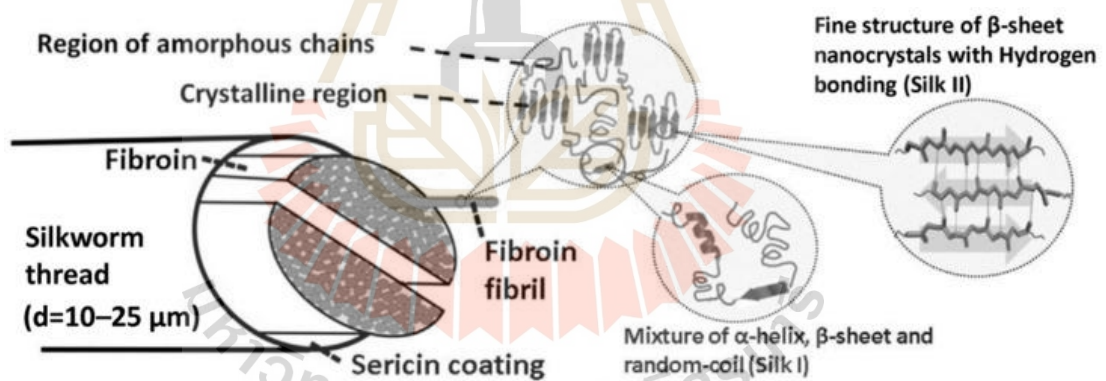
Figure 2.7 Silk fibroin structure (Qi et al., 2017)
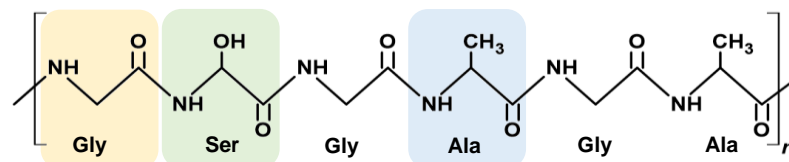
Figure 2.8 Silk fibroin chemical structure (Promnil, Ruksakulpiwat, Ruksakulpiwat, & Numpaisal, 2022)

SF is a semi-crystalline protein with a fibrous structure (Figure 2.7) that offers stiffness and strength. The stiffness and tensile strength of SF are considerably enhanced by the presence of strong hydrogen bonding between neighboring segments. (Qi et al., 2017). Heavy chain (390 kDa) and light chain (26 kDa) are the two major chains that make up SF, and they are connected by disulphide bonds to build the H-L complex (Sun, Gregory, Tomeh, & Zhao, 2021). In heavy chain, SF is made up of only 5% of the other 15 amino acid types and contains 46% glycine, 30% alanine, 12% serine, 5% tyrosine, and 2% valine which is hydrophobic domains of amino acids (Figure 2.8) (Zhou et al., 2001).

It has been demonstrated that SF is an enzymatically degradable polymer and rarely causes a significant immunological reaction (Long, Cheng, Tang, & Chen, 2021). The degradation process is started when enzymes are firstly adsorbed via surface-bonding domains onto the SF fibers. In the following step, the enzymes degrade SF by hydrolyzing ester bonds (Arai, Freddi, Innocenti, & Tsukada, 2004). Therefore, SF composite materials offer superior biocompatibility and better degradability for bioscaffolds (X. Liu et al., 2020).

2.5   Poly(lactic) acid

Poly(lactic acid) (PLA) based polymers are widely used in the biomedical field due to their biocompatibility and hydrolytic degradation. PLA is an aliphatic polyester which synthesized from lactic acid. There are two enantiomeric forms, namely L-lactic acid and D-lactic acid, as shown in Figure 2.8.

Stereochemistry has effects related to material properties. For example, PLLA is a semicrystalline polymer, while PDLLA is an amorphous polymer. Moreover, degradation rate of PLLA is significantly slower than PDLLA, because of the presence of crystalline regions (Casalini, Rossi, Castrovinci, & Perale, 2019). PLA crystallinity effects physical properties and mechanical properties such as tensile strength, Young's modulus, elongation and melting point.
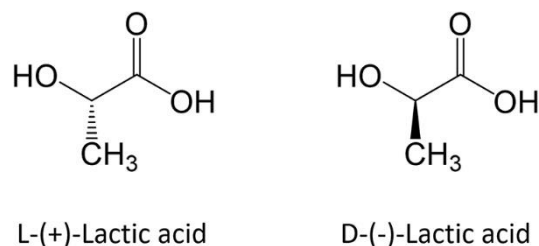
Figure 2.9 Lactic acid enantiomeric forms (Casalini et al., 2019)

2.6 Electrospinning

Electrospinning is an electrohydrodynamic process which a liquid droplet is electrified to generate a jet, followed by stretching fibers. This process is very simple to set up. A typical electrospinning device comprises a high-voltage power supply, a syringe pump, a spinneret with a metallic needle and a rotating collector The polymer solution is loaded in the syringe and extruded to form a droplet as a result of surface tension (Chen et al., 2019).

The polymer solution droplet is deformed into Taylor cone, which a charge jet is ejected. After that, the jet initially extends in a straight line by the electric field force. As the jet is stretched into finer diameters, it solidifies quickly, leading to the deposition of random fibers on the grounded collector.
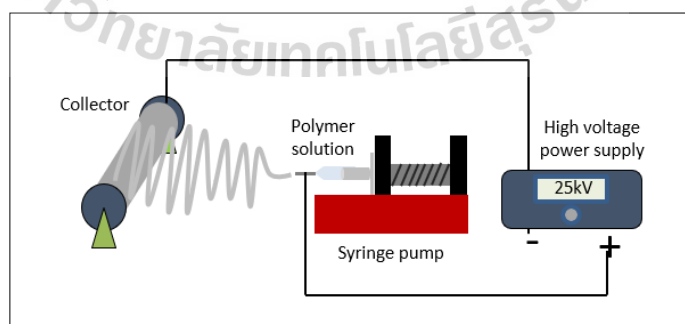
Figure 2.10 Schematic drawing of electrospinning process (Promnil et al., 2022).

The formation and diameter of electrospun fibers were controlled by the processing parameters, including flow rate, voltage, and the distance between the needle tip and the fiber collector. An electrospinning technique has been utilized to fabricate nanofibers from various types of materials. Normally, the success of electrospinning of polymer solutions and the structure and morphology of the resulting polymer nanofibers are determined by the polymer, solvent, polymer solution, processing parameters, and several parameters related to environmental conditions. The presence of a sufficient high molecular weight polymer and a suitable polymer solvent are the two general requirements for good solution electrospinning. The polymer molecular weight has a dominant impact on the rheological behavior of the polymer solution, while the homogeneous solution relies on the solubility parameter of the solvent (Xue, Wu, Dai, & Xia, 2019).

Electrospinning is considered to be the most versatile technique for producing nanofibers. Electrospun fibers have a high surface area, desired mechanical properties, a controlled structure, and ease of biochemical functionalization. The three-dimensional electrospun fibrous structures nearly mimic the architecture and features of the extracellular matrix (ECM) which significantly influences biomaterial design to promote tissue regeneration (Su et al., 2021).

2.7 Poly(lactic) acid-based scaffold

Gao et al. (2018) fabricated a scaffold with a scaffold should have a distributed architecture, remarkable mechanical strengths, and good biocompatibility. Electrospun into nanofiber yarns and woven into multilayer fabrics, a polylactic acid (PLA) and Tussah silk fibroin (TSF) solution was used to create these materials. After electrospinning, scaffolds were mineralized in simulated body fluid (SBF) to develop polymer nanofibers, usually as a composite with hydroxyapatite (HA) which constitutes the majority of natural bone's inorganic material, to better imitate natural bone. The PLA/TSF multilayer nanofiber textiles' compressive modulus and stress after mineralization were increased; these values were 32.8 and 3.0 times higher than those

of the composite scaffolds without mineralization, respectively. These values were significantly higher than those of a scaffold comprised of randomly arranged nanofibers because of the ordered and hierarchical structure of the nanofiber fabric template. Mesenchymal stem cells (MSCs) were transplanted onto PLA/TSF fabric, PLA/TSF/HA nanofiber fabric, and PLA/TSF/HA nanofiber fabric mats in order to test and evaluate the scaffolds' cytocompatibility. Cell proliferation on the PLA/TSF/HA multilayered nanofiber fabric and PLA/TSF/HA multilayered nanofiber mats was considerably higher than that on the PLA/TSF multilayered nanofiber fabric on days four and seven, while it was lower on the reference sample, according to the results of an MTT cell proliferation assay done on MSCs growing on various scaffolds, revealing that the mineral crystals on the nanofibers surface can promote cell proliferation. Confocal fluorescence microscopy of MSCs cells on various materials revealed that the cells were distributed randomly over the PLA/TSF/HA nanofiber mats while being oriented on the surface of the nanofiber fabric along the axial direction of the yarn. Furthermore, compared to the PLA/TSF/HA nanofibrous mats, the cells fluoresced more intensely on the PLA/TSF/HA fabric group. This demonstrated that, when compared to other materials, multilayered nanofiber textiles may provide a three-dimensional culture environment more conducive to MSCs cell growth.

Gutiérrez-Sánchez, Escobar-Barrios, Pozos-Guillén, and Escobar-García (2019) developed new polymeric compound for bone tissue engineering. The goal of this study is to evaluate cell adhesion produced by starch and poly (lactic acid) (PLA) combinations that have been treated with arginine-glycine-aspartic acid peptides (RGD), one of the peptide sequences most frequently employed to mimic cell adhesion. Using the electrospinning technique, PLA non-woven fibers with varying starch contents (0.0, 2.5, 5.0, and 10% w/v) were created. Through examination of the water contact angle, the wettability of scaffolds was assessed (WCA). The outcome demonstrated that the scaffold had a hydrophobic nature before being treated with RGD, and that after the surface treatment, the WCA decreased by about 18% as a result of the incorporation of surface groups of the RGD's amino acid sequence on the surface of

the various PLA scaffolds with starch. Subsequently, interaction with water molecules was made simpler and more effective thanks to a hydrogen bond between the amine group and the proton of the water molecules. However, the PLA's starch had no influence on the WCA, suggesting that it is more deeply embedded in the polymer matrix than on the surface. Over the end of five weeks, the hydrolytic degradation of the scaffolds was examined in phosphate buffer solution (PBS) at 37 °C. The sample weights were kept under observation. The outcome showed that the sample hydrolytic degradation did not appear to be affected by the addition of starch. MTS testing was used to assess cell growth. After 48 hours of incubation, the osteoblast content that was discovered for each scaffold may be appreciated. The outcome shown that the osteoblast cells multiplied on the PLA and PLA scaffolds that included 5.0 % starch. The data, however, could not clearly demonstrate a pattern based on the starch content. This may be due to the morphology of the scaffold, which is drastically affected with the starch content.

Yin Gui-Bo (2009) investigated the possibility of PLA/SF-gelatin use as scaffolds by fabricating a nanofibrous composite scaffold of poly L-lactic acid (PLA)/silk fibroin (SF)-gelatin using an electrospinning process. The air-dried SF membranes or a blend of gelatin and air-dried SF membranes (70:30:50:50) were dissolved in formic acid at a concentration of 98 percent (w/w). To achieve a concentration of 5%, PLA was dissolved in a mixture of solvents with a volume ratio of 2:1 (chloroform: acetone). By electrospinning, SF and SF-gelatin mix nanofibers in various ratios were applied to the PLA fibrous membranes. These membranes were submerged in 100% methanol for 10 minutes before being dried at room temperature for 24 hours. Utilizing the mitochondrial metabolic (MTT) activity test, cell proliferation was detected. The ability of PLA/SF-gelatin (70:30), PLA/SF-gelatin (50:50), and chemically treated PLA/SF-gelatin fiber membranes to sustain cell growth and proliferation implies that the scaffolds are not cytotoxic. Over the course of 12 cell culture days, the vitality of 3T3 murine fibroblasts cultivated on each membrane rose and eventually fell. Furthermore, the proliferation dramatically increased as the gelatin content rose, indicating that the

scaffold compositions had an impact on the development of the cells. The composite fiber membrane made of PLA/SF-gelatin (50:50) proven to be the best choice for scaffolds.

2.8   Silk fibroin-based scaffold

Panjapheree et al. (2018) studied scaffolds with 2 phases of silk fibroin film attached to a silk fibroin and chitosan sponge that were created for osteoarthritis treatment. Before being applied to the silk fibroin and chitosan sponge phase, silk fibroin film was created in the following ratios: 100:0 (SF), 70:30 (SF70), 50:50 (SF50), 30:70 (SF30), and 0:100. (CS). Film casting was used to create the silk fibroin, which was then allowed to air dry for two days before being submerged in methanol to change its random coil structure into a beta sheet structure. For sample preparation, the SF film was trimmed into 1x1 cm pieces. A 3 % SF solution and a 3 % CS solution were mixed for the porous phase. 48 well plates were filled with about 1 mL of each solution, lyophilized for freeze-drying, allowed to dry, and then submerged in methanol. The samples were then divided into 2x10 mm plates. The biphasic scaffolds were fully constructed by attaching two phases together with a silk solution and letting them rest at room temperature for two days. Biphasic scaffolds' mechanical characteristics were shown using ultimate tensile strength and elastic modulus. The findings showed that as the amount of chitosan grew, the stress at maximum load dropped. When the quantity of chitosan was raised, the elastic modulus of silk fibroin and chitosan part dropped. The breakdown of biphasic scaffolds by lysozyme was used to gauge their physical stability. The findings showed that CS had the greatest degree of deterioration. The least level of deterioration was seen in SF. As the amount of chitosan grew, the degradation accelerated.

L.-P. Yan et al. (2012) have studied silk fibroin scaffolds which obtained from high concentration of aqueous silk fibroin solutions. The salt-leaching and freeze-drying techniques were used to create the silk fibroin scaffolds, which were created with a range of starting concentrations (8, 10, 12, and 16 percent in weight percent). The

scaffolds were made by pouring a solution of silk fibroin (8–16%) into a silicon tube, then adding granular sodium chloride. To eliminate sodium chloride, the silicon tubing was exposed to distilled water for three days before being dried at room temperature for 48 hours. The scaffolds were then created by punching the produced skin with a stainless-steel tool, freezing it at -80 ℃ for a day, and then freeze-drying it. The compressive tests were performed using a universal testing machine. When the concentration of silk fibroin was elevated from 8 to 16 percent, the dried silk fibroin scaffolds' static compressive modulus significantly rose from 0.81 to 0.29 to 15.14 to 1.70 MPa. The compressive strength of the scaffolds significantly rose, from 0.05 to 0.79 MPa, as silk content grew from 8 to 16 percent and stiffness also increased, as seen by the example stress-strain curve. As a result, the created silk fibroin scaffolds are suitable for application in tissue-engineered scaffolding, particularly for the regeneration of cartilage and meniscus.

Mandal, Park, Gil, and Kaplan (2011) fabricated knee meniscus scaffold system with three-layered wedge-shaped structure. The freeze-drying three-layer silk meniscus scaffolding method was designed to resemble the natural meniscus structure. A single layer of aqueous silk 3D scaffolds is produced with various pore sizes and orientations. The first two layers of the three were created using the salt-porogen leaching method mentioned above, while the third layer was created using the lyophilization method. Using a universal testing equipment, the compressive and tensile mechanical characteristics of hydrated scaffolds were determined (Instron 3366). For the first, second, and third scaffold layers, respectively, the compressive modulus varied between 293.78 ±47.56, 347.58±62.39, and 164.80±14.24 kPa. The first through third scaffold layers had compressive strengths of 67.23±27.30, 75.62±15.76, and 70.44±09.07 kPa, respectively.

Comparing the stated axial (83.4 kPa) and radial (76.1 kPa) compressive moduli of natural human medial meniscus, the silk meniscus layers possessed greater compressive moduli. The outcome showed how to create a multilamellar,

multiporous, wedge-shaped silk meniscus scaffold with promising mechanical characteristics.

2.9 Effect of polymer molecular weight on mechanical properties of electrospun nanofibers

Zhang et al. (2014) studied the mechanical characteristics of electrospun poly(ε-caprolactone) (PCL) mats with varying PCL average molecular weights (40,0000, 80,000 and 120,000 g/mol). The PCL was dissolved in mixed solvents, chloroform/methanol (6:1, v/v), in which the PCL concentration was 12% (w/w). In order to create the nanofiber mats, electrospinning was used. PCL-40 nanofibrous scaffolds have a beads-on-string structure that is difficult to manage, making it unable to conduct a tensile test on them. The high molecular weight PCL-based electrospun mat is somewhat stronger but less flexible than the low molecular weight sample, according to the tensile test. Young's modulus and ultimate strength both rise from 8.41 MPa to 8.77 MPa and from 1.13 MPa to 2.25 MPa, respectively, as average molecular weight varies from 80,000 to 120,000 g/mol. The mat's elongation at break decreases dramatically to only 63.5%. The significant reduction in flexibility is due to two aspects: First, excessively entangled PCL chains are unable to react quickly to shifting stresses. The second aspect is that some fine fibers are weak and reduce the electrospun mat's ability to resist deformation. The results show that the PCL-80 scaffold achieves the desired levels of strength, modulus, and flexibility.

Ngadiman, Noordin, Idris, Shakir, and Kurniawan (2015) investigated the influence of molecular weight (M_w) of polyvinyl alcohol (PVA) on electrospun nanofibers. PVA was utilized in four different molecular weights: 60,000 Da, 124,000 Da, 145,000 Da, and 200,000 Da. PVA polymer powder was dissolved in deionized water to create an aqueous PVA solution with a 10% w/v concentration. The electrospinning method was used to construct the PVA nanofibers. The higher mechanical properties were obtained from high molecular weight PVA (200kDa). The tensile strength increases from 20.5±0.9 to 29.8 ±0.3 MPa and the Young's modulus increases from 55.5±0.3 to

77.9±0.8 MPa. Above 145 kDa, the increase in tensile strength and modulus that occurs with molecular weight increase appears to have reached saturation. Longer PVA polymer chains are the cause of the increase in molecular weight, which often corresponds to better mechanical properties.

2.10 Effect of polymer concentration on mechanical properties of electrospun nanofibers

Ngadiman et al. (2015) studied the effect of PVA concentration on mechanical properties of electrospun nanofiber mats. Aqueous PVA (60k Da, 124 k Da, 145kDa, and 200k Da) solutions with 5% and 10% w/v were prepared by dissolving PVA polymer powder in deionized water. The nanofiber mats were constructed by using electrospining. The higher solution concentration (10% w/v) has higher mechanical properties compared to the lower solution concentration for all the different molecular weights of PVA. For 60 kDa PVA, the tensile strength increases from 16.8±0.4 MPa to 20.5±0.9 MPa when the concentration is increased.

Tarus et al. (2016) investigated the mechanical properties of electrospun poly(vinyl chloride) (PVC) nanofiber mats. PVC solutions of 12, 14 and 16 wt.% PVC concentration were prepared in a 1:1 (w/w) N,N-dimethylformamide (DMF) /Tetrahydrofuran (THF) solvent system. The nanofiber mats were fabricated by using an electrosoinning process. The tensile strengths of PVC mats are 0.003, 0.007, and 00.1 N/tex, respectively. The tensile strength increases with an increase in polymer concentration. The presence of beads in nanofiber mats at low concentration causes fewer fiber-to-fiber interactions and increased weakness of individual fibers, resulting in low tensile strength values.

2.11 Effect of polymer concentration on morphology of electrospun nanofibers

Ma, Yamane, and Kimura (2010) studied the effect of PLLA solution concentration on nanofiber morphology. The PLA sample was dissolved in a dichloromethane (DCM)/ N,N-dimethylformamide (DMF) mixture (9:1 wt%) at a concentration of 1, 4, and 8 wt.%. The nanofibers were fabricated by electrospinning. The fibers electrospun from 1 wt.% solution showed morphologies of bead-on-string because the viscosity was not sufficiently high to yield continuous fiber during electrospinning. With the dopes containing 4 wt.% of PLLA, the bead-on-string formation was observed. The suitable fiber formation was achieved at an 8 wt.% concentration. The average fiber diameter increases with increasing viscosity.

Tarus et al. (2016) investigated the effect of polymer concentration on PVC nanofiber morphology. In a 1:1 (w/w) N,N-dimethylformamide (DMF)/Tetrahydrofuran (THF) solvent system, PVC solutions of 12, 14, and 16 % (wt.) PVC concentration were produced. The creation of the nanofibers using electrospinning. Beaded fibers were formed at 12 weight percent from the SEM micrographs, whereas smooth fibers were obtained at 14 and 16 % concentrations. 12%, 14 %, and 16 % PVC have fiber diameters of 121, 253, and 275 nm, respectively. It was discovered that as the concentration of the solution increased, so did the diameters of the nanofibers.

2.12 Effect of silk fibroin content on mechanical properties of scaffold

L.-P. Yan et al. (2012) studied the developmental properties of silk fibroin scaffolds derived from high-concentration aqueous silk fibroin solutions. The silk fibroin scaffolds were prepared with different initial concentrations (8, 10, 12, and 16%, in wt.%) and obtained by combining the salt-leaching and freeze-drying methodologies. The universal testing machine was used for the compressive tests. When the concentration of silk fibroin was raised from 8 to 16 %, the static compressive modulus

of the dried silk fibroin scaffolds increased drastically from 0.81 to 0.29 to 15.14 to 1.70 MPa. The compressive strength of the scaffolds significantly rose, from 0.05 to 0.79 MPa, as silk content grew from 8 to 16 % and stiffness also increased, as seen by the example stress-strain curve. As a result, the created silk fibroin scaffolds are suitable for application in tissue engineering scaffold, particularly for the regeneration of cartilage and meniscus.

Roy et al. (2018) investigated the impact of silk fibroin content on the mechanical characteristics of an electrospun core-shell nanofibrous scaffold made of polycaprolactone and silk fibroin (PCL/SF). PCL was dissolved in chloroform (10% w/v), while SF was dissolved in formic acid (10% w/v). For electrospinning, the PCL and SF solution was combined in a variety of ratios, including 100:0, 70:30, and 50:50. According to the findings of the tensile testing, the elastic modulus of PCL/SF 50:50 nanofibers (448.8±198.0 MPa) were much higher than that of PCL/SF 70:30 nanofibers (333.66±0.4 MPa). For PCL/SF 70:30 nanofibers, a maximum ultimate tensile strength of 4.7±0.16 MPa was recorded. The high SF concentration increased the nanofibers' stiffness, while the high PCL content enhanced their ductility, leading to a high degree of nanofiber elongation.

The influence of silk fibroin content on the shape of an electrospun polycaprolactone/silk fibroin (PCL/SF) nanofibrous scaffold was examined by Nazeer, Yilgor, and Yilgor (2019). Different PCL/SF solutions with SF concentrations (20 wt. percent and 40 % wt.). Formic acid was used to make the solution. created by combining a certain amount of PCL with a certain amount of SF after the SF has been dissolved in formic acid. The scaffolds were made with the help of electrospinning. There are no appreciable differences in the ultimate tensile strength values of PCL and PCL/SF composites. Elongation at break values were found to be much lower, dropping from 42.22.4 %(PCL) to 21.10.4 % (PCL/SF-40). The elastic modulus values, on the other hand, dramatically rise from 21.6±1.7 MPa (PCL) to 49.3± 6 MPa (PCL/SF-20) and 98.1±23.7 MPa (PCL/SF-40).

W. Liu et al. (2016b) studied the effect of silk fibroin content on the mechanical properties of the fibrous SF/PLLA scaffold. SF and PLLA at different mass ratios (S40P60, S50P50, and S60P40) were dissolved in trifluoroacetic acid (TFA) and 1,1,1,3,3,3-Hexafluoro-2-propanol (HFIP), respectively, and then mixed together. Electrospinning was used to create the aligned fibrous SF/PLLA at a working voltage provided by a high voltage power supply. A universal testing device was used to conduct tensile testing on the fibrous SF/PLLA scaffolds to assess their mechanical characteristics. When the SF:PLLA mass ratio was S50P50, the scaffold's highest tensile strength (1.5 MPa) was achieved (Collector distance of 20 cm, working voltage of 15 kV).

2.13 Effect of silk fibroin content on morphology of electrospun nanofibers

Nazeer et al. (2019) investigated the effect of silk fibroin content on the morphology of an electrospun polycaprolactone/silk fibroin (PCL/SF) nanofibrous scaffold. To create PCL/SF solutions with various SF concentrations, formic acid was applied (20 % and 40 % wt.). A portion of SF was dissolved in formic acid, then a portion of PCL was added to create the solution. The scaffolds were constructed using electrospinning. The production of precise electrospun mats is visible in the SEM pictures. The average fiber diameter dramatically increased with the addition of SF, increasing from 150 nm for PCL fiber to 200 nm and 280 nm for blends with 20 and 40 weight percent of SF, respectively.

Roy et al. (2018) investigated how the amount of silk fibroin affected the shape of a core-shell nanofibrous scaffold electrospun from polycaprolactone and silk fibroin (PCL/SF). PCL was dissolved in chloroform (10% w/v), while SF was dissolved in formic acid (10% w/v). For electrospinning, numerous ratios of PCL and SF solutions were used, including 100:0, 70:30, 50:50, and 30:70. A scanning electron microscope was used to examine the electrospun fibers. Although the diameter distribution curve of the PCL fibers revealed significant variance in the nanofiber diameter range (539.8–93.2 nm), the native PCL nanofibers displayed smooth fiber morphology without beads.

With an increase in SF concentration, the fiber diameter rose as well. When the SF ratio is raised from 30 to 70, the fiber diameter grows from 333.6 nm to 1021.6 nm.

2.14 Effect of silk fibroin content on in vitro cell culture studies of electrospun nanofibers

Pillai et al. (2016) examined at how much silk was present in SF/PVA electrospun nanofibers as well as how much DNA was present. SF solution (10% w/v) was produced in 98 percent formic acid. Water was used to dissolve PVA (10% w/v). Blends of SF/PVA were created in the following proportions: 2:1, 3:1, and 4:1 (v/v). Electrospinning was used to create the scaffolds. To evaluate the cytotoxicity of the nanofibrous scaffolds, the MTT assay was used. All of the scaffolds-maintained cell growth, were non-toxic, and shown rising cell viability with time. The most viable formulation was the 3:1 SF/PVA (103.20.4% at day 5). When compared to the 6th day control, DNA content significantly increased in all scaffolds as incubation days progressed.

Nazeer et al. (2019) studied the effect of silk fibroin content on cell viability of electrospun polycaprolactone/silk fibroin (PCL/SF) nanofibrous scaffold. Different PCL/SF solutions with SF concentrations (20% and 40% wt.). The solutions were made by first dissolving a certain quantity of SF in formic acid, then adding a certain amount of PCL. The scaffolds were made with the help of electrospinning. Due to an increase in cell density from Day 1 to Day 4, the results of the cell viability tests demonstrated that none of the scaffolds were hazardous to cells. In the presence of SF, a significant proliferation rate was seen.

CHAPTER 3

RESEARCH METHODOLOGY

3.1 Materials

Two commercially available non-medical grades of PLA with different molecular weights, PLA3251D (99% L-lactide and 1% D-lactide; low molecular weight; PLAL) and PLA4043D (94% L-lactide and 6% D-lactide; high molecular weight; PLAH) provided by NatureWorks LLC (Minnetonka, MN, USA) and a PLA medical grade, Resomer L209S (pure PLLA; PLAmed) from Sigma-Aldrich (Burlington, MA, USA.) were utilized. Chloroform RPE was purchased from Carlo Erba Reagents (Milano, Italy). Formic acid was purchased from Merck (Darmstadt, Germany). Bombyx mori cocoons were arranged by the Queen Sirikit Sericulture Center (Nakhon Ratchasima, Thailand). Sodium carbonate (Na_2CO_3, analytically pure) and calcium chloride ($CaCl_2$, analytically pure) were purchased from Carlo Erba (Milano, Italy). HPLC chloroform was purchased from RCI Labscan (Bangkok, Thailand).

3.2 Method

3.2.1 Extraction of silk fibroin

Silk cocoons were cut into small pieces, put in a 1% Na_2CO_3 boiled solution for 30 minutes to remove the sericin, and washed with distilled water. The ratio between Na_2CO_3 and cutting cocoon is 1:20. 2.0 g of degummed silk was added to 10 g of $CaCl_2$ solution and boiled for 1 hour at 98±2°C before being cooled and filtered. The filtrate was removed into a dialysis bag soaked with distilled water. The distilled water was changed three times a day. The regenerated silk fibroin solution after dialysis was stored at 4°C in the refrigerator.

3.2.2 Preparation of electrospinning solution

        Two commercial grades of PLA (PLAL and PLAH) with various molecular weights were produced in chloroform at various concentrations (10%, 15%, and 20% w/v). 98–100% of the SF was dissolved in formic acid at a 12 % (w/v) concentration. For SF solution mixing, an electrospun PLA sample with a high molecular weight at a 15% w/v concentration has been chosen (PLAH75:SF25, PLAH50:SF50, and PLAH25SF75). Medical grade was made at a 6 % concentration and blended 50:50 with SF in the meanwhile. To make a PLA/SF emulsion, a magnetic stirrer was used. The PLA/SF emulsion was stirred for 24 h to make it homogenous.

Table 3.1. PLA sample nomenclature.

Sample	Grade	Manufacturer	Molecular Weight (g/mol)	Concentration (% w/v)
PLAL–10	3251D	NatureWorks LLC	55,400 (Friné, Hector, Manuel, Estrella, & Antonio, 2019; Jazrawi, Noroozi, Ansari, & Hatzikiriakos, 2013)	10
PLAL–15	3251D	NatureWorks LLC	55,400 (Friné et al., 2019; Jazrawi et al., 2013)	15
PLAL–20	3251D	NatureWorks LLC	55,400 (Friné et al., 2019; Jazrawi et al., 2013)	20

Table 3.1. PLA sample nomenclature (continued).

Sample	Grade	Manufacturer	Molecular Weight (g/mol)	Concentration (% w/v)
PLAH–10	4043D	NatureWorks LLC	127,300–147,400 (Meng, Nguyen, Tekinalp, Lara-Curzio, & Ozcan, 2018; Ortenzi et al., 2020)	10
PLAH–15	4043D	NatureWorks LLC	127,300–147,400 (Meng et al., 2018; Ortenzi et al., 2020)	15
PLAH–20	4043D	NatureWorks LLC	127,300–147,400 (Meng et al., 2018; Ortenzi et al., 2020)	20
PLAmed–6	L209S	Sigma-Aldrich LLC	177,000 (BAYDEMİR, 2009; Torino, Aruta, Sibillano, Giannini, & Netti, 2016)	6

3.2.3 Preparation of scaffold by electrospinning process

The polymer solution was filled into a 10 mL syringe equipped with a 20-gauge blunt needle, and the solution was pumped out with a flow rate of 2.0 mL/h. Electrospinning was used to acquire the samples. The application of a 20 kV electrical field was made via a high voltage power supply. At a distance of 15 cm from the needle tip, PLA and PLA/SF samples were collected on a grounded rotating collector.

3.3   Characterization

3.3.1   Characterization of PLA solutions

The PLA solution viscosities were evaluated by rotational rheometry using a DV3T cone-plate viscometer (AMETEK Brookfield, Middleboro, MA, USA) at a controlled temperature of 25 °C. The temperature control was prepared by a circulating refrigerated bath. The cone type used and the shear rate range were selected in consideration of the relationship between the apparent viscosity and the measurement range of the device.

3.3.2   Scaffolds morphology

Field emission scanning electron microscopy (FESEM; Carl Zeiss Auriga, Oberkochen, Germany) with gold coating was used to investigate the morphology of electrospun fiber. Using image analysis software (ImageJ), the diameter of 100 randomly selected electrospun fibers was calculated from SEM micrographs. The OriginLab program was used to plot the diameter distribution curves of fiber diameter.

3.3.3   Scaffolds mechanical properties

Using an Instron Universal Testing Machine (Instron 5565, Norwood, MA, USA) with a crosshead speed of 10 mm/min and a 1 kN load cell operating at room temperature, the tensile characteristics of the materials were evaluated. The prepared electrospun specimens had initial lengths of 10 cm and a width of 1 cm. The statistics for Young's modulus, elongation at break, and tensile strength are the average outcomes from five test specimens (n=5).

3.3.4   Thermal properties

Using a TGA/DSC1 thermogravimetric analyzer (Mettler Toledo, Greifensee, Switzerland) and a nitrogen atmosphere between 25 and 500 °C, the thermal stabilities of all scaffolds were examined. Differential scanning calorimetry (DSC) was used on a Pyris Diamond DSC machine (PerkinElmer, Waltham, MA, USA) in a nitrogen gas flow to examine the thermal characteristics of all samples. The samples were heated at a rate of 10 °C/min from 25 to 200 °C (first-heating scan). The samples

were cooled to 25 °C at a rate of 10 °C/min after 5 minutes at 200 °C. They were then heated to 200 °C at a rate of 10 °C/min (second-heating scan).

The first and second heating scans were used to calculate the glass transition temperature (T_g), melting temperature (T_m) cold crystallization temperature (T_{cc}), cold crystallization enthalpy (ΔH_{cc}), and melting enthalpy (ΔH_m). The cooling scan was used to determine the melt crystallization temperature (T_c) and crystallization enthalpy (ΔH_c). Equation 3.1 was used to calculate the percent (%χ_c) of crystallinity in PLA and biocomposite scaffolds.

$$\% \text{ Crystallinity } (\chi_c) = [(\frac{\Delta H_m}{\Delta H_m^0}) \times 100] \times \frac{1}{W_{PLA}} \qquad (3.1)$$

which ΔH_m is the melting enthalpy (J/g) from the heating scan, ΔH_m^0 is the theoretical melting enthalpy of completely crystalline PLA (93.7 J/g) (Nguyen, Ruksakulpiwat, & Ruksakulpiwat, 2016), and W_{PLA} is the PLA weight fraction in the biocomposites scaffolds.

3.3.5 Fourier-transform infrared spectroscopy (FTIR)

A FTIR spectrophotometer (Bruker Tensor 27, Billerica, MA, USA) was used to measure the FT-IR spectra of PLA, PLA/SF nanofibrous scaffolds, and SF powder. In the spectral region of 4000-400 cm^{-1}, attenuated total reflectance (ATR-FTIR) mode was used to directly analyze all samples.

3.3.6 In vitro degradation of constructed scaffolds

Scaffolds of 1 cm width and 1 cm length (n = 3) were submerged in phosphate buffered saline (PBS, pH = 7.4) and kept incubating for 14, 28, 42, and 84 days at 37 °C with 5 percent carbon dioxide (CO_2) for 14, 28, 42, and 84 days. Every three days, PBS was replaced. Every two weeks, the total scaffold weight was measured. The scaffolds underwent a distilled water wash, drying, and weighing process. Equation 3.2 (Wongnarat & Srihanam, 2013) was used to get the residual weight %.

$$\% \text{ Residual weight} = 100 - [\frac{(W_i - W_f)}{W_i} \times 100] \qquad (3.2)$$

which W_i is initial weight of scaffold sample, while W_f is the scaffold sample weight after submerging in PBS.

3.3.7 Scaffold surface wettability

To evaluate the surface wettability qualities of the PLA/SF electrospun scaffolds, the water contact angle was measured. On top of each sample, 15 μL of specified volume distilled pipet. Images of water drops on the sample surface were captured using a USB digital micro-scope (1600x) after a 60-second exposure at room temperature, and they were processed using ImageJ software. Measurements were made at three distinct sample locations (n = 3).

3.3.8 In vitro cell viability

The scaffolds were cut to dimensions of 4 mm x 4 mm (n = 3) and divided into two groups. The first group was soaked in 70% alcohol, dried at 30 ° C for 24 hours and sterilized under ultraviolet (UV) light for 30 minutes, while the second group was not soaked in alcohol. The scaffolds were then placed in 96-well plates and the human chondrocyte cells (HCPCs) with 5×10^3 cells were seeded onto the scaffolds. The scaffold in which the cells were seeded was Dulbecco's Modified Eagle's Medium (DMEM) containing 1% L-glutamine, 1% penicillin-streptomycin and 10% fetal bovine serum. It was cultured in 37 °C with a 5% CO_2 humidified incubator. Cell viability was assessed on days 1, 3, and 7 using the MTT (3-[4,5-dimethylthiazole-2-yl]-2,5-diphenyltetrazolium bromide) assay. A microplate reader was used to measure the optical density of each well at 590 nm. By comparing the absorbance of cells growing on the scaffold with the absorbance of the reference equation (3.3), cell viability was estimated.

$$\% \text{ Cell viability} = \frac{\text{(O.D.of treatment)}}{\text{(O.D.of control)}} \times 100 \qquad (3.3)$$

3.3.9 Quantitative analysis for gene expression

The PLAmed-6 and PLAmed50:SF50 scaffolds were used to measure gene expression in accordance with the results of the cell viability tests. The

electrospun scaffold sheet was cut into a 12-mm-diameter circular and sanitized for 30 minutes under UV light. Following that, the ready scaffolds (n = 3) were put in 24 wells and allowed to incubate in the medium for 4 hours. Each scaffold of the HCPCs received 2.5 ×10^4 cells as seeding. Following that, samples of the cell-seeded scaffold were grown for 7, 14, and 28 days. Using the RNeasy mini-Kit (Qiagen, Hilden, Germany), total RNA was extracted from the HCPCs on the scaffolds for quantitative gene analysis. An SYBR Green kit (Thermo Fisher Scientific, Waltham, Massachusetts, USA) and a Fluorescein kit (BIOLINE, London, UK) were used to perform a quantitative real-time polymerase chain reaction (qRT-PCR). Type I collagen (COL1A1), which had fibrogenic characteristics, and type II collagen (COL2A1), which demonstrated a chondrogenic phenotype, were the target genes. The 18S rRNA was employed as a housekeeping gene, as can be seen in Table 3.2.

Table 3.2. Sequences of the primer sets for qRT-PCR.

Genes		Primer Sequence (5′ to 3′)
Type I collagen	Sense	GGAGGAGAGTCAGGAAGG
(COL1A1)	Antisense	GCAACACAGTTACACAAGG
Type II collagen	Sense	GGCAGAGGTATAATGATAAG
(COL2A1)	Antisense	ATGTCGTCGCAGAGG
18S rRNA	Sense	ATACCGTCGTAGTTCC
	Antisense	GTCTCGTTCGTTATCG

CHAPTER 4

RESULTS AND DISCUSSION

4.1 Effect of the PLA molecular weight and concentration on the physical properties and mechanical properties of electrospun PLA scaffolds

4.1.1 PLA solution viscosities

The electrospun solution viscosities were shown in Table 4.1. PLAL solutions showed lower viscosity than PLAH at the same concentration. Increasing concentration led to a significant increase in viscosity. While, PLAmed solution at a lower concentration (6%) showed higher solution viscosity than PLAH (10%).

Viscosity was a crucial solution parameter that impacted the capacity to generate fibers during the electrospinning process (L. Li et al., 2011). Concentration and polymer molecular weight were two significant factors that affected the viscosity of the solution (Kim et al., 2005). Higher concentrations cause the polymer chains to become more entangled, increasing viscosity.

Table 4.1 PLA solution viscosity for scaffold electrospinning.

PLA Solution (w/v)	Viscosity (cP)
PLAL-10	58.02 ± 0.80
PLAL-15	278.68 ± 5.47
PLAL-20	690.54 ± 30.18
PLAH-10	652.98 ± 36.15
PLAH-15	2304.73 ± 74.49
PLAH-20	9319.67 ± 91.40
PLAmed-6	1024.81 ± 83.15

PLAH has a higher molecular weight and therefore has a higher viscosity than PLAL. PLAmed-6 has a higher viscosity than PLAH-10. During the polymer-solvent interaction, solvent molecules penetrate the polymer and chain segmentation increases chain mobility.

4.1.2 Morphology of electrospun PLA scaffold

Scanning electron microscope micrographs of electrospun PLAL, PLAH, and PLAmed nanofibers and diameter distribution curves of the electrospun fibers are shown in Figures 4.1 and 4.2, respectively.

Each sample PLA fiber surfaces had tiny holes dispersed at random on them. Instead of a fibrous structure, PLAL10 (Figure 4.1a–c) displayed a significant number of droplets or beaded particles. The electrospun fibers for PLAL15 (Figure 4.1d-e), also known as bead-on-string fibers, still had beads on them, but PLAL20 (Figure 4.1g-i) produced porous fibers without any beads. Small fiber diameter and high entanglement were also obtained by PLAH-10 (Figure 4.2c-l). When compared to other samples, PLAH15 displayed consistent fibers with variable orientation (Figure 4.1m–o), while PLAH20 (Figure 4.1p–r) offered bigger diameter fibers (Figure 4.2e), although it was challenging to produce.

The increased fiber diameter of the electrospun fibrous scaffold was made possible by the higher molecular weight of PLA. In comparison to electrospun PLAL and PLAH fibers, PLAmed6 (Figure 4.1s-u) produced the biggest fibers with the largest average diameter (Figure 4.2f). When the surface tension of the charged jet is sufficient to convert it into droplets and reduce surface area, beads develop in electrospun fibers (Williams, Raimi-Abraham, & Luo, 2018). Viscoelastic forces in the jet that oppose changes to the fiber shape work against this. Contrarily, as a result of the solution's increased viscosity, stronger viscoelastic forces were generated, resisting the axial stretching that occurred during whipping and leading to a bigger fiber diameter. This was supported by the fact that PLA fiber diameter increased as PLA concentration increased.
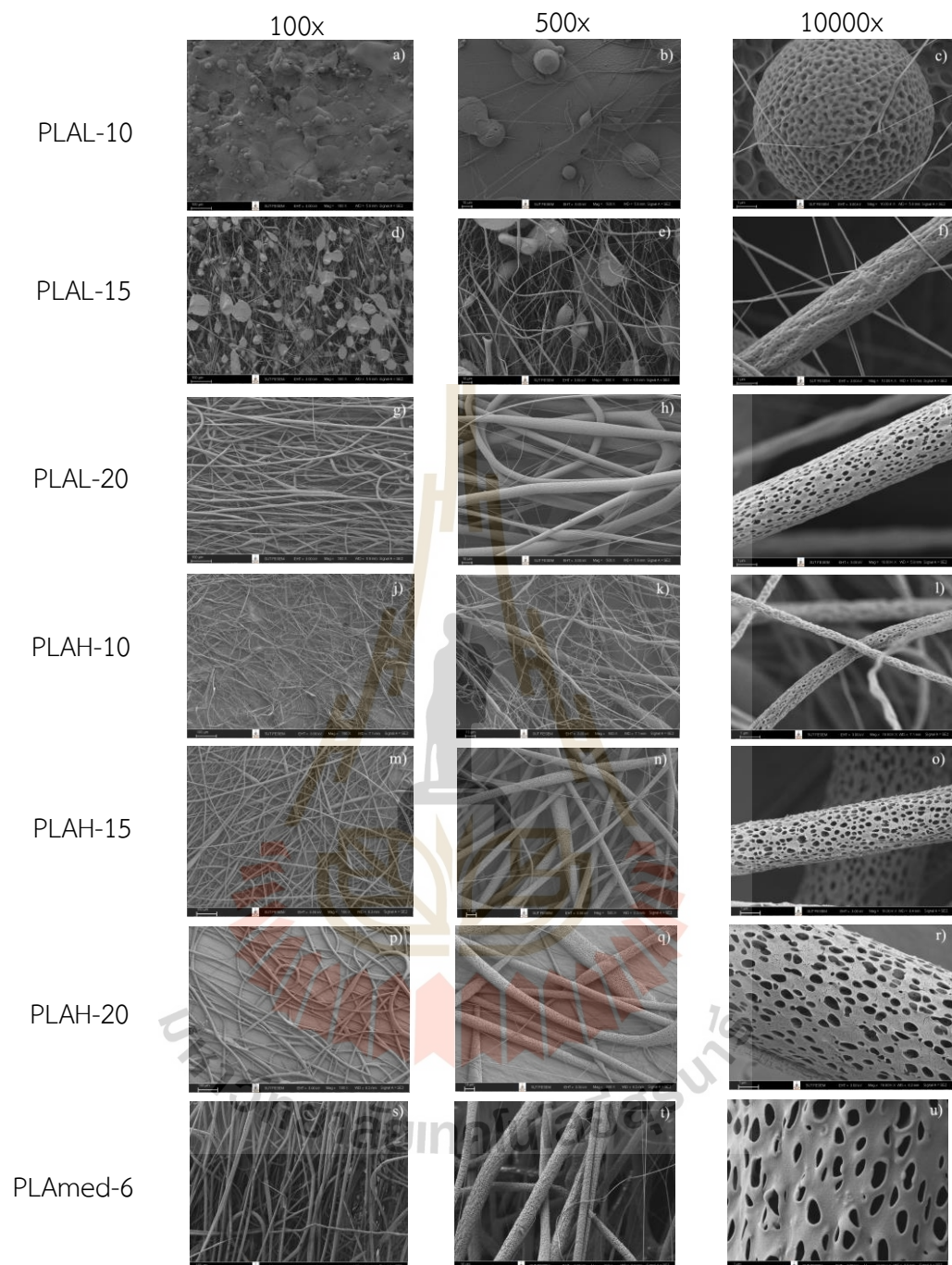
Figure 4.1. Scanning electron micrographs of pure PLAL, PLAH, and PLAmed fibers which was prepared by using various concentrations; (a–c) PLAL–10;(d–f) PLAL–15; (g–i) PLAL–20; (j–l) PLAH–10; (m–o) PLAH–15; (p–r) PLAH–20; and (s–u) PLAmed–6 at different magnifications (100×, 500×, and 10000×).
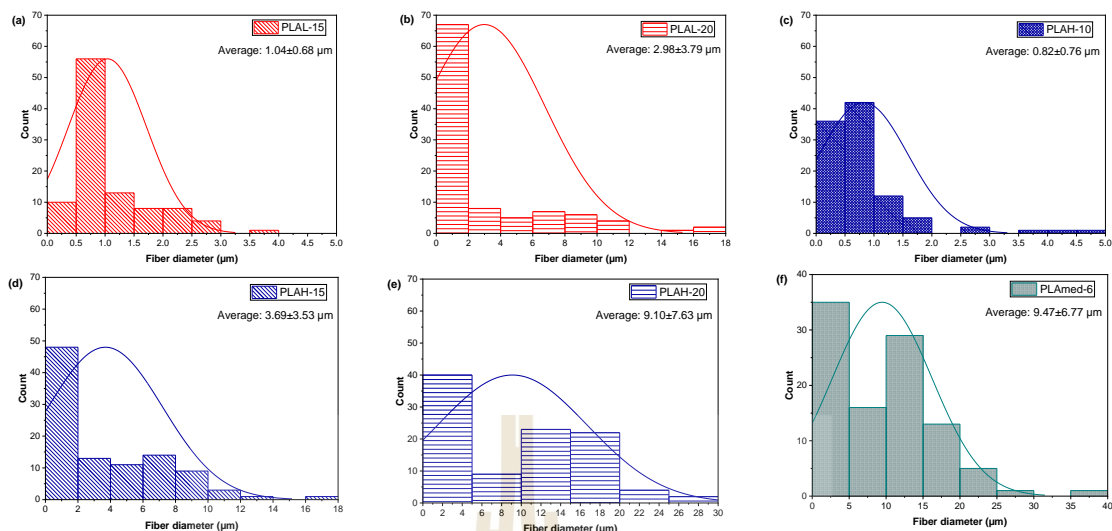
Figure 4.2 Diameter distribution curves of electrospun fibers (a) PLAL–15; (b) PLAL–20; (c) PLAH–10; (d) PLAH–15; (e) PLAH–20; and (f) PLAmed–6.

However, PLAH-20 solution viscosity was very high, making it difficult to spin and readily clogging the needle. When compared to the restricted distribution of fiber diameter in PLA/SF scaffolds, pure PLA scaffolds (both PLAH and PLAmed) showed a large variety of fiber diameter. Due to solvent evaporation, PLA fibers have tiny holes scattered throughout them at random (Promnil, Numpaisal, & Ruksakulpiwat, 2021). Additionally, due to complexity during jet ejection, the PLAmed-6 offers the largest fiber diameter (Mehta & Pawar, 2018).

4.1.3 Mechanical properties of electrospun PLA scaffold

Effect of molecular weight of PLA on mechanical properties of electrospun PLA nanofiber sheets was shown in Table 4.3. PLA with higher molecular weight exhibited higher %elongation at break due to higher chain entanglement. Young's modulus was reduced with increasing molecular weight of PLA. The tensile strength was not significantly increased.

Table 4.2 PLA scaffold mechanical properties

Samples	Ultimate tensile strength (MPa)	Elongation at break (%)	Young's modulus (MPa)
PLAH-10	1.18±0.12	17.8±1.93	52.25±6.77
PLAH-15	1.14±0.09	10.19±1.20	70.21±4.99
PLAH-20	2.08±0.10	25.87±6.47	113.95±5.80
PLAL-15	0.99±0.17	2.21±0.14	80.45±11.70
PLAL-20	2.21±0.37	17.47±2.03	107.54±16.54

Due to thicker fiber with increasing PLA percentage, PLA with greater solution concentration displayed better tensile strength and Young's modulus. The thicker fibers are produced by the polymer solution at increasing concentrations. The explanation is that when the concentration of the polymer solution rises, the viscosity of the polymer also raises. The increased viscosity of the polymer prevents the stretching of the fibers (Riley, 2012).

4.2 Effect of the SF content on the physical properties and mechanical properties of electrospun PLA scaffolds.

4.2.1 Characteristic of electrospun PLA/SF scaffolds

Fourier transform infrared spectroscopy spectra in Figure 4.3 displayed the characteristic absorption peaks of SF powder that emerged at 1626 cm^{-1} (C=O. stretching vibration of Amide I), 1512 cm^{-1} (in-plane N-H bending of Amide II), and 1228 cm^{-1} (C-N stretching vibration of Amide III). Electrospun PLA scaffold exhibited important absorption peaks at 1752 cm^{-1} (carbonyl stretching vibration), 1452 cm^{-1} (carbon hydrogen bond deformation vibration), 1368 cm^{-1}, 1261 cm^{-1} (carbonyl antisymmetric stretching vibration), 1184 cm^{-1} (carbonyl stretching vibration), 1084

cm^{-1} (carbon-oxygen bond antisymmetric stretching vibration), 868 cm^{-1}, 755 cm^{-1}, and 694 cm^{-1} (carbon-hydrogen bond bending vibration). In PLA/SF scaffolds (both PLAH and PLAmed), identical typical peaks for SF and PLA were seen, confirming the presence of SF.
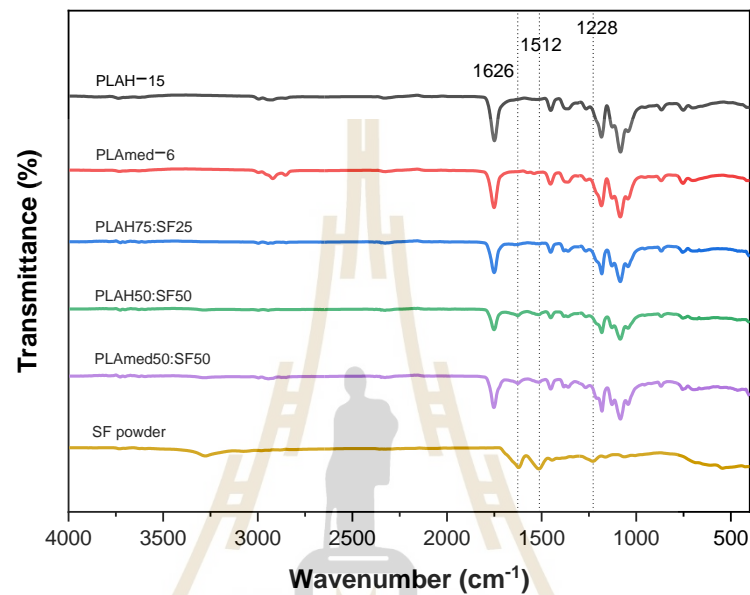
Figure 4.3 Fourier transform infrared spectroscopy spectra of SF powder, PLAH –15, PLAH75:SF25, PLAH50:SF50, PLAmed–6, and PLAmed50:SF50 fibers.

The primary bands in the SF protein structure generated by amide I (1626 cm^{-1}) and amide II (1512 cm^{-1}) could be recognized with the typical peaks (denoted by hashed lines), SF on the scaffold surfaces, demonstrating. (He, Qin, Cui, Gao, & Wang, 2011; Taddei et al., 2017; Fang Wang et al., 2020).

4.2.2 Morphology of electrospun PLA/SF scaffolds

The impact of SF content on PLA/SF electrospun fiber shape is depicted in Figure 4.4. Figure 4.4a-b depicts beads on the fiber surface of an electrospun PLA75:SF25 sample, with an average fiber diameter of 0.29±0.20 m. (Figure 4.5a).

	100x	500x	10000x

PLAH75:SF25

PLAH50:SF50

PLAH25:SF75
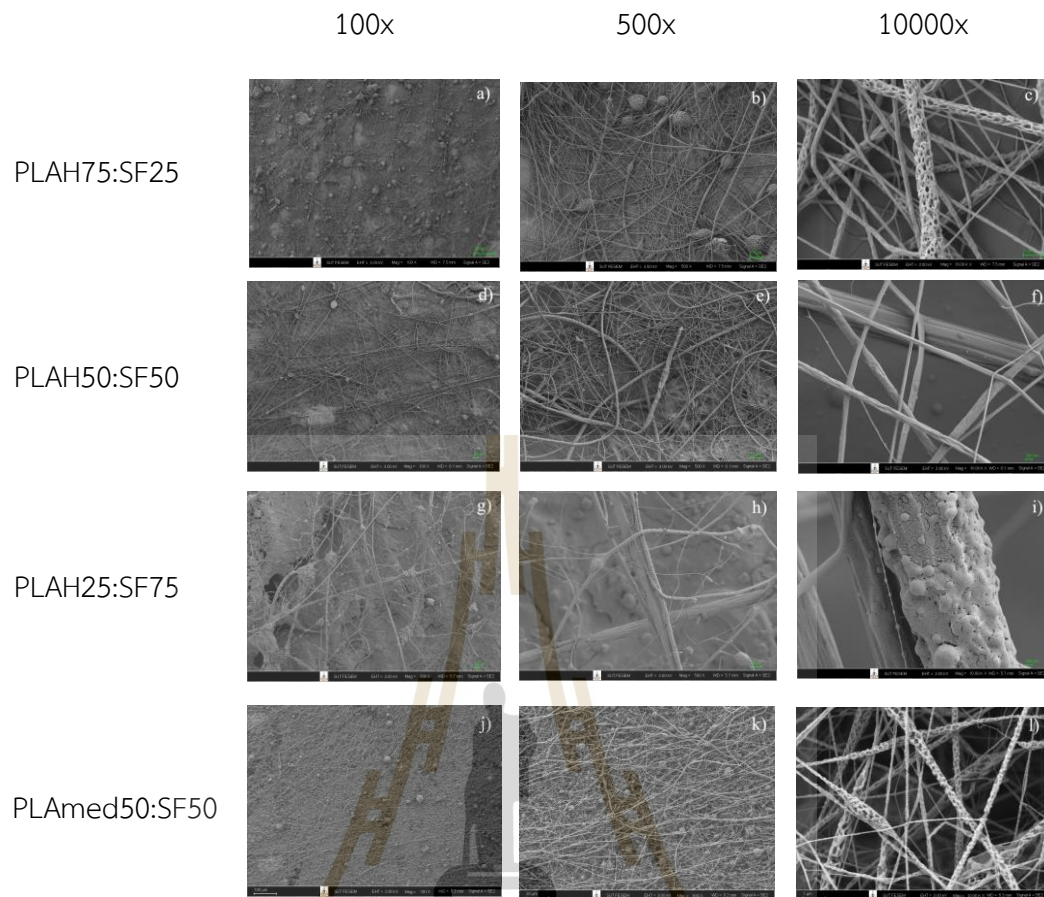
PLAmed50:SF50

Figure 4.4 Scanning electron micrographs of (a–c) PLAH75:SF25; (d–f) PLAH50:SF50; (g-i) PLAH50:SF50; and (j–l) PLAmed50:SF50 fibers at different magnifications (100×, 500×, and 10000×).

In a sample of PLA50: SF50 (Figure 4.4d–f), the average fiber diameter was 0.32 ± 0.26 μm (Figure 4.5b), and the surface of the fiber was smoother. Compared to other samples, the PLA25:SF75 sample (Figure 4.4g–i) had less fiber on the rotating collector. It was challenging to process when it broke up into electrospray at this ratio. The fibers had an average diameter of 2.19 ± 1.71 μm (Figure 4.5c). The fiber diameter increased as SF content increased. In comparison to pure PLA fiber, the fiber diameter reduced after the addition of SF (Figure 4.1). It was decided to compare PLAH50:SF50 with PLAmed50:SF50. For PLAmed50:SF50, the tiny beads and fine porous fiber were

visible on the scaffold (Figure 4.4j–l). The fiber diameter was 0.18 ± 0.08 µm (Figure 4.5d), which was smaller than that of PLAH50:SF50 fibers.

While the emulsion solution was flowing, the addition of SF to PLA caused a gradient in the solution's viscosity and surface tension. The average diameter of the PLA/SF fibers was comparatively smaller because they were pulled with more force (Roy et al., 2018). The PLAH/SF fiber diameters in the two distinct ratios (PLAH75: SF25 and PLAH50: SF50) did not clearly differ from one another. Very thin fibers with beads and holes were created together with nanofiber for the PLAmed50: SF50 sample.
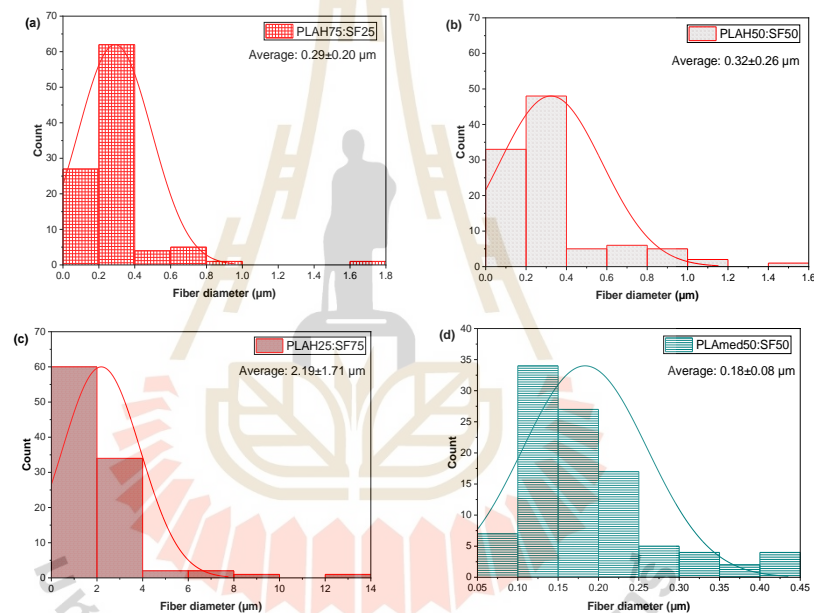
Figure 4.5. Diameter distribution curves of electrospun fibers (a) PLAH75:SF25, (b)PLAH50:SF50; (c) PLAH25:SF75 and (d) PLAmed50:SF50.

4.2.3 Mechanical properties of electrospun PLA/SF scaffolds

The tensile characteristics of PLAH-15, PLAH75: SF25, PLAH50: SF50, PLAmed-6, and PLAmed50: SF50 are displayed in Table 4.4. The PLAH-15 scaffolds outperformed the PLAH75: SF25 and PLAH50: SF50 scaffolds in terms of tensile strength and modulus. In comparison to pure PLAH15, the tensile strength of the

PLAH75: SF25 scaffold reduced with the addition of SF, from 1.14±0.09 MPa to 0.47 ±0.07 MPa, but the elongation at break rose from 15.97±1.80 percent to 26.22±10.64 percent. Compared to PLAH75:SF25, PLAH50:SF50 has a better tensile strength but a lower elongation at break.

Table 4.3 PLA based scaffold mechanical properties

Samples	Ultimate tensile strength (MPa)	Elongation at break (%)	Young's modulus (MPa)
PLAH–15	1.14 ± 0.09	15.97 ± 1.80	70.21 ± 4.99
PLAH75:SF25	0.47 ± 0.07	26.22 ± 10.64	20.51 ± 3.97
PLAH50:SF50	1.05 ± 0.43	17.51 ± 3.89	16.49 ± 8.71
PLAmed–6	2.06 ± 0.28	14.34 ± 1.00	109.38 ± 12.21
PLAmed50:SF50	0.85 ± 0.11	12.14 ± 2.20	22.59 ± 6.59

For meniscus tissue engineering applications, electrospun scaffolds' mechanical characteristics and structural stability were crucial factors. Numerous crucial biomechanical tasks are carried out by the meniscus, including load transfer, shock absorption, stability, and joint congruency (Fox et al., 2012). The tension resistance of electrospun scaffolds, which preserves the scaffold's integrity after transplantation, is a sign of mechanical strength (Thanh Tam, Abdul Hamid, & Cheong, 2018). The shape of electrospun fibers is associated with the mechanical characteristics of the scaffold (Tertyshnaya, Karpova, Moskovskiy, & Dorokhov, 2021). The addition of the SF solution to the electrospinning solution clearly enhanced the elongation at break of the PLAH/SF scaffold. Modulus and tensile strength were somewhat decreased as a result of adding SF content (Promnil et al., 2022). Electrospun fibrous scaffolds' mechanical characteristics are correlated with fiber connectivity and density (Wu & Hong, 2016). Because of the beads and tiny porous fibers, PLAmed/SF scaffolds have inferior mechanical characteristics than pure PLAmed scaffolds in terms of tensile

strength and modulus. Pure PLLA, which has a high molecular weight, can be used in medical applications as a load-bearing material (Maharana, Mohanty, & Negi, 2009).

In addition, varieties with low D-lactide content have higher crystallization capacity (Pölöskei, Csézi, Hajba, & Tábi, 2020). D-lactide causes a twist in the normal poly (L-lactide) molecular structure. Both the rate and the extent of poly (L-lactide) crystallization are affected by molecular defects (Auras, Harte, & Selke, 2004). Larger or more organized PLA crystals that can withstand greater tensile strengths are often linked to increased crystallinity (Oksiuta, Jalbrzykowski, Mystkowska, Romanczuk, & Osiecki, 2020).

Elastic modulus (3.77±2.81 to 16.90±9.70 MPa), tensile strength (0.60±0.43 to 3.40±1.10 MPa), and percent elongation (3.28±1.49 to 20.09±5.89) were reported as the mechanical parameters of scaffold augmented suture(Rothrauff et al., 2016; Shimomura, Bean, Lin, Nakamura, & Tuan, 2015; S. Yan et al., 2016). This study determined the Young's modulus, percent elongation, and tensile strength of scaffolds made of PLA and PLA/SF. This research measurement of the scaffold's percent elongation at break can be utilized to demonstrate that the scaffold won't be cut through during repair (Shimomura et al., 2015). By seeding cells on the scaffold's integrated suture, we may use our scaffold to facilitate tissue repair. It was demonstrated that the cell-seeded scaffold may speed up tissue recovery and close gaps around repair sites.

4.2.4 Thermal properties of electrospun PLA/SF scaffolds

Figure 4.6 demonstrates the effects of the PLA/SF scaffold's SF content on thermal decomposition.

SF contained about 10% water content by weight, while PLA had a very low water content. The sample's water content considerably increased with the addition of SF. Due of the limited thermal stability of SF, the decomposition temperature of PLA with SF added was changed to a lower temperature. Upon initial heating from room temperature to 250 ° C, evaporation of water or solvent molecules resulted in the loss of mass of all samples. In the presence of SF, the water content

increased significantly. This is due to the excellent hydrophilicity and hygroscopicity of silk fibroin (F. Wang, Li, Gough, Liu, & Hu, 2021)
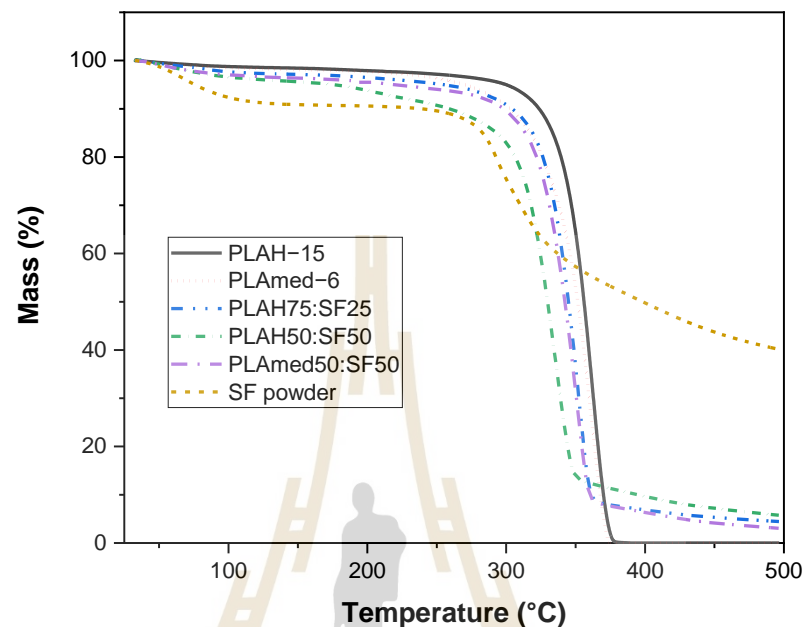
Figure 4.6 Thermogravimetric analysis thermograms of SF, PLAH–15, PLAH75:SF25, PLA50:SF50, PLAmed–6, and PLAmed50:SF50.

       Figure 4.7 shows DSC thermograms of electrospun scaffolds during the first heating scan (Figure 4.7a), cooling scan (Figure 4.7b), and second-heating scan (Figure 4.7c). In Tables 4.5 and 4.6, thermal characteristics derived from Figure 4.7 are displayed. based on the first-heating scan, which showed the electrospun scaffold thermal characteristics acquired after the electrospinning process. In comparison to the PLAH–15 scaffold, the PLAmed–6 scaffold showed a greater glass transition, a lower cold crystallization temperature, and a higher melting temperature. The change to a higher cold crystallization temperature and a somewhat higher melting temperature in the PLAH75:SF25 and PLAH50:SF50 scaffold was seen with the addition of SF to PLA solution. As opposed to pure PLAmed scaffold, PLAmed50:SF50 demonstrated a reduced cold crystallization temperature. However, a second heating scan revealed

no obvious variations in the glass transition temperature, cold crystallization temperature, or melting temperature among PLAH15, PLAH75:SF25, and PLAH50:SF50 after the thermal history had been deleted and the samples had been cooled.

It is interesting to highlight the difference in crystallization behavior between medical PLA and commercial PLA during cooldown scans. PLAmed-6 and PLAmed50: SF50 showed clear melt crystallization peaks during cooling. In contrast, PLAH with and without SF did not show a melt crystallization peak. The crystallinity of medical grade PLA was higher than that of commercial grade PLA in both the first heat scan and the second heat scan. This indicates that it has a higher ability to crystallize medical grade PLA than commercial grade PLA.

Because the amorphous phase structure in the silk fibroin progressively rises with an increase in SF, the percent crystallinity of the electrospun fibrous PLA/SF scaffolds decreased with an increase in SF (Holjevac Grgurić et al., 2021; Taddei et al., 2017; F. Wang et al., 2021). In comparison to the PLAH scaffold, the electrospun PLAmed scaffold had higher T_m and a higher percentage of crystallinity. Both the PLAmed and PLAmed/SF scaffolds showed a cold crystallization peak after cooling, proving that both specimens reached a semi-crystalline state (Yu, Wang, Ferraris, & Zhang, 2019). This might be as a result of the higher L-lactide content of medical grade PLA. The α crystalline form of PLAmed is optically pure PLLA, with a melting point range of around 170-180 °C (Burg, 2014; Torino et al., 2016). A greater T_m suggested a lower D-Lactide content (Pölöskei et al., 2020). The purity of the PLA, the kinetics of crystallization, and the melting behavior of the PLA all affect the T_m and degree of crystallinity (Farah, Anderson, & Langer, 2016).
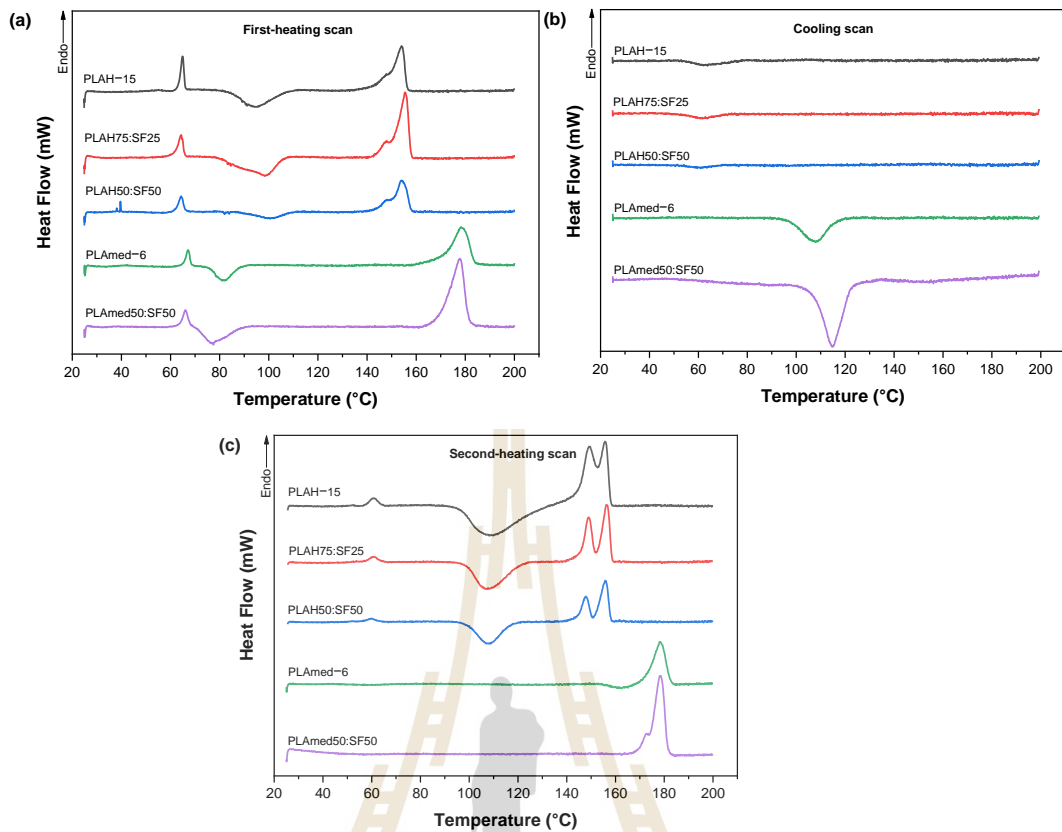
Figure 4.7 Differential scanning calorimetry thermograms of (a) first-heating scan, (b) cooling scan, and (c) second-heating scan of PLAH–15, PLAH75:SF25, PLAH50:SF50, PLAmed–6, and PLAmed50:SF50 scaffolds

Table 4.4 Scaffold thermal properties during during first-heating and cooling scan.

Samples	First-Heating Scan							Cooling Scan		
	T_g (°C)	T_{cc} (°C)	ΔH_{cc} (Jg^{-1})	T_{m_1} (°C)	T_{m_2} (°C)	ΔH_m (Jg^{-1})	χ_c (%)	T_g (°C)	T_c (°C)	ΔH_c (Jg^{-1})
PLAH−15	64.90	94.22	14.81	148.05	154.07	20.53	21.94	63.68	-	-
PLAH75:SF25	64.38	98.44	13.35	147.81	155.49	25.86	21.83	62.66	-	-
PLAH50:SF50	64.32	100.55	9.09	148.12	154.19	21.41	12.81	61.55	-	-
PLAmed−6	67.19	82.01	12.00	-	178.61	42.61	45.52	-	107.91	19.01
PLAmed50:SF50	66.03	77.42	8.56	-	177.82	42.71	25.55	-	114.84	30.52

Table 4.5 Scaffold thermal properties during second-heating scan.

Samples	Second-Heating Scan						
	T_g (°C)	T_{cc} (°C)	ΔH_{cc} (Jg^{-1})	T_{m_1} (°C)	T_{m_2} (°C)	ΔH_m (Jg^{-1})	χ_c (%)
PLAH–15%	59.28	108.78	14.48	149.42	155.76	21.53	23.00
PLAH75:SF25	58.55	107.67	24.21	149.03	156.40	25.71	21.70
PLAH50:SF50	57.41	107.79	21.58	147.85	155.92	23.71	14.19
PLAmed–6%	67.57	-	-	-	178.33	39.97	42.71
PLAmed50:SF50	63.94	-	-	172.50	178.41	41.04	24.56

4.2.5 In vitro degradation behavior of electrospun PLA/SF scaffolds

Figure 4.8 showed how SF content affected the degradation of the PLA/SF scaffold. By time, degradation profiles were displayed as a percentage of the scaffolds' remaining weight. Both the pure PLA and PLA/SF scaffolds degraded gradually throughout the investigation. While the weight of the PLAH50:SF50 and PLAmed50:SF50 scaffolds declined over time, PLAH, PLAH75:SF25, and PLAmed showed very little degradation.
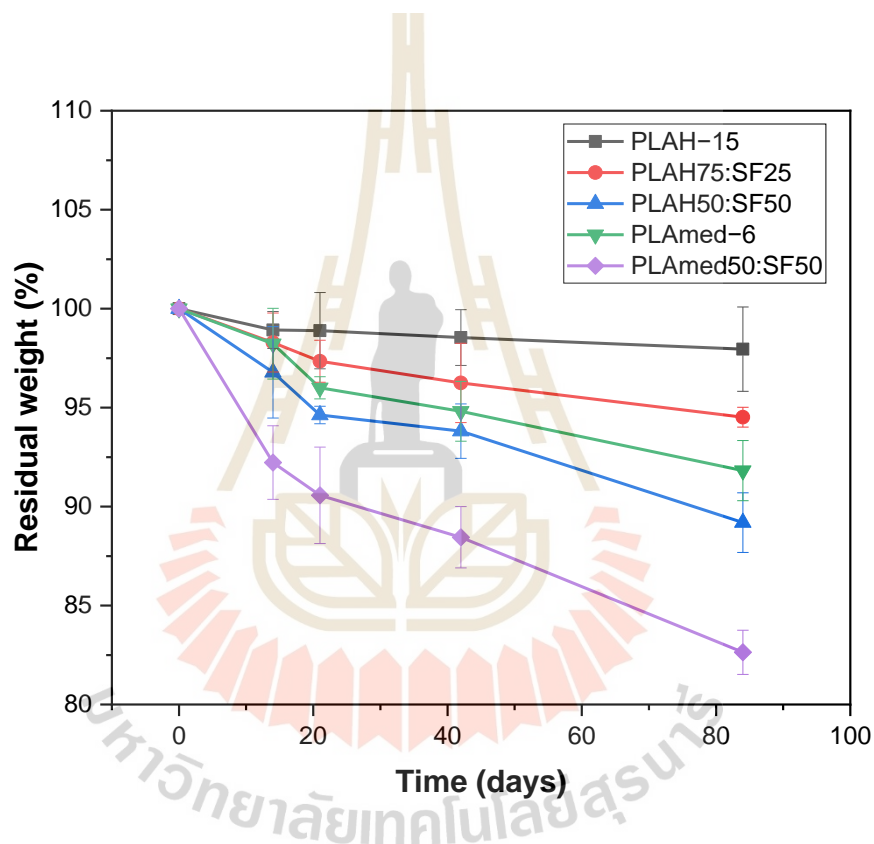
Figure 4.8 In vitro degradation behavior of electrospun scaffolds after immersing in phosphate buffered saline (PBS, pH = 7.4) as a function of time.

Biodegradability is another important aspect of the scaffold. Scaffolds must be degraded at the desirable time to ensure proper tissue remodeling or regeneration [60]. Figure 8 shows the effect of SF content on the degradation of the PLA / SF scaffold. All scaffolds displayed very low degradation. The weight loss

obtained can be observed to be a function of the amount of silk fibroin present in the electrospun fibers (S. Wang, Zhang, Wang, Yin, & Dong, 2009). PLA consists of crystalline and amorphous regions. The long polymer chain segments are more regularly arranged and packed more strongly in the crystalline phase than in the amorphous phase. Small water molecules can more easily attack polymer chains in the amorphous phase (Leonés, Peponi, Lieblich, Benavente, & Fiori, 2020). Adding SF can increase the amorphous region and increase the degradation of the scaffold. Silk fibroin degradation involves both hydrophilic interaction and specific nanostructures. During the degradation process, the hydrophilic block was first degraded (Lu et al., 2011). It was shown that the degradation of the PLA / SF scaffold prepared in this study can be controlled by adjusting the PLA / SF ratio (W. Liu et al., 2016a).

4.2.6 Surface wettability of electrospun PLA/SF scaffolds

Figure 4.9 indicated that the water contact angle of the scaffolds as determined by the droplet photographs.
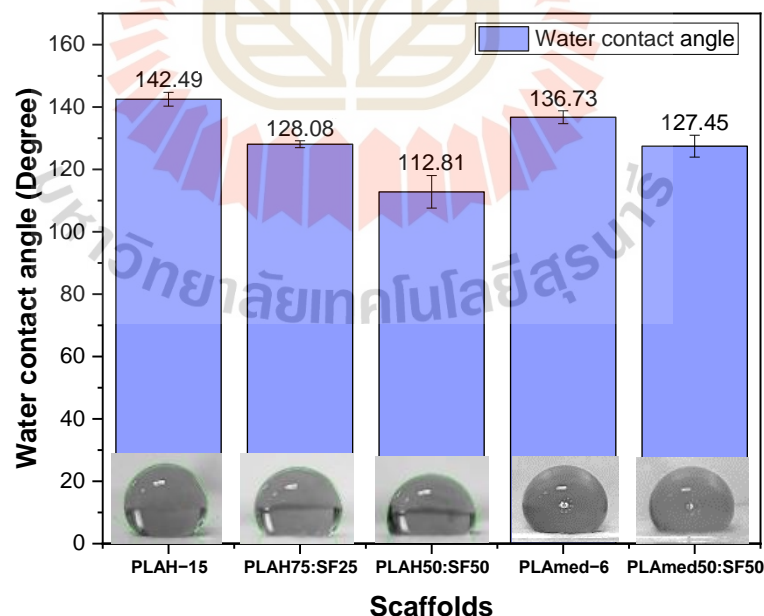
Figure 4.9 Water contact angle of PLAH−15, PLAH75:SF25, PLAH50:SF50, PLAmed−6, and PLAmed50:SF50 scaffolds.

The contact angles for electrospun pure PLAH and PLAmed scaffolds were highly hydrophobic, with a contact angle of 142.49 ± 2.22° and 136.73 ± 2.09°, respectively. Electrospun PLAH:SF and PLAmed:SF scaffolds demonstrated a slight decrease to 128.08 ± 1.10° (PLAH75:SF25), 112.81 ± 5.22° (PLAH50:SF50), and 127.45 ± 3.49° (PLAmed50:SF50). The hydrophilic properties of the PLA/SF scaffolds increased with the addition of SF.

Biomaterials surface wettability has a significant impact on how cells adhere, proliferate, and migrate (Gui-Bo et al., 2010). The water contact angle was evaluated to clarify the impact of SF and its concentration on the surface wettability of electrospun scaffolds. Results for water contact angles (Figure 4.9) revealed that adding SF to PLA scaffolds lowered their hydrophobicity compared to pure PLA scaffolds. The backbone of SF contains naturally hydrophilic amino groups, carboxylic groups, and other functional groups, which may account for the condition (L. Li et al., 2011; Roy et al., 2018).

4.2.7 In vitro cell viability of electrospun PLA/SF scaffolds

The viability of human chondrocyte cells on PLA and PLA/SF electrospun scaffolds was assessed using the MTT technique. Figure 4.10 displays the influence of ethanol treatment (+) on cell viability rather than the PLA/SF ratio and PLA.

In general, ethanol-treated scaffold groups (+) had better HCPC viability than untreated groups. Except for PLA50:SF50, which had better vitality relative to the control group at days 3 and 7, the cell viability in untreated scaffold groups was lower than the control group at every time point. When compared to medical grade PLA scaffolds, PLAH+ scaffolds in the alcohol-treated group (+) showed poorer cell survival. Among the PLAH+ groups, cell vitality varied somewhat at days 1 and 3, and at day 7, PLAH15+ had greater cell viability than PLAH50:SF50+ and PLAH75:SF25+, respectively. At every time point, PLAmed6+ demonstrated slightly greater cell viability than PLAmed50:SF50+.

The outcomes showed that biodegradability and cellular induction were provided by medical grade PLA electrospun scaffolds for the regeneration of meniscus tissue. After seeding HCPCs which possess chondrogenic potential on the PLA and PLA/SF scaffolds, initial cell viability and the viability at days 3 and 7 were evaluated.
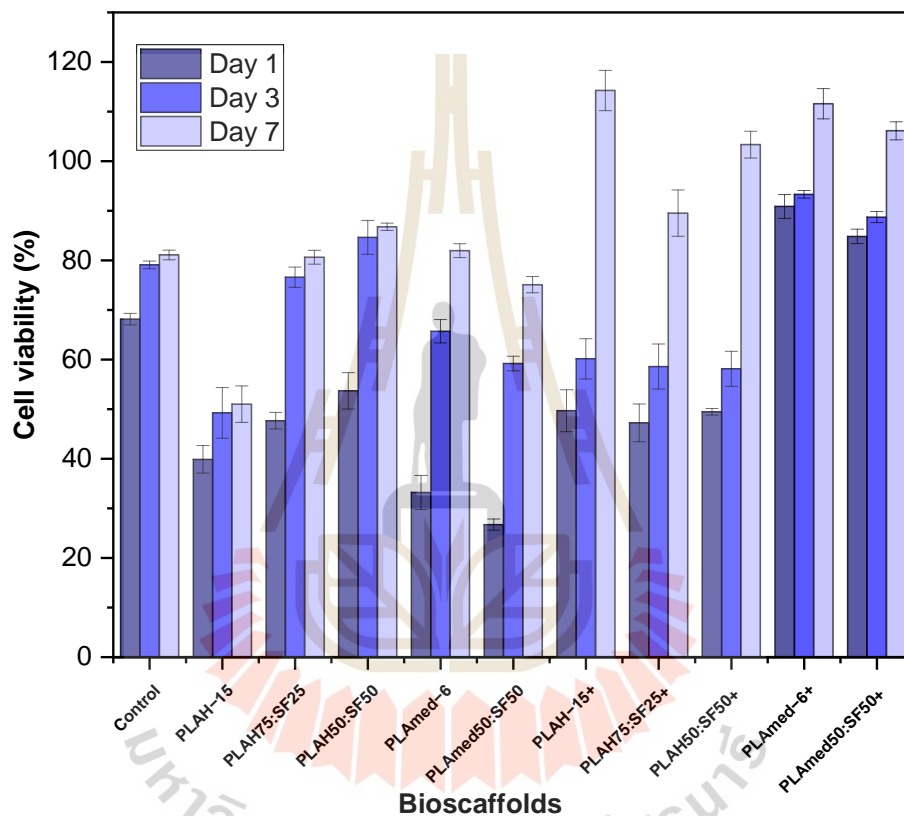
Figure 4.10 Comparison of human chondrocyte cell viability (%) on electrospun scaffolds after 1, 3, and 7 days. The plus sign (+) demonstrated ethanol treated scaffolds.

Even though the cell viability of PLA/SF scaffolds with higher SF contents was higher than that of the control group, it was still lower. Medical grade PLA scaffolds had higher cell viability; however, ethanol treatment was required to reduce SF toxicity during fabrication (Gholipourmalekabadi, Mozafari, Bandehpour,

Sameni, & Ghanbarian, 2015). In the PLA/SF composite scaffold, cell viability was lower when compared to PLAmed6 and PLAmed50:SF50.

4.2.8 Quantitative gene expression of electrospun PLA/SF scaffolds

The gene expression analyses of human chondrocyte cell seeded scaffolds were observed to demonstrate cellular phenotype. Three triplicate sample sets were used for each group of scaffolds. The results are shown in Figure 4.11. COL1A1 expression from PLAmed-6 and PLAmed50: SF50 was greater than that of cells without scaffold at all time points. COL1A1 expression from PLAmed-6 was significantly higher on day 7 than PLAmed50: SF50 and slightly higher on day 28. On the contrary, PLAmed-6 and PLAmed50: SF50 showed equivalent COL2A1 expression on days 7 and 28 than in the control group. The highest expression of COL2A1 was observed on day 14.
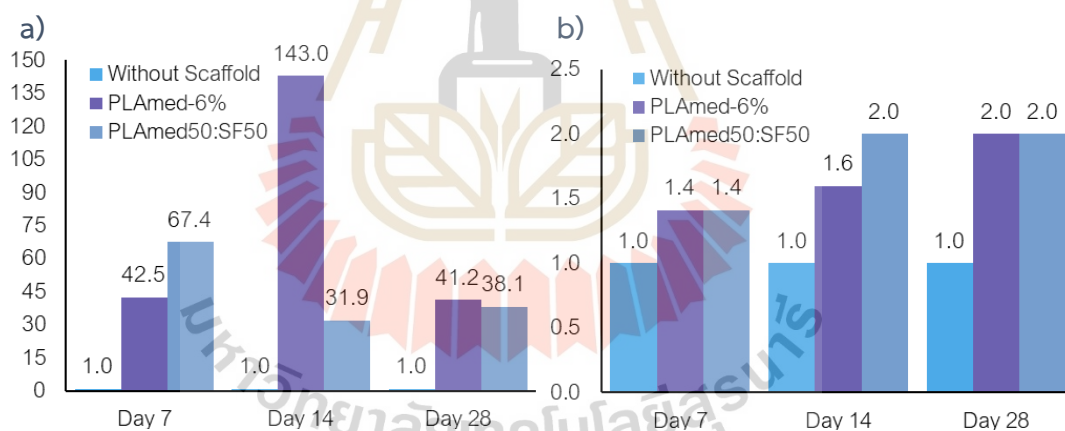
Figure 4.11 The gene expression of COL1A1 (a) and COL2A1 (b) at days 7, 14, and 28.

Cells in PLAmed-6 scaffolds were more fibrogenic, whereas cells in PLAmed50:SF5 scaffolds were more chondrogenic, according to these presentations. Because the cell seeded scaffolds were cultured in plain expanded medium without growth factors or localized mechanical stimulation, the cells' chondrogenic phenotype might diminish over time (Numpaisal, Jiang, Hsieh, Chiang, & Chien, 2022).

CHAPTER 5
CONCLUSION AND RECOMMENDATION

5.1   Conclusion

Higher PLA concentrations resulted in higher mechanical properties in this study. The thicker the fibers formed, the higher the concentration. PLAH-15 produced randomly oriented uniform fibers. Furthermore, electrospinning is used to favorably manufacture PLA / SF nanofiber scaffolds. This study discovered that viscosity is important in determining fiber formability, morphology, and size. With increasing solution viscosity, the average fiber diameter enlarged. PLA concentration, structure, and molecular weight were significant parameters that influenced polymer solution viscosity. For meniscus tissue regeneration, the PLAmed-6 scaffold demonstrated excellent mechanical properties, degradability, and cell viability. However, due to its toxicity, the non-medical PLA used in this study was not recommended for medical use.

SF dominated nanofiber morphology, diameter distribution, mechanical properties, decomposition temperature, crystallinity, biodegradability, surface wettability, and cell viability have all been added. Based on mechanical properties, cell viability, gene expression, surface wettability, and in vitro degradation, PLAmed50: SF50 scaffold could be used as a biomimetic meniscus scaffold for scaffold enhanced sutures.

5.2   Recommendation

5.2.1 Use other solvents or mixing solvents for dissolving PLA pellet to get different fiber surface morphology.

5.2.2 Determine the scaffold weight after the electrospinning process to check the material content.

5.2.3 Check the stability of the PLA/SF emulsion before fabrication by leaving it for 5 minutes after stirring.

5.2.4 Determine the PLA/SF emulsion viscosity.

5.2.5 Determine the surface chemistries of PLA/SF scaffold.
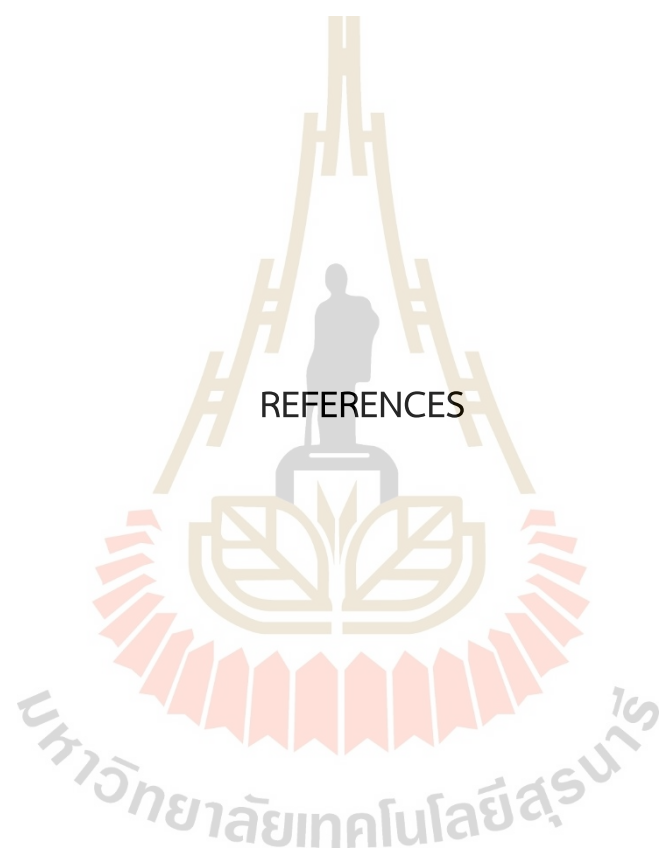
REFERENCES

REFERENCES

Ahmed, M., Ramos, T. A. d. S., Damanik, F., Quang Le, B., Wieringa, P., Bennink, M., Moroni, L. (2015). A combinatorial approach towards the design of nanofibrous scaffolds for chondrogenesis. *Scientific reports, 5*(1), 14804. doi:10.1038/srep14804

Arai, T., Freddi, G., Innocenti, R., & Tsukada, M. (2004). Biodegradation of Bombyx mori silk fibroin fibers and films. *Journal of Applied Polymer Science, 91*(4), 2383-2390. doi:https://doi.org/10.1002/app.13393

Asadian, M., Chan, K. V., Norouzi, M., Grande, S., Cools, P., Morent, R., & De Geyter, N. (2020). Fabrication and Plasma Modification of Nanofibrous Tissue Engineering Scaffolds. *Nanomaterials, 10*(1). doi:10.3390/nano10010119

Auras, R., Harte, B., & Selke, S. (2004). An overview of polylactides as packaging materials. *Macromol Biosci, 4*(9), 835-864. doi:10.1002/mabi.200400043

Baek, J., Chen, X., Sovani, S., Jin, S., Grogan, S. P., & D'Lima, D. D. (2015). Meniscus tissue engineering using a novel combination of electrospun scaffolds and human meniscus cells embedded within an extracellular matrix hydrogel. *J Orthop Res, 33*(4), 572-583. doi:10.1002/jor.22802

BAYDEMİR, T. (2009). *INVESTIGATIONS ON THE PROPERTIES AND DRUG RELEASES OF BIODEGRADABLE POLYMER COATINGS ON METAL SUBSTRATES AS DRUG CARRIERS.* (Doctor of Philosophy). Middle East Technical University, Turkey.

Bryceland, J. K., Powell, A. J., & Nunn, T. (2017). Knee Menisci. *Cartilage, 8*(2), 99-104. doi:10.1177/1947603516654945

Buma, P., Ramrattan, N. N., van Tienen, T. G., & Veth, R. P. H. (2004). Tissue engineering of the meniscus. *Biomaterials, 25*(9), 1523-1532. doi:https://doi.org/10.1016/S0142-9612(03)00499-X

Burg, K. (2014). Chapter 6 - Poly(α-ester)s. In S. G. Kumbar, C. T. Laurencin, & M. Deng (Eds.), *Natural and Synthetic Biomedical Polymers* (pp. 115-121). Oxford: Elsevier.

Casalini, T., Rossi, F., Castrovinci, A., & Perale, G. (2019). A Perspective on Polylactic Acid-Based Polymers Use for Nanoparticles Synthesis and Applications. *Frontiers in Bioengineering and Biotechnology, 7*. doi:10.3389/fbioe.2019.00259

Chan, B. P., & Leong, K. W. (2008). Scaffolding in tissue engineering: general approaches and tissue-specific considerations. *Eur Spine J, 17 Suppl 4* (Suppl 4), 467-479. doi:10.1007/s00586-008-0745-3

Chen, K., Chou, W., Liu, L., Cui, Y., Xue, P., & Jia, M. (2019). Electrochemical Sensors Fabricated by Electrospinning Technology: An Overview. *Sensors, 19*(17). doi:10.3390/s19173676

Coluccino, L., Gottardi, R., Ayadi, F., Athanassiou, A., Tuan, R. S., & Ceseracciu, L. (2018). Porous Poly(vinyl alcohol)-Based Hydrogel for Knee Meniscus Functional Repair. *ACS Biomaterials Science & Engineering, 4*(5), 1518-1527. doi:10.1021/acsbiomaterials.7b00879

Dang, M., Saunders, L., Niu, X., Fan, Y., & Ma, P. (2018). Biomimetic delivery of signals for bone tissue engineering. *Bone Research, 6*, 25. doi:10.1038/s41413-018-0025-8

de Caro, F., Perdisa, F., Dhollander, A., Verdonk, R., & Verdonk, P. (2020). Meniscus Scaffolds for Partial Meniscus Defects. *Clin Sports Med, 39*(1), 83-92. doi:10.1016/j.csm.2019.08.011

DeBari, M. K., King, C. I., Altgold, T. A., & Abbott, R. D. (2021). Silk Fibroin as a Green Material. *ACS Biomaterials Science & Engineering, 7*(8), 3530-3544. doi:10.1021/acsbiomaterials.1c00493

Dou, H., & Zuo, B. (2015). Effect of sodium carbonate concentrations on the degumming and regeneration process of silk fibroin. *J. Text. Inst., 106*(3), 311.

Englund, M., Guermazi, A., & Lohmander, S. (2009). The Role of the Meniscus in Knee Osteoarthritis: a Cause or Consequence? *Radiologic clinics of North America, 47*, 703-712. doi:10.1016/j.rcl.2009.03.003

Farah, S., Anderson, D. G., & Langer, R. (2016). Physical and mechanical properties of PLA, and their functions in widespread applications — A comprehensive

review. *Advanced drug delivery reviews, 107*, 367-392.
doi:https://doi.org/10.1016/j.addr.2016.06.012

Fox, A. J. S., Bedi, A., & Rodeo, S. A. (2012). The basic science of human knee menisci: structure, composition, and function. *Sports health, 4*(4), 340-351. doi:10.1177/1941738111429419

Friné, V.-C., Hector, A.-P., Manuel, N.-D. S., Estrella, N.-D., & Antonio, G. J. (2019). Development and Characterization of a Biodegradable PLA Food Packaging Hold Monoterpene-Cyclodextrin Complexes against Alternaria alternata. *Polymers, 11*(10), 1720. doi:10.3390/polym11101720

Gao, Y., Shao, W., Qian, W., He, J., Zhou, Y., Qi, K., . . . Wang, R. (2018). Biomineralized poly (l-lactic-co-glycolic acid)-tussah silk fibroin nanofiber fabric with hierarchical architecture as a scaffold for bone tissue engineering. *Materials Science and Engineering: C, 84*, 195-207. doi:https://doi.org/10.1016/j.msec.2017.11.047

Gautam, S., & Ambwani, S. (2019). Tissue Engineering: New Paradigm of Biomedicine. *Biosciences Biotechnology Research Asia, 16*, 521-532. doi:10.13005/bbra/2766

Gholipourmalekabadi, M., Mozafari, M., Bandehpour, M., Sameni, M., & Ghanbarian, H. (2015). How Ethanol Treatment Affects The Physico-chemical And Biological Characteristics Of Silk Fibroin Nanofibrous Scaffolds. *Advanced Materials Letters, 6*(5), 391-394. doi:10.5185/amlett.2015.5739

Gui-Bo, Y., You-Zhu, Z., Shu-Dong, W., De-Bing, S., Zhi-Hui, D., & Wei-Guo, F. (2010). Study of the electrospun PLA/silk fibroin-gelatin composite nanofibrous scaffold for tissue engineering. *J Biomed Mater Res A, 93*(1), 158-163. doi:10.1002/jbm.a.32496

Gutiérrez-Sánchez, M., Escobar-Barrios, V. A., Pozos-Guillén, A., & Escobar-García, D. M. (2019). RGD-functionalization of PLA/starch scaffolds obtained by electrospinning and evaluated in vitro for potential bone regeneration. *Materials Science and Engineering: C, 96*, 798-806. doi:https://doi.org/10.1016/j.msec.2018.12.003

Haider, A., Haider, S., Rao Kummara, M., Kamal, T., Alghyamah, A.-A. A., Jan Iftikhar, F., Khan, R. (2020). Advances in the scaffolds fabrication techniques using biocompatible polymers and their biomedical application: A technical and statistical review. *Journal of Saudi Chemical Society, 24*(2), 186-215. doi:https://doi.org/10.1016/j.jscs.2020.01.002

He, J., Qin, Y., Cui, S., Gao, Y., & Wang, S. (2011). Structure and properties of novel electrospun tussah silk fibroin/poly(lactic acid) composite nanofibers. *Journal of Materials Science, 46*, 2938-2946. doi:10.1007/s10853-010-5169-x

Hirano, N., Kusuhara, H., Sueyoshi, Y., Teramura, T., Murthy, A., Asamura, S., Landis, W. J. (2021). Ethanol treatment of nanoPGA/PCL composite scaffolds enhances human chondrocyte development in the cellular microenvironment of tissue-engineered auricle constructs. *PLOS ONE, 16*(7), e0253149. doi:10.1371/journal.pone.0253149

Holjevac Grgurić, T., Mijović, B., Zimić, I., Dolenec, T., Kuzmić, S., Mrkonjić, N., Govorcin Bajsic, E. (2021). Preparation and Characterization of Electrospun PCL/Silk Fibroin Scaffolds. *Chemical & biochemical engineering quarterly, 35*, 31-42. doi:10.15255/CABEQ.2020.1834

Jazrawi, B., Noroozi, N., Ansari, M., & Hatzikiriakos, S. (2013). Processing aids for biodegradable polymers. *Journal of Applied Polymer Science, 128*, 3592-3600. doi:10.1002/app.38562

Jenkins, T., & Little, D. (2019). Synthetic scaffolds for musculoskeletal tissue engineering: cellular responses to fiber parameters. *npj Regenerative Medicine, 4*, 15. doi:10.1038/s41536-019-0076-5

Jeong, H. J., Lee, S. H., & Ko, C. S. (2012). Meniscectomy. *Knee Surg Relat Res, 24*(3), 129-136. doi:10.5792/ksrr.2012.24.3.129

Kesireddy, V., & Kasper, F. K. (2016). Approaches for building bioactive elements into synthetic scaffolds for bone tissue engineering. *Journal of materials chemistry. B, 4*(42), 6773-6786. doi:10.1039/C6TB00783J

Kim, G.-T., Lee, J.-S., Shin, J.-H., Ahn, Y.-C., Hwang, Y.-J., Shin, H.-S., Sung, C.-M. (2005). Investigation of pore formation for polystyrene electrospun fiber: Effect of

relative humidity. *Korean Journal of Chemical Engineering - KOREAN J CHEM ENG, 22*, 783-788. doi:10.1007/BF02705799

Kurtis Kasper, M. S. F., & Mikos, A. G. (2013). Chapter II.6.3 - Tissue Engineering Scaffolds. In B. D. Ratner, A. S. Hoffman, F. J. Schoen, & J. E. Lemons (Eds.), *Biomaterials Science (Third Edition)* (pp. 1138-1159): Academic Press.

Leonés, A., Peponi, L., Lieblich, M., Benavente, R., & Fiori, S. (2020). In Vitro Degradation of Plasticized PLA Electrospun Fiber Mats: Morphological, Thermal and Crystalline Evolution. *Polymers, 12*(12). doi:10.3390/polym12122975

Li, H., Li, P., Yang, Z., Gao, C., Fu, L., Liao, Z., . . . Guo, Q. (2021). Meniscal Regenerative Scaffolds Based on Biopolymers and Polymers: Recent Status and Applications. *Frontiers in Cell and Developmental Biology, 9*. doi:10.3389/fcell.2021.661802

Li, L., Li, H., Qian, Y., Li, X., Singh, G. K., Zhong, L., . . . Yang, L. (2011). Electrospun poly (ε-caprolactone)/silk fibroin core-sheath nanofibers and their potential applications in tissue engineering and drug release. *Int J Biol Macromol, 49*(2), 223-232. doi:10.1016/j.ijbiomac.2011.04.018

Liu, W., Li, Z., Zheng, L., Zhang, X., Liu, P., Yang, T., & Han, B. (2016a). Electrospun fibrous silk fibroin/poly(L-lactic acid) scaffold for cartilage tissue engineering. *Tissue Engineering and Regenerative Medicine, 13*(5), 516-526. doi:10.1007/s13770-016-9099-9

Liu, W., Li, Z., Zheng, L., Zhang, X., Liu, P., Yang, T., & Han, B. (2016b). Electrospun fibrous silk fibroin/poly(L-lactic acid) scaffold for cartilage tissue engineering. *Tissue Engineering and Regenerative Medicine, 13*, 516-526. doi:10.1007/s13770-016-9099-9

Liu, X., Chen, B., Li, Y., Kong, Y., Gao, M., Zhang, L. Z., & Gu, N. (2020). Development of an electrospun polycaprolactone/silk scaffold for potential vascular tissue engineering applications. *Journal of Bioactive and Compatible Polymers, 36*(1), 59-76. doi:10.1177/0883911520973244

Long, Y., Cheng, X., Tang, Q., & Chen, L. (2021). The antigenicity of silk-based biomaterials: sources, influential factors and applications. *Journal of Materials Chemistry B, 9*(40), 8365-8377. doi:10.1039/D1TB00752A

Lu, Q., Zhang, B., Li, M., Zuo, B., Kaplan, D. L., Huang, Y., & Zhu, H. (2011). Degradation mechanism and control of silk fibroin. *Biomacromolecules, 12*(4), 1080-1086. doi:10.1021/bm101422j

Ma, A., Yamane, H., & Kimura, Y. (2010). Effect of Polymer Molecular Weight on the Electrospinning of Polylactides in Entangled and Aligned Fiber Forms. *Sen-i Gakkaishi, 66*, 35-42. doi:10.2115/fiber.66.35

Maharana, T., Mohanty, B., & Negi, Y. S. (2009). Melt–solid polycondensation of lactic acid and its biodegradability. *Progress in Polymer Science, 34*, 99-124. doi:10.1016/j.progpolymsci.2008.10.001

Makris, E. A., Hadidi, P., & Athanasiou, K. A. (2011). The knee meniscus: structure-function, pathophysiology, current repair techniques, and prospects for regeneration. *Biomaterials, 32*(30), 7411-7431. doi:10.1016/j.biomaterials.2011.06.037

Mandal, B. B., Park, S.-H., Gil, E. S., & Kaplan, D. L. (2011). Multilayered silk scaffolds for meniscus tissue engineering. *Biomaterials, 32*(2), 639-651. doi:https://doi.org/10.1016/j.biomaterials.2010.08.115

McDermott, I. D., & Amis, A. A. (2006). The consequences of meniscectomy. *J Bone Joint Surg Br, 88*(12), 1549-1556. doi:10.1302/0301-620x.88b12.18140

Mehta, P. P., & Pawar, V. S. (2018). 22 - Electrospun nanofiber scaffolds: Technology and applications. In Inamuddin, A. M. Asiri, & A. Mohammad (Eds.), *Applications of Nanocomposite Materials in Drug Delivery* (pp. 509-573): Woodhead Publishing.

Meng, X., Nguyen, N. A., Tekinalp, H., Lara-Curzio, E., & Ozcan, S. (2018). Supertough PLA-Silane Nanohybrids by in Situ Condensation and Grafting. *ACS Sustainable Chemistry & Engineering, 6*(1), 1289-1298. doi:10.1021/acssuschemeng.7b03650

Murphy, C., O'Brien, F., Little, D., & Schindeler, A. (2013). Cell-scaffold interactions in the bone tissue engineering triad. *European cells & materials, 26*, 120-132. doi:10.22203/eCM.v026a09

Myers, K. R., Sgaglione, N. A., & Goodwillie, A. D. (2014). Meniscal scaffolds. *J Knee Surg, 27*(6), 435-442. doi:10.1055/s-0034-1388656

Nazeer, M. A., Yilgor, E., & Yilgor, I. (2019). Electrospun polycaprolactone/silk fibroin nanofibrous bioactive scaffolds for tissue engineering applications. *Polymer, 168*, 86-94. doi:https://doi.org/10.1016/j.polymer.2019.02.023

Ngadiman, N. H. A., Noordin, M. Y., Idris, A., Shakir, A. S. A., & Kurniawan, D. (2015). Influence of Polyvinyl Alcohol Molecular Weight on the Electrospun Nanofiber Mechanical Properties. *Procedia Manufacturing, 2*, 568-572. doi:https://doi.org/10.1016/j.promfg.2015.07.098

Nguyen, T. C., Ruksakulpiwat, C., & Ruksakulpiwat, Y. (2016). The Study on the Grafting of Glycidyl Methacrylate onto Poly(lactic acid) in an Internal Mixer. *Walailak Journal of Science and Technology (WJST), 13*(12), 1037-1046. Retrieved from https://wjst.wu.ac.th/index.php/wjst/article/view/2385

Numpaisal, P.-o., Jiang, C.-C., Hsieh, C.-H., Chiang, H., & Chien, C.-L. (2022). Prospective Application of Partially Digested Autologous Chondrocyte for Meniscus Tissue Engineering. *Pharmaceutics, 14*(3). doi:10.3390/pharmaceutics14030605

Oksiuta, Z., Jalbrzykowski, M., Mystkowska, J., Romanczuk, E., & Osiecki, T. (2020). Mechanical and Thermal Properties of Polylactide (PLA) Composites Modified with Mg, Fe, and Polyethylene (PE) Additives. *Polymers, 12*(12). doi:10.3390/polym12122939

Ortenzi, M. A., Gazzotti, S., Marcos, B., Antenucci, S., Camazzola, S., Piergiovanni, L., Verotta, L. (2020). Synthesis of Polylactic Acid Initiated through Biobased Antioxidants: Towards Intrinsically Active Food Packaging. *Polymers, 12*(5), 1183. doi:10.3390/polym12051183

Panjapheree, K., Kamonmattayakul, S., & Meesane, J. (2018). Biphasic scaffolds of silk fibroin film affixed to silk fibroin/chitosan sponge based on surgical design for cartilage defect in osteoarthritis. *Materials & Design, 141*, 323-332. doi:https://doi.org/10.1016/j.matdes.2018.01.006

Petersen, W., Karpinski, K., Bierke, S., Müller Rath, R., & Häner, M. (2022). A systematic review about long-term results after meniscus repair. *Archives of Orthopaedic and Trauma Surgery, 142*(5), 835-844. doi:10.1007/s00402-021-03906-z

Petersen, W., & Tillmann, B. (1998). Collagenous fibril texture of the human knee joint menisci. *Anat Embryol (Berl), 197*(4), 317-324. doi:10.1007/s004290050141

Pillai, M. M., Gopinathan, J., Indumathi, B., Manjoosha, Y. R., Santosh Sahanand, K., Dinakar Rai, B. K., . . . Bhattacharyya, A. (2016). Silk–PVA Hybrid Nanofibrous Scaffolds for Enhanced Primary Human Meniscal Cell Proliferation. *The Journal of Membrane Biology, 249*(6), 813-822. doi:10.1007/s00232-016-9932-z

Pina, S., Ribeiro, V. P., Marques, C. F., Maia, F. R., Silva, T. H., Reis, R. L., & Oliveira, J. M. (2019). Scaffolding Strategies for Tissue Engineering and Regenerative Medicine Applications. *Materials (Basel, Switzerland), 12*(11), 1824. doi:10.3390/ma12111824

Pölöskei, K., Csézi, G., Hajba, S., & Tábi, T. (2020). Investigation of the thermoformability of various D-Lactide content poly(lactic acid) films by ball burst test. *Polymer Engineering & Science, 60*. doi:10.1002/pen.25378

Promnil, S., Numpaisal, P.-o., & Ruksakulpiwat, Y. (2021). Effect of molecular weight on mechanical properties of electrospun poly (lactic acid) fibers for meniscus tissue engineering scaffold. *Materials Today: Proceedings, 47*, 3496-3499. doi:https://doi.org/10.1016/j.matpr.2021.03.504

Promnil, S., Ruksakulpiwat, Y., Ruksakulpiwat, C., & Numpaisal, P.-o. (2022). Effect of Silk Fibroin Content on Physical and Mechanical Properties of Electrospun Poly(lactic acid)/Silk Fibroin Nanofibers for Meniscus Tissue Engineering Scaffold. *Journal of Physics: Conference Series, 2175*(1), 012016. doi:10.1088/1742-6596/2175/1/012016

Qi, Y., Wang, H., Wei, K., Yang, Y., Zheng, R.-Y., Kim, S. I., & Zhang, K.-Q. (2017). A Review of Structure Construction of Silk Fibroin Biomaterials from Single Structures to Multi-Level Structures. *International journal of molecular sciences, 18*(3). doi:10.3390/ijms18030237

Reddy, M. S., Ponnamma, D., Choudhary, R., & Sadasivuni, K. K. (2021). A Comparative Review of Natural and Synthetic Biopolymer Composite Scaffolds. *Polymers, 13*(7). doi:10.3390/polym13071105

Ridley, T. J., McCarthy, M. A., Bollier, M. J., Wolf, B. R., & Amendola, A. (2017). Age Differences in the Prevalence of Isolated Medial and Lateral Meniscal Tears in Surgically Treated Patients. *Iowa Orthop J, 37*, 91-94.

Riley, A. (2012). 14 - Plastics manufacturing processes for packaging materials. In A. Emblem & H. Emblem (Eds.), *Packaging Technology* (pp. 310-360): Woodhead Publishing.

Rothrauff, B. B., Numpaisal, P.-O., Lauro, B. B., Alexander, P. G., Debski, R. E., Musahl, V., & Tuan, R. S. (2016). Augmented repair of radial meniscus tear with biomimetic electrospun scaffold: an in vitro mechanical analysis. *Journal of experimental orthopaedics, 3*(1), 23-23. doi:10.1186/s40634-016-0058-0

Roy, T., Maity, P. P., Rameshbabu, P. A., Das, B., John, A., Dutta, A., . . . Dhara, S. (2018). Core-Shell Nanofibrous Scaffold Based on Polycaprolactone-Silk Fibroin Emulsion Electrospinning for Tissue Engineering Applications. *Bioengineering, 5*(3). doi:10.3390/bioengineering5030068

Sari, A., Gunaydin, B., & dinçel, y. (2018). Meniscus Tears and Review of the Literature. In.

Shimomura, K., Bean, A. C., Lin, H., Nakamura, N., & Tuan, R. S. (2015). In Vitro Repair of Meniscal Radial Tear Using Aligned Electrospun Nanofibrous Scaffold. *Tissue Eng Part A, 21*(13-14), 2066-2075. doi:10.1089/ten.TEA.2014.0549

Song, R., Murphy, M., Li, C., Ting, K., Soo, C., & Zheng, Z. (2018). Current development of biodegradable polymeric materials for biomedical applications. *Drug design, development and therapy, 12*, 3117-3145. doi:10.2147/DDDT.S165440

Spalding, T., Damasena, I., & Lawton, R. (2020). Meniscal Repair Techniques. *Clin Sports Med, 39*(1), 37-56. doi:10.1016/j.csm.2019.08.012

Su, Y., Toftdal, M. S., Le Friec, A., Dong, M., Han, X., & Chen, M. (2021). 3D Electrospun Synthetic Extracellular Matrix for Tissue Regeneration. *Small Science, 1*(7), 2100003. doi:https://doi.org/10.1002/smsc.202100003

Sun, W., Gregory, D. A., Tomeh, M. A., & Zhao, X. (2021). Silk Fibroin as a Functional Biomaterial for Tissue Engineering. *Int J Mol Sci, 22*(3). doi:10.3390/ijms22031499

Taddei, P., Tozzi, S., Zuccheri, G., Martinotti, S., Ranzato, E., Chiono, V., Tsukada, M. (2017). Intermolecular interactions between B. mori silk fibroin and poly(l-lactic acid) in electrospun composite nanofibrous scaffolds. *Materials Science and Engineering: C, 70*, 777-787. doi:https://doi.org/10.1016/j.msec.2016.09.055

Talukdar, S., Nguyen, Q. T., Chen, A. C., Sah, R. L., & Kundu, S. C. (2011). Effect of initial cell seeding density on 3D-engineered silk fibroin scaffolds for articular cartilage tissue engineering. *Biomaterials, 32*(34), 8927-8937. doi:https://doi.org/10.1016/j.biomaterials.2011.08.027

Tarus, B., Fadel, N., Al-Oufy, A., & El-Messiry, M. (2016). Effect of polymer concentration on the morphology and mechanical characteristics of electrospun cellulose acetate and poly (vinyl chloride) nanofiber mats. *Alexandria Engineering Journal, 55*(3), 2975-2984. doi:https://doi.org/10.1016/j.aej.2016.04.025

Tertyshnaya, Y., Karpova, S., Moskovskiy, M., & Dorokhov, A. (2021). Electrospun Polylactide/Natural Rubber Fibers: Effect Natural Rubber Content on Fiber Morphology and Properties. *Polymers, 13*(14). doi:10.3390/polym13142232

Thanh Tam, T., Abdul Hamid, Z., & Cheong, K. Y. (2018). A Review of Mechanical Properties of Scaffold in Tissue Engineering: Aloe Vera Composites. *Journal of Physics: Conference Series, 1082*, 012080. doi:10.1088/1742-6596/1082/1/012080

Torino, E., Aruta, R., Sibillano, T., Giannini, C., & Netti, P. A. (2016). Synthesis of semicrystalline nanocapsular structures obtained by Thermally Induced Phase Separation in nanoconfinement. *Scientific reports, 6*, 32727-32727. doi:10.1038/srep32727

Trivedi, H., Gupta, N., Bey, A., & Kirmani, M. (2016). Engineering of Tissues: A Boon For Medical Science. *International Journal of Contemporary Medical Research, 3*, 2393-2915.

Vadodaria, K., Kulkarni, A., Santhini, E., & Vasudevan, P. (2019). Materials and structures used in meniscus repair and regeneration: a review. *Biomedicine (Taipei), 9*(1), 2. doi:10.1051/bmdcn/2019090102

Wang, F., Li, Y., Gough, C. R., Liu, Q., & Hu, X. (2021). Dual-Crystallizable Silk Fibroin/Poly(L-lactic Acid) Biocomposite Films: Effect of Polymer Phases on Protein Structures in Protein-Polymer Blends. *Int J Mol Sci, 22*(4). doi:10.3390/ijms22041871

Wang, F., Liu, H., Li, Y., Li, Y., Ma, Q., Zhang, J., & Hu, X. (2020). Tunable Biodegradable Polylactide–Silk Fibroin Scaffolds Fabricated by a Solvent-Free Pressure-Controllable Foaming Technology. *ACS Applied Bio Materials, 3*(12), 8795-8807. doi:10.1021/acsabm.0c01157

Wang, S., Zhang, Y., Wang, H., Yin, G., & Dong, Z. (2009). Fabrication and Properties of the Electrospun Polylactide/Silk Fibroin-Gelatin Composite Tubular Scaffold. *Biomacromolecules, 10*(8), 2240-2244. doi:10.1021/bm900416b

Wang, Z., Xiong, Y., Tang, X., Li, Q., Zhang, Z., Li, J., & Chen, G. (2019). An arthroscopic repair technique for meniscal tear using a needle and suture: outside-in transfer all-inside repair. *BMC Musculoskeletal Disorders, 20*(1), 614. doi:10.1186/s12891-019-2984-3

Warnecke, D., Stein, S., Haffner-Luntzer, M., de Roy, L., Skaer, N., Walker, R., Dürselen, L. (2018). Biomechanical, structural and biological characterisation of a new silk fibroin scaffold for meniscal repair. *Journal of the Mechanical Behavior of Biomedical Materials, 86*, 314-324. doi:https://doi.org/10.1016/j.jmbbm.2018.06.041

Williams, G. R., Raimi-Abraham, B. T., & Luo, C. J. (2018). Electrospinning fundamentals. In *Nanofibres in Drug Delivery* (pp. 24-59): UCL Press.

Wongnarat, C., & Srihanam, P. (2013). Degradation Behaviors of Thai Bombyx mori Silk Fibroins Exposure to Protease Enzymes. *Engineering, Vol.05No.01*, 6. doi:10.4236/eng.2013.51010

Wu, J., & Hong, Y. (2016). Enhancing cell infiltration of electrospun fibrous scaffolds in tissue regeneration. *Bioactive Materials, 1*(1), 56-64. doi:https://doi.org/10.1016/j.bioactmat.2016.07.001

Xue, J., Wu, T., Dai, Y., & Xia, Y. (2019). Electrospinning and Electrospun Nanofibers: Methods, Materials, and Applications. *Chemical reviews, 119*(8), 5298-5415. doi:10.1021/acs.chemrev.8b00593

Yan, L.-P., Oliveira, J. M., Oliveira, A. L., Caridade, S. G., Mano, J. F., & Reis, R. L. (2012). Macro/microporous silk fibroin scaffolds with potential for articular cartilage and meniscus tissue engineering applications. *Acta Biomaterialia, 8*(1), 289-301. doi:https://doi.org/10.1016/j.actbio.2011.09.037

Yan, S., Ou-Yang, H.-K., Shan, Y.-L., Luo, D.-Z., Wang, H., & Zhang, K. (2016). Tensile biomechanical characteristics of human meniscus. *Emerging Materials Research, 5*, 1-6. doi:10.1680/jemmr.15.00031

Yin Gui-Bo, Z. Y. Z., Wang Shu-Dong, Shi De-Bing, Dong Zhi-Hui, Fu Wei-Guo. (2009). Study of the electrospun PLA/silk fibroin-gelatin composite nanofibrous scaffold for tissue engineering. *Journal of Biomedical Material Research*. doi:https://doi.org/10.1002/jbm.a.32496

Yu, W., Wang, X., Ferraris, E., & Zhang, J. (2019). Melt crystallization of PLA/Talc in fused filament fabrication. *Materials & Design, 182*, 108013. doi:https://doi.org/10.1016/j.matdes.2019.108013

Zhang, J., Liu, H., Xu, H., Ding, J., Zhuang, X., Chen, X., . . . Li, Z.-M. (2014). Molecular Weight-Modulated Electrospun Poly(Ɛ-caprolactone) Membranes for Postoperative Adhesion Prevention. *RSC Adv., 4*. doi:10.1039/C4RA07216B

Zhou, C.-Z., Confalonieri, F., Jacquet, M., Perasso, R., Li, Z.-G., & Janin, J. (2001). Silk fibroin: Structural implications of a remarkable amino acid sequence. *Proteins: Structure, Function, and Bioinformatics, 44*(2), 119-122. doi:https://doi.org/10.1002/prot.1078
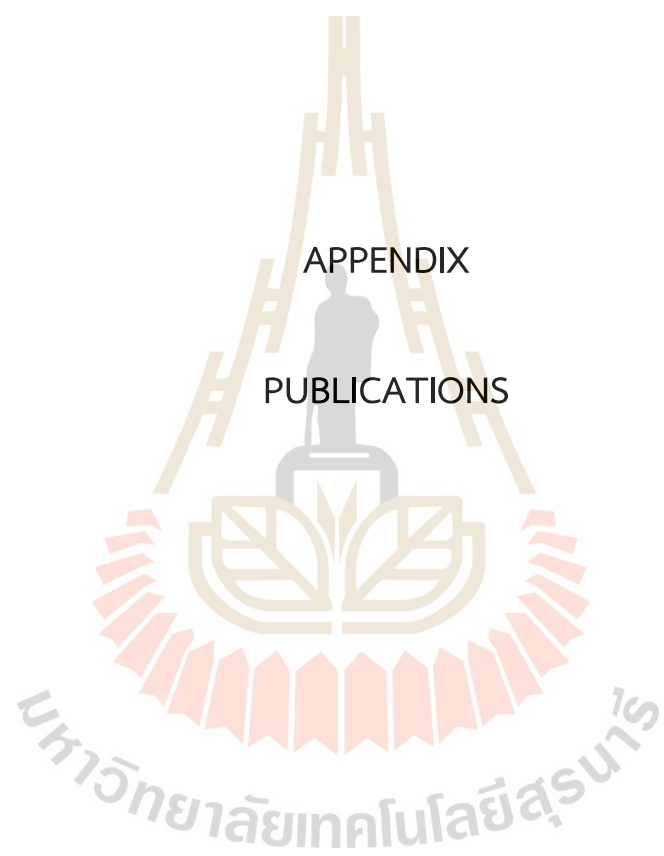
APPENDIX

PUBLICATIONS

List of Publications

Promnil, S., Numpaisal, P.-o., & Ruksakulpiwat, Y. (2021). Effect of molecular weight on mechanical properties of electrospun poly (lactic acid) fibers for meniscus tissue engineering scaffold. Materials Today: Proceedings, 47, 3496-3499. doi:https://doi.org/10.1016/j.matpr.2021.03.504

Promnil, S., Ruksakulpiwat, C., Numpaisal, P.-o., & Ruksakulpiwat, Y. (2022). Electrospun Poly(lactic acid) and Silk Fibroin Based Nanofibrous Scaffold for Meniscus Tissue Engineering. Polymers, 14(12). doi:10.3390/polym14122435

Promnil, S., Ruksakulpiwat, Y., Ruksakulpiwat, C., & Numpaisal, P.-o. (2022). Effect of Silk Fibroin Content on Physical and Mechanical Properties of Electrospun Poly(lactic acid)/Silk Fibroin Nanofibers for Meniscus Tissue Engineering Scaffold. Journal of Physics: Conference Series, 2175(1), 012016. doi:10.1088/1742-6596/2175/1/012016

polymers

Article

Electrospun Poly(lactic acid) and Silk Fibroin Based Nanofibrous Scaffold for Meniscus Tissue Engineering

Siripanyo Promnil [1,2,3], Chaiwat Ruksakulpiwat [1,2,3], Piya-on Numpaisal [3,4,*] and Yupaporn Ruksakulpiwat [1,2,3,*]

1 School of Polymer Engineering, Institute of Engineering, Suranaree University of Technology, Nakhon Ratchasima 30000, Thailand; siripanyo.pn@gmail.com (S.P.); charuk@sut.ac.th (C.R.)
2 Center of Excellence on Petrochemical and Materials Technology, Chulalongkorn University, Bangkok 10330, Thailand
3 Research Center for Biocomposite Materials for Medical Industry and Agricultural and Food Industry, Suranaree University of Technology, Nakhon Ratchasima 30000, Thailand
4 School of Orthopaedics, Institute of Medicine, Suranaree University of Technology, Nakhon Ratchasima 30000, Thailand
* Correspondence: piya-on@sut.ac.th (P.-o.N.); yupa@sut.ac.th (Y.R.); Tel.: +66-44-22-3917 (P.-o.N.); +66-44-22-3033 (Y.R.)

Abstract: Biopolymer based scaffolds are commonly considered as suitable materials for medical application. Poly(lactic acid) (PLA) is one of the most popular polymers that has been used as a bioscaffold, but it has poor cell adhesion and slowly degrades in an in vitro environment. In this study, silk fibroin (SF) was selected to improve cell adhesion and degradability of electrospun PLA. In order to fabricate a PLA/SF scaffold that offered both biological and mechanical properties, related parameters such as solution viscosity and SF content were studied. By varying the concentration and molecular weight of PLA, the solution viscosity significantly changed. The effect of solution viscosity on the fiber forming ability and fiber morphology was elucidated. In addition, commercial (L-lactide, D-lactide PLA) and medical grade PLA (pure PLLA) were both investigated. Mechanical properties, thermal properties, biodegradability, wettability, cell viability, and gene expression of electrospun PLA and PLA/SF based nanofibrous scaffolds were examined. The results demonstrated that medical grade PLA electrospun scaffolds offered superior mechanical property, degradability, and cellular induction for meniscus tissue regeneration. However, for commercial non-medical grade PLA used in this study, it was not recommended to be used for medical application because of its toxicity. With the addition of SF in PLA based scaffolds, the in vitro degradability and hydrophilicity were improved. PLAmed50:SF50 scaffold has the potential to be used as biomimetic meniscus scaffold for scaffold augmented suture based on mechanical properties, cell viability, gene expression, surface wettability, and in vitro degradation.

Keywords: PLA; silk fibroin; electrospinning; tissue engineering; gene expression; cell viability

1. Introduction

Poly(lactic acid) (PLA) is a linear aliphatic polyester that was originally obtained from natural crops [1]. Lactide is an intermediate for the production of the high molar mass PLA via ring opening polymerization (ROP). This monomer has large importance because it controls the synthesis of polymer production. The monomer exists as two stereo isomers, L-lactide and D-Lactide [2]. The processing, crystallization, and degradation behavior of PLA all depend on the stereochemical structure and composition of the polymer chains, which is influenced by the lactide isomers [3]. The presence of L- or D-lactide monomer affects the physical and mechanical characteristics of the final polymer. PLLA polymer has the highest melting point among the other PLA forms due to its crystalline nature. As D-isomer is incorporated in the PLA chain, it reduces its crystallinity, lowering the melting

points of PLA copolymers. In addition to that, PLLA (higher crystallinity) is often more used than PDLA [4]. PLA and its copolymers were developed as biomedical materials based on their bioabsorbable and biocompatible properties and have been widely used in orthopedic surgery including sutures, prostheses, and tissue engineering scaffold in which high- and low-molecular-weight PLAs are utilized [5].

Due to the manufacturing process, the cost of medical grade PLA is much higher than the commercial grade PLA. It must be synthesized under a physician's license to pass the validation requirements of the regulatory agencies. This meant that polymer manufacturers would need to have controls over their design and development processes, including strict controls of the raw materials and components used to manufacture the finished product [6]. Thus, it is interested to compare the scaffold properties obtained from medical grade PLA (pure PLLA) to the commercial grade PLA (L-lactide, D-lactide PLA) at the comparable molecular weight in order to study the difference of physical and mechanical properties of PLA and PLAmed scaffolds. However, PLA has slow degradation, poor hydrophilicity, and poor cell adhesion. To eliminate the drawback of PLA, a combination of PLA and silk fibroin (SF) scaffold was studied [7].

Silk is a fibrous protein produced by silkworms. Silk consists of two components; the main part is fibroin, which is the core fiber and the coverage protein called sericin [8,9]. Silk fibroin is a biocompatible natural polymer which is non-toxic, immunogenically inert and provides good elasticity. Moreover, it has been fabricated and used as the medical suture and has a long safety record. Therefore, SF is a good candidate natural polymer for our PLA composite scaffold in meniscus tissue engineering [10]. PLA/SF composite scaffolds have good cell compatibility and are conducive to cell adhesion and growth [11–14]. The presence of silk fibroin also significantly enhanced the enzymatic degradation ability of the PLA matrix, which is good for bone tissue engineering application [7,15].

Meniscus is a fibrocartilageous structure which covers the tibial articular surface. Meniscus functions to distribute, absorb, and transmit load across the knee joint. Meniscus also enhances knee stability by increasing joint congruity and contact surface area [16]. From this reason, meniscus is vulnerable to injury which caused a meniscus tear to become a common injury in the knee joint. Unfortunately, the efficacy of meniscus repair depends on location with respect to the vascular supply. Outer and middle meniscus is avascular and can heal with some fibroblasts. The inner avascular zone presents a limited amount of chondrocyte like cells that possess poor healing potential [17]. Since inner menisci have pool healing potential, an unhealed meniscus ends up with meniscus resection that causes high contact stress on the articular surface and leads to osteoarthritis [18].

For the aforementioned reason, tissue engineering and cell-based therapy have been proposed as a biological augmentation for meniscus repair. There are three main components in tissue engineering: cells, scaffolds, and bio-active molecules. Cells and bioactive molecules function simultaneously to produce new tissue formation. Scaffold is a cell shelter and delivery system. Scaffolds is made from biocompatible material and should support target tissue regeneration as well as provide mechanical competent [19]. Currently, a three-dimensional biomimetic scaffold which imitates a host tissue environment has been studied. Collagen is a major component of the meniscus extracellular matrix. Collagen fibers mostly align longitudinally in a circumferential orientation; some fibers lie perpendicularly as a radial fiber. Electrospinning is an interesting technique to fabricate the fibrous scaffold. Electrospun fibers can be fabricated on a micro to nano-scale with a great surface area and high porosity that is similar to a natural extracellular matrix (ECM) in both architecture and mechanical properties [20].

Our research aimed to develop a PLA/SF composite biomimetic meniscus scaffold using an electrospinning technique. The application of our scaffold will be used for a scaffold augmented suture. The effect of molecular weight and concentration of PLA on viscosity and fiber morphology was observed. Moreover, the effect of SF contents on fiber morphology, thermal properties, wettability, degradability, mechanical properties, and cytotoxicity of the PLA/SF scaffold were examined. Comparison of these properties

between commercial grade PLA (L-lactide, D-lactide PLA) and medical grade of PLA (PLLA) based scaffold was also made.

2. Materials and Methods

2.1. Materials

Two commercial non-medical grade PLA with different molecular weight, PLA3251D (low molecular weight with 99% L-lactide and 1% D-lactide; PLAL [21]) and PLA4043D (high molecular wight with 94% L-lactide and 6% D-lactide content; PLAH [22]) provided by NatureWorks LLC(Minnetonka, MN, USA) and a medical grade, Resomer L209S (pure PLLA; PLAmed) from Sigma-Aldrich (Burlington, MA, USA.) were used. PLAH and PLAmed have a molecular weight in a comparable range. Chloroform RPE was purchased from Carlo Erba Reagents (Milano, Italy). Formic acid was obtained from Merck (Darmstadt, Germany). Bombyx mori cocoons were provided by Queen Sirikit Sericulture Center, Nakhon Ratchasima, Thailand. Sodium carbonate (Na_2CO_3, analytically pure) and calcium chloride ($CaCl_2$, analytically pure) were purchased from Carlo Erba (Milano, Italy).

2.2. Silk Fibroin Preparation

Cocoons were degummed in Na_2CO_3 solution at 98 ± 2 °C for 30 min, rinsed with distilled water and dried overnight. Degummed silk fibers were dissolved in $CaCl_2$ solution by stirring at 98 ± 2 °C for 1 h. Then, the SF aqueous solution was filtered to remove undissolved component, and dialyzed against distilled water for 3 days. The SF solution was filtered and lyophilized to obtain the SF powder.

2.3. Electrospinning Solution Preparation

PLA was dissolved in chloroform at various concentrations as indicated in Table 1. SF solution was prepared by dissolving SF in formic acid (12% w/v). The solution of PLA commercial grade and SF were mixed in three different ratios of PLAH:SF (75:25, 50:50 and 25:75). The solution of PLA medical grade and SF was mixed at a 50:50 ratio. The symbols used for PLA/SF samples were shown in Table 2. The emulsion was created by magnetic stirring for 12 h to obtain uniform emulsion. The electrospinning parameters were as follows: a positive voltage of 20 kV, a collector distance of 15 cm, and the flow rate of 2.0 mL/h.

Table 1. PLA sample nomenclature.

Sample	Grade	Manufacturer	Molecular Weight (g/mol)	Concentration (% w/v)
PLAL−10	3251D	NatureWorks LLC	55,400 [21,23]	10
PLAL−15	3251D	NatureWorks LLC	55,400 [21,23]	15
PLAL−20	3251D	NatureWorks LLC	55,400 [21,23]	20
PLAH−10	4043D	NatureWorks LLC	127,300–147,400 [24,25]	10
PLAH−15	4043D	NatureWorks LLC	127,300–147,400 [24,25]	15
PLAH−20	4043D	NatureWorks LLC	127,300–147,400 [24,25]	20
PLAmed−6	L209S	Sigma-Aldrich LLC	177,000 [26,27]	6

Table 2. PLA/SF electrospun samples.

Samples	PLA Concentration (% w/v)	SF Concentration (% w/v)	PLA Ratio (Volume)	SF Ratio (Volume)
PLAH75:SF25	15	12	75	25
PLAH50:SF50	15	12	50	50
PLAH25:SF75	15	12	25	75
PLAmed50:SF50	15	12	50	50

73

2.4. Characterization of PLA Solutions

The viscosity of PLA solutions was measured by a Brookfield rheometer (AMETEK Brookfield, Middleboro, MA, USA) with a cone-plate at constant temperature (25 °C).

2.5. Fiber Morphology

The microstructure of electrospun fibers was observed under field emission scanning electron microscopy (FESEM; Carl Zeiss Auriga, Oberkochen, Germany) with gold coating. The diameter of the fibers was measured from the micrographs using image analysis software (ImageJ) in 100 random fibers, and the diameter distribution histograms were plotted by OriginLab software.

2.6. Mechanical Properties

Tensile properties were determined by using an Instron Universal Testing Machine (Instron 5565, Norwood, MA, USA) with crosshead speed on 10 mm/min, 1 kN load cell at room temperature. The electrospun test specimens with 1 cm width and 10 cm original length were prepared. The reported data of tensile strength, elongation at break and Young's modulus represent the average results from five test specimens ($n = 5$).

2.7. Thermal Properties

The thermal stabilities of PLA and PLA/SF scaffolds were analyzed by a TGA/DSC1 thermogravimetric analyzer (Mettler Toledo, Greifensee, Switzerland) at a heating rate of 10 °C/min under nitrogen from 25 to 500 °C. The thermal properties of scaffolds were analyzed by differential scanning calorimetry (DSC) on a Pyris Diamond DSC machine (PerkinElmer, Waltham, MA, USA) in nitrogen atmosphere. The samples were heated from 25 to 200 °C at a rate of 10 °C/min (first-heating scan). After keeping the specimens at 200 °C for 5 min, they were cooled to 25 °C at 10 °C/min. Then, they were heated again to 200 °C at 10 °C/min (second-heating scan). The glass transition temperature (T_g), the melting temperature (T_m), the cold crystallization temperature (T_{cc}), the cold crystallization enthalpy (ΔH_{cc}), and the melting enthalpy (ΔH_m) were determined from the first and second heating scan. The melt crystallization temperature (T_c) and the crystallization enthalpy (ΔH_c) were obtained from the cooling scan. The degree of crystallinity ($\%\chi_c$) of PLA and biocomposites was determined by Equation (1):

$$\% \text{ Crystallinity } (\chi_c) = \left[(\Delta H_m) / \left(\Delta H_m^0 \right) \right] \times 100 \times 1/W_{PLA} \tag{1}$$

in which ΔH_m is the measured melting enthalpy (J/g) from the heating scan, ΔH_m^0 is the theoretical melting enthalpy of completely crystalline PLA (93.7 J/g) [28,29], and W_{PLA} is the PLA weight fraction in the biocomposites.

2.8. Fourier-Transform Infrared Spectroscopy (FTIR)

The FT-IR spectra with characteristic absorption peaks of SF powder, PLA, and PLA/SF nanofibers were determined by a FTIR spectrophotometer (Bruker Tensor 27, Billerica, MA, USA). All samples were directly characterized in attenuated total reflectance (ATR-FTIR) mode in the spectral range of 4000–400 cm^{-1}.

2.9. In Vitro Degradation

Scaffolds with dimensions of 1 cm width and 1 cm length ($n = 3$) were immersed in phosphate buffered saline (PBS, pH = 7.4) and incubated at 37 °C with 5% carbon dioxide (CO_2) for 14, 28, 42, and 84 days (2, 4, 6, and 12 weeks). PBS was changed every 3 days. The appearance of all scaffolds was observed every 2 weeks. The scaffolds were washed with distilled water, dried, and weighed. The percentage of residual weight was calculated by Equation (2) [30]:

$$\% \text{ Residual weight} = 100 - \left[((W_i - W_f)/W_i) \times 100 \right] \tag{2}$$

where W_i is initial weight of sample, while W_f is the weight of sample after immersing in PBS.

2.10. Surface Wettability

Water contact angle was studied to assess the surface wettability properties of the PLA/SF electrospun nanofibers. Distilled water with controlled volume of 15 µL was dropped on the surface of each sample. After a 60 s exposure at ambient temperature, the images of water drop on the sample surface were recorded by a USB digital microscope (1600×) and analyzed with ImageJ software. Three different points ($n = 3$) were measured for each sample.

2.11. In Vitro Cell Culture Studies

Scaffolds were cut into 4 mm x 4 mm dimension ($n = 3$), separated into two groups. The first group was plunged into 70% alcohol, dried at 30 °C for 24 h, and sterilized under ultraviolet (UV) light for 30 min while the second group was not plunged into alcohol. The scaffolds were then placed in 96-well plates and 5×10^3 human chondrocyte cells were seeded onto the scaffolds. The cell seeded scaffolds were cultured in Dulbecco's modified Eagle's medium (DMEM) with 10% fetal bovine serum, 1% L-glutamine, and 1% penicillin-streptomycin, put in 37 °C with a 5% CO_2 humidified incubator. The cell viability was assessed with an MTT (3-[4,5-dimethylthiazol-2-yl]-2,5 diphenyl tetrazolium bromide) assay at days 1, 3, and 7. Optical density of each well was read at 590 nm using a microplate reader. The percentage of cell viability was calculated by comparing the absorbance of cells cultured on scaffolds to that of control Equation (3):

$$\% \text{ Cell viability} = (\text{O.D.of treatment})/(\text{O.D.of control}) \times 100 \tag{3}$$

2.12. Quantitative Analysis for Gene Expression

According to cell viability results, PLAmed−6% and PLAmed50:SF50 scaffold were used to assess gene expression. The nanofibrous scaffold sheets were cut into a circle, 12 mm in diameter, and sterilized under UV light for 30 min. Then, the prepared scaffolds ($n = 3$) were put in 24 wells and incubated in culture media for 4 h. The HCPCs were seeded with 2.5×10^4 cells in each scaffold. A cell seeded scaffold was then cultured for 7, 14, and 28 days. Total RNA was extracted from the HCPCs on the scaffolds for quantitative gene-analysis using RNeasy mini-Kit (Qiagen, Hilden, Germany). Quantitative real-time polymer chain reaction (qRT-PCR) was done with an SYBR Green kit (Thermo Fisher Scientific, Waltham, MA, USA) and Fluorescein Kit (BIOLINE, London, UK). The target genes were type I collagen (COL1A1), which represented a fibrogenic property, and type II collagen (COL2A1), which demonstrated a chondrogenic phenotype. The 18S rRNA was used as a housekeeping gene (Table 3).

Table 3. Sequences of the primer sets for qRT-PCR.

Genes		Primer Sequence (5' to 3')
Type I collagen	Sense	GGAGGAGAGTCAGGAAGG
(COL1A1)	Antisense	GCAACACAGTTACACAAGG
Type II collagen	Sense	GGCAGAGGTATAATGATAAG
(COL2A1)	Antisense	ATGTCGTCGCAGAGG
18S rRNA	Sense	ATACCGTCGTAGTTCC
	Antisense	GTCTCGTTCGTTATCG

3. Results

3.1. Viscosity of PLA Solutions

PLA solution viscosities were shown in Table 4. PLAL showed lower viscosity than PLAH at the same concentration. Increasing concentration led to a significant increase in viscosity. PLAmed solution at a lower concentration (6%) showed higher solution viscosity than PLAH (10%).

Table 4. PLA solution viscosity for electrospinning.

PLA Solution (*w/v*)	Viscosity (cP)
PLAL−10	58.02 ± 0.80
PLAL−15	278.68 ± 5.47
PLAL−20	690.54 ± 30.18
PLAH−10	652.98 ± 36.15
PLAH−15	2304.73 ± 74.49
PLAH−20	9319.67 ± 91.40
PLAmed−6	1024.81 ± 83.15

3.2. Fiber Morphology

3.2.1. PLA Fiber Morphology

SEM micrographs of electrospun PLAL, PLAH, and PLAmed nanofibers, and their diameter distribution curves of electrospun fiber were shown in Figures 1 and 2, respectively.

PLA fiber surfaces of each sample contained small pores randomly distributed on the fibers. PLAL−10 (Figure 1a–c) showed a large number of droplets or beaded particles instead of a fibrous structure. For PLAL−15 (Figure 1d,e), the beads still appeared on the electrospun fibers, or they can be called bead-on-string fibers, while PLAL−20 (Figure 1g–i) gave the porous fibers with no beads. PLAH−10 provided a small fiber diameter (Figure 2c) with high entanglement (Figure 1j–l). PLAH−15 exhibited the uniform fibers with random orientation (Figure 1m–o) when compared to other samples, while PLAH−20 (Figure 1p–r) gave larger diameter fibers (Figure 2e), but it was difficult to be processed. The higher molecular weight of PLA gave a larger fiber diameter of electrospun fibrous scaffold. PLAmed−6 (Figure 1s–u) provided the large fibers with the highest average diameter (Figure 2f) compared to electrospun PLAL and PLAH fibers.

3.2.2. PLA/SF Fiber Morphology

Figure 3 shows the effect of SF content on PLA/SF electrospun fiber morphology. An electrospun PLA75:SF25 sample showed beads on the fiber surface (Figure 3a,b) with the average fiber diameter of 0.29 ± 0.20 µm (Figure 4a). A PLA50: SF50 sample (Figure 3d–f) showed a smoother fiber surface and smaller beads, with an average fiber diameter of 0.32 ± 0.26 µm (Figure 4b). For the PLA25:SF75 sample (Figure 3g–i), there was less fiber on the collector than in other samples. At this ratio, it tended to break up into electrospray instead, and it was difficult to process. The average fiber diameter was 2.19 ± 1.71 µm (Figure 4c). As SF content increased, the fiber diameter increased. With the addition of SF, the fiber diameter decreased compared to that of pure PLA fiber (Figure 1). PLAH50:SF50 was selected to compare with PLAmed50:SF50. For PLAmed50:SF50 (Figure 3j–l), the fine porous fiber and small beads appeared on the scaffold. The fiber diameter was 0.18 ± 0.08 µm (Figure 4d), which was smaller than that of PLAH50:SF50 fibers.
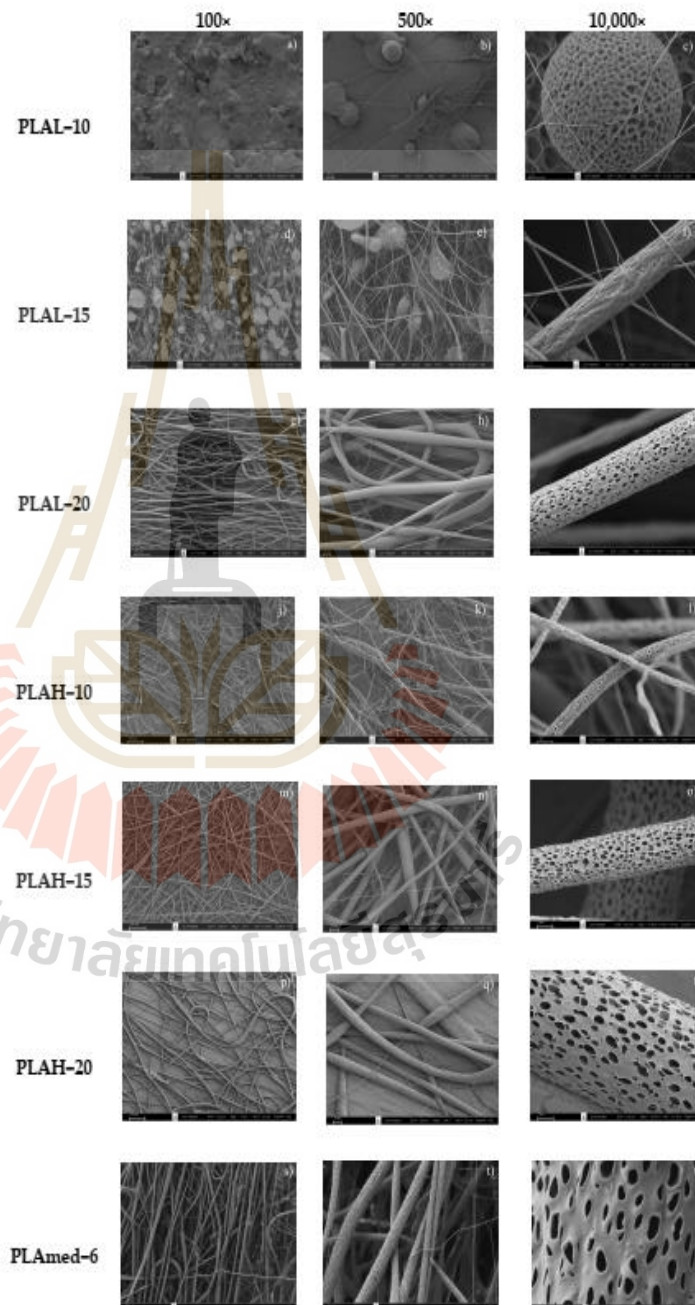
Figure 1. The morphology of pure PLAL, PLAH, and PLAmed fibers, which was fabricated by using various concentrations; (a–c) PLAL−10; (d–f) PLAL−15; (g–i) PLAL−20; (j–l) PLAH−10; (m–o) PLAH−15; (p–r) PLAH−20; and (s–u) PLAmed−6 at different magnifications (100×, 500×, and 10,000×).
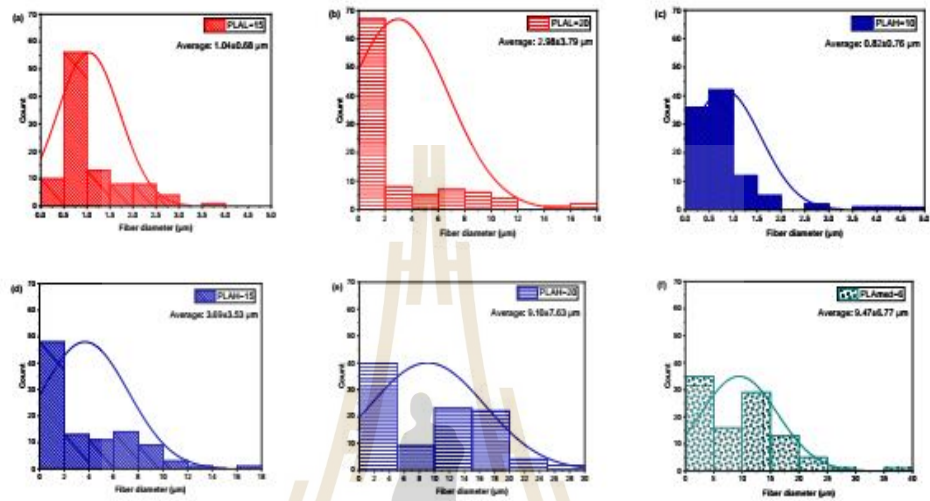
Figure 2. Histograms of electrospun fibers (**a**) PLAL−15; (**b**) PLAL−20; (**c**) PLAH−10; (**d**) PLAH−15; (**e**) PLAH−20; and (**f**) PLAmed−6.
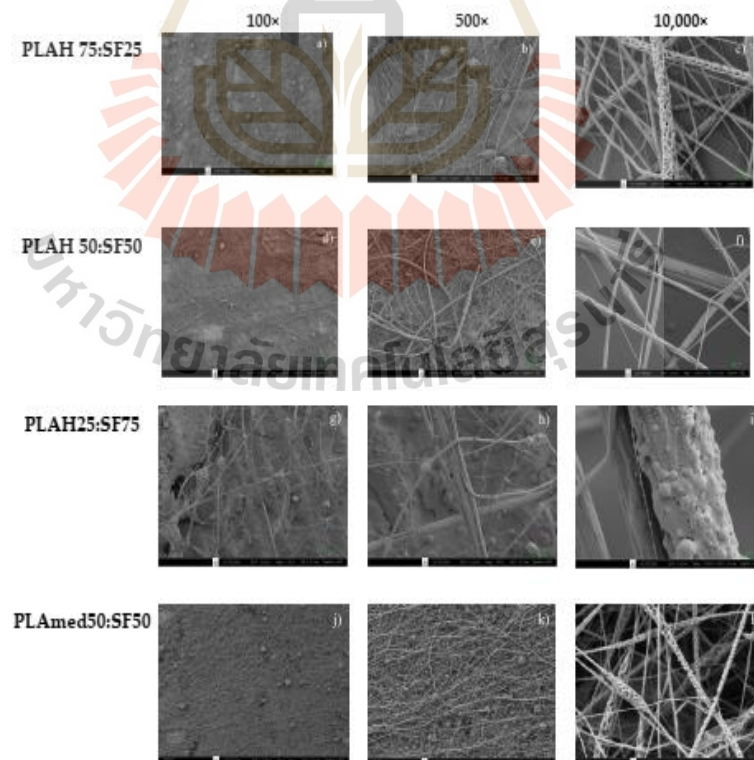

Figure 3. The morphology of (**a–c**) PLAH75:SF25; (**d–f**) PLAH50:SF50; (**g–i**) PLAH50:SF50; and (**j–l**) PLAmed50:SF50 fibers at different magnifications (100×, 500×, and 10,000×).
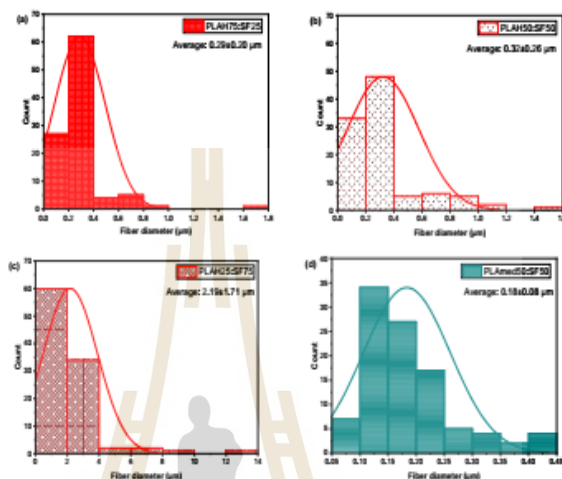
Figure 4. Histograms of electrospun fibers (**a**) PLAH75:SF25, (**b**)PLAH50:SF50; (**c**) PLAH25:SF75 and (**d**) PLAmed50:SF50.

3.3. FTIR Spectra

FTIR spectroscopy in Figure 5 showed the strong characteristic absorption bands of SF powder that appeared at 1626 cm^{-1} (Amide I), 1512 cm^{-1} (Amide II), and 1228 cm^{-1} (Amide III). Electrospun pure PLA samples demonstrated significant absorption bands at 1752 cm^{-1} (the stretching vibration of carbonyl), 1452 cm^{-1} (the deformation vibration of a carbon hydrogen bond), 1368 cm^{-1}, 1261 cm^{-1} (the antisymmetric stretching vibration of carbonyl), 1184 cm^{-1} (the stretching vibration of carbonyl), 1084 cm^{-1} (the antisymmetric stretching vibration of a carbon-oxygen bond), 868 cm^{-1}, 755 cm^{-1}, and 694 cm^{-1} (the bending vibration of carbon-hydrogen bond). Similar characteristic peaks for SF and PLA were observed in PLA/SF scaffolds (both PLAH and PLAmed), which confirmed the presence of both SF and PLA in the scaffolds.
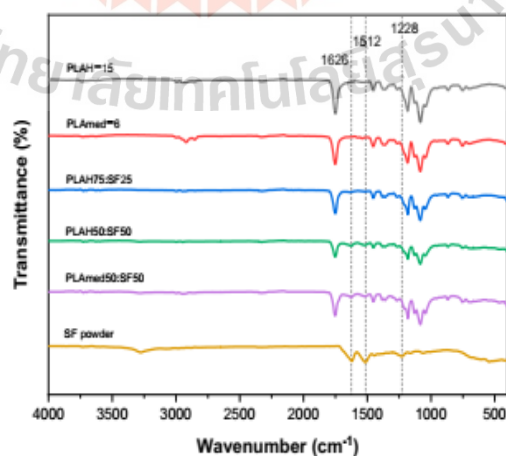

Figure 5. FTIR spectra of SF powder, PLAH −15, PLAH75:SF25, PLAH50:SF50, PLAmed−6, and PLAmed50:SF50 fibers.

3.4. Mechanical Properties

Tensile properties of PLAH−15, PLAH75:SF25, PLAH50:SF50, PLAmed−6, and PLAmed50:SF50 were shown in Table 5. PLAH−15 scaffold gave the highest tensile strength and highest Young's modulus when compared to PLAH75:SF25 and PLAH50:SF50 scaffolds. After adding SF, the tensile strength of PLAH75:SF25 scaffolds decreased from 1.14 ± 0.09 MPa to 0.47 ± 0.07 MPa, while the elongation at break increased from 15.97 ± 1.80% to 26.22 ± 10.64% compared to that of pure PLAH−15. For PLAH50:SF50, the tensile strength was higher than PLAH75:SF25, but the elongation at break was lower.

Table 5. Mechanical properties of PLA based scaffolds.

Samples	Ultimate Tensile Strength (MPa)	Elongation at Break (%)	Young's Modulus (MPa)
PLAH−15	1.14 ± 0.09 *	15.97 ± 1.80 *	70.21 ± 4.99 *
PLAH75:SF25	0.47 ± 0.07 *	26.22 ± 10.64 *	20.51 ± 3.97 *
PLAH50:SF50	1.05 ± 0.43 *	17.51 ± 3.89 *	16.49 ± 8.71 *
PLAmed−6	2.06 ± 0.28	14.34 ± 1.00	109.38 ± 12.21
PLAmed50:SF50	0.85 ± 0.11	12.14 ± 2.20	22.59 ± 6.59

* From previous study [31].

The mechanical properties of PLAmed−6 scaffold showed higher values than the PLAmed50:SF50 scaffold. Incorporation of SF in PLA scaffolds slightly increased in elongation at break but decreased the tensile strength and Young's modulus of electrospun scaffold.

3.5. Thermal Properties

The effect of SF content of PLA/SF scaffold on thermal degradation was shown in Figure 6. SF contained moisture content about 10% wt., while PLA showed very low moisture content. With the addition of SF, the moisture content in the sample slightly increased. The decomposition temperatures of PLA with the addition of SF shifted to a lower temperature due to the low thermal stability of SF.
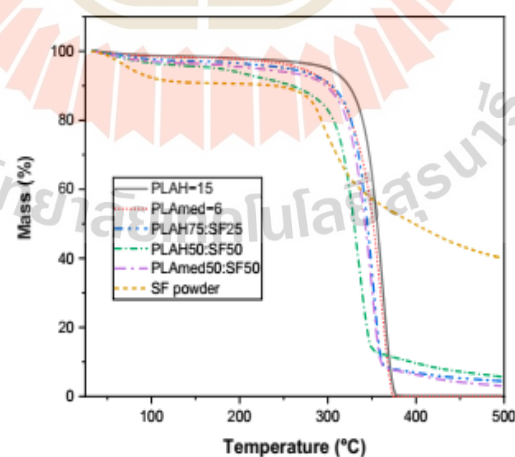

Figure 6. TGA thermograms of SF, PLAH−15, PLAH75:SF25, PLA50:SF50, PLAmed−6, and PLAmed50:SF50.

Figure 7 shows DSC thermograms of electrospun scaffolds during the first heating scan (Figure 7a), cooling scan (Figure 7b), and second heating scan (Figure 7c). Thermal properties obtained from this figure were shown in Tables 6 and 7. From the first heating scan which represented the thermal properties of the electrospun scaffolds obtained after the electrospinning process, the PLAmed−6 scaffold showed a higher glass transition, lower cold crystallization temperature, and higher melting temperature than the

PLAH−15 scaffold. With the addition of SF into PLA, the shift to higher cold crystallization temperature and slightly higher melting temperature was observed in PLAH75:SF25 and PLAH50:SF50 scaffold. On the other hand, PLAmed50:SF50 showed lower cold crystallization temperature than pure PLAmed scaffold. However, after removing thermal history and cooling in DSC, no significant differences in glass transition temperature, cold crystallization temperature, and melting temperature among PLAH−15, PLAH75:SF25, and PLAH50:SF50 were observed from a second heating scan.
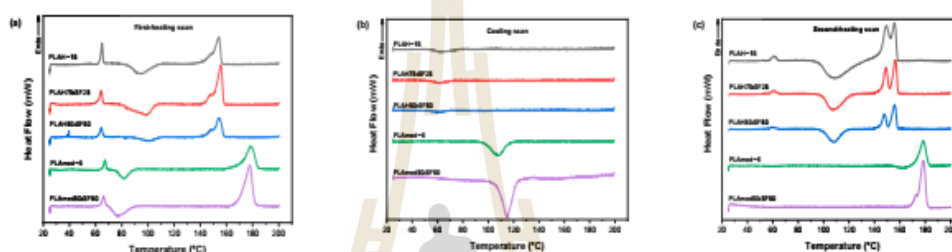

Figure 7. DSC thermograms from (a) first-heating scan, (b) cooling scan, and (c) second-heating scan of PLAH−15, PLAH75:SF25, PLAH50:SF50, PLAmed−6, and PLAmed50:SF50 scaffolds.

Table 6. Thermal properties of PLAH−15, PLAH75:SF25, PLAH50:SF50, PLAmed−6, and PLAmed50:SF50 obtained from DSC thermogram during first-heating and cooling scan.

Samples	First-Heating Scan							Cooling Scan		
	T_g (°C)	T_{cc} (°C)	ΔH_{cc} (Jg^{-1})	T_{m_1} (°C)	T_{m_2} (°C)	ΔH_m (Jg^{-1})	χ_c (%)	T_g (°C)	T_c (°C)	ΔH_c (Jg^{-1})
PLAH−15	64.90	94.22	14.81	148.05	154.07	20.53	21.94	63.68	-	-
PLAH75:SF25	64.38	98.44	13.35	147.81	155.49	25.86	21.83	62.66	-	-
PLAH50:SF50	64.32	100.55	9.09	148.12	154.19	21.41	12.81	61.55	-	-
PLAmed−6	67.19	82.01	12.00	-	178.61	42.61	45.52	-	107.91	19.01
PLAmed50:SF50	66.03	77.42	8.56	-	177.82	42.71	25.55	-	114.84	30.52

Table 7. Thermal properties of PLAH−15, PLAH75:SF25, PLAH50:SF50, PLAmed−6, and PLAmed50:SF50 obtained from DSC thermogram during second-heating scan.

Samples	Second-Heating Scan						
	T_g (°C)	T_{cc} (°C)	ΔH_{cc} (Jg^{-1})	T_{m_1} (°C)	T_{m_2} (°C)	ΔH_m (Jg^{-1})	χ_c (%)
PLAH−15%	59.28	108.78	14.48	149.42	155.76	21.53	23.00
PLAH75:SF25	58.55	107.67	24.21	149.03	156.40	25.71	21.70
PLAH50:SF50	57.41	107.79	21.58	147.85	155.92	23.71	14.19
PLAmed−6%	67.57	-	-	-	178.33	39.97	42.71
PLAmed50:SF50	63.94	-	-	172.50	178.41	41.04	24.56

It is interesting to point out the difference in crystallization behavior between medical grade PLA and commercial grade PLA during a cooling scan. For PLAmed−6 and PLAmed50:SF50, a clear melt crystallization peak during cooling was presented. In contrast, no melt crystallization peak was shown for PLAH with and without SF. The %crystallinity of medical grade of PLA was higher than that of commercial grade of PLA both from the first heating scan and second heating scan. This indicated a higher ability to crystallize medical grade PLA than commercial grade PLA.

3.6. In Vitro Degradation

The effect of SF content on PLA/SF scaffold degradation was shown in Figure 8. Degradation profiles were shown as a percentage of residual weight of scaffolds by time. During the study period, both pure PLA and PLA/SF scaffolds degraded slowly. PLAH, PLAH75:SF25, and PLAmed exhibited very low degradation, while the weight of PLAH50:SF50 and PLAmed50:SF50 scaffolds decreased by time
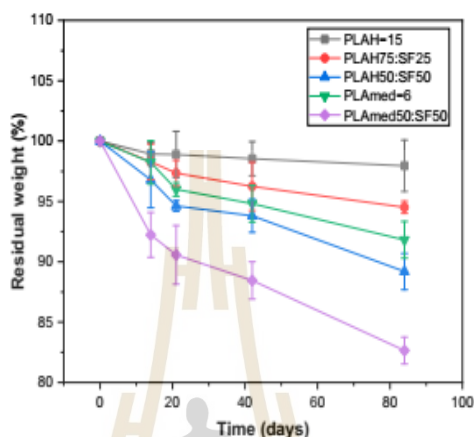
Figure 8. Residual weight (%) of electrospun scaffolds after degradation in phosphate buffered saline (PBS, pH = 7.4) as a function of time.

3.7. Surface Wettability

The water contact angle of scaffolds measured from the droplet images was shown in Figure 9. The contact angle for electrospun pure PLAH and PLAmed scaffolds was highly hydrophobic with a contact angle of $142.49 \pm 2.22°$ and $136.73 \pm 2.09°$, respectively. Electrospun PLAH:SF and PLAmed:SF scaffolds showed a slight decrease to $128.08 \pm 1.10°$ (PLAH75:SF25), $112.81 \pm 5.22°$ (PLAH50:SF50), and $127.45 \pm 3.49°$ (PLAmed50:SF50). With the incorporation of SF, the PLA/SF scaffolds became more hydrophilic.
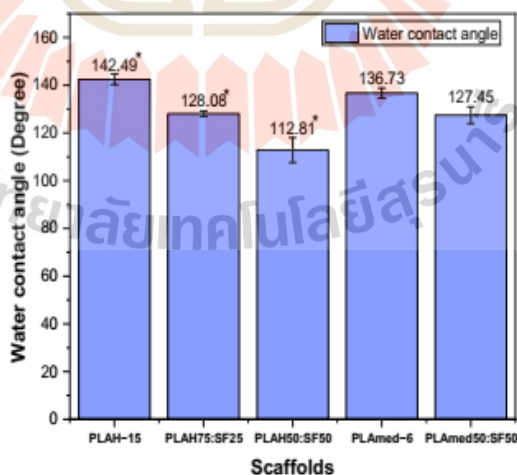
Figure 9. Water contact angle of PLAH−15, PLAH75:SF25, PLAH50:SF50, PLAmed−6, and PLAmed50:SF50 scaffolds; * From previous study [31].

3.8. Cell Viability Test

MTT assay was carried out to evaluate HCPCs viability on PLA and PLA/SF electrospun scaffolds. Rather than the PLA/SF ratio and PLA grading, the effect of ethanol treatment (+) on cell viability is shown in Figure 10. Generally, the HCPC viability of ethanol treated scaffold groups (+) was higher than that of the non-treated groups. The

cell viability in untreated scaffold groups was lower than the control group at every time point except PLA50:SF50, which presented higher viability compared to the control group at days 3 and 7. In the alcohol treated group (+), PLAH+ scaffolds had lower cell viability compared to medical grade PLA scaffolds. Cell viability at days 1 and 3 were slightly different among PLAH+ groups and, at day 7, PLAH−15+ had higher cell viability than PLAH50:SF50+ and PLAH75:SF25+, respectively. PLAmed−6+ had slightly higher cell viability than PLAmed50:SF50+ at every time point.
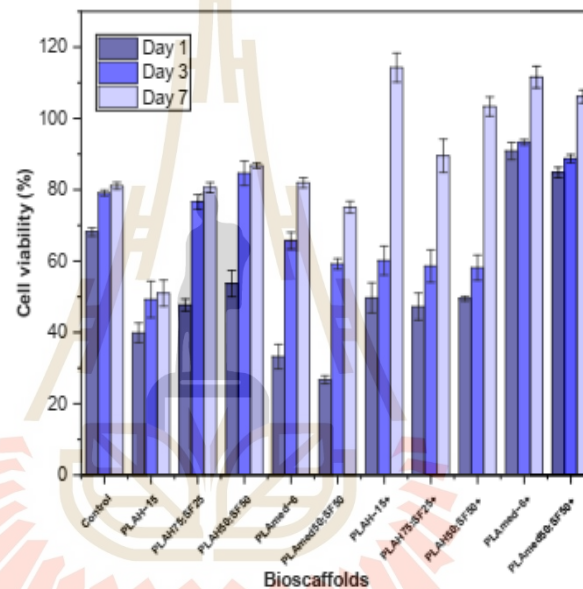

Figure 10. MTT assay for human chondrocyte cells viability on electrospun scaffolds after 1, 3, and 7 days. The plus sign (+) represents ethanol treated scaffolds (group 1).

3.9. Quantitative Gene Expression

The gene expression analyses of HCPC seeded scaffolds were examined to demonstrate cellular phenotype. All groups of scaffolds were repeated with triplicate sample sets. The results were shown in Figure 11, and the expressions of COL1A1 of PLAmed−6 and PLAmed50:SF50 were higher than the cell without a scaffold at every time point. The expression of COL1A1 of PLAmed−6 was obviously higher than PLAmed50:SF50 (143.0 and 31.9) at day 7 and slightly higher at day 28 (41.2 and 38.1). On the other hand, PLAmed−6 and PLAmed50:SF50 had equivalent COL2A1 expression, which was higher than the control group at days 7 (1.4, 1.4) and 28 (2.0, 2.0). The highest expression of COL2A1 was observed at day 14 (2.0).
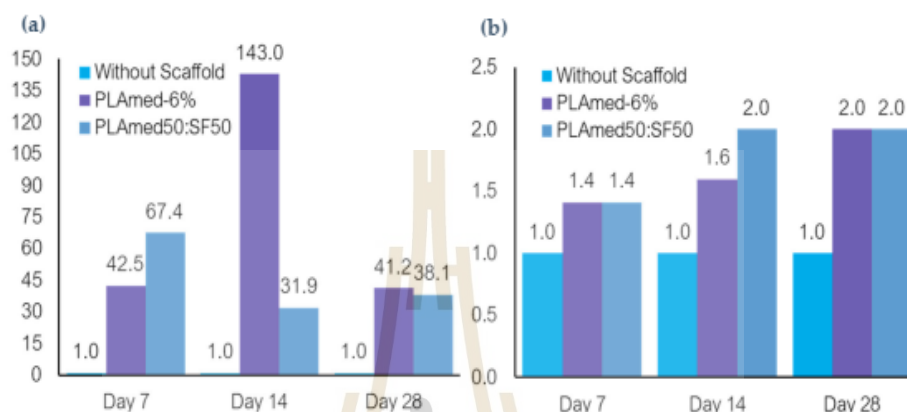
(a)

(b)

Figure 11. The expression of COL1A1 and COL2A1 at days 7, 14, and 28 were demonstrated in (a,b), respectively.

4. Discussion

For the electrospinning process, viscosity was an important solution parameter that affected the fiber formation ability [32]. Solution viscosity was affected by two important parameters, concentration [33] and molecular weight of polymer. An increase in concentration led to an increase in viscosity due to the longer chain entanglement of polymer. This can be seen from Table 4. PLAH showed higher viscosity than PLAL because of its higher molecular weight. The PLAmed−6 show higher viscosity when compared to PLAH−10. During polymer–solvent interaction, the solvent molecules go into the polymer and increase the chain mobility because of chain segmental relaxation [34]. The increase in the D-lactide content in the copolymer increases disorder in the polymer chains and reduces the crystallinity. Because of the less compact packing of D-lactide enantiomers, poly (D,L-lactide) is more amorphous, while poly (L-lactide) is enantiomerically pure poly-lactides [35,36]. The higher the L-lactide content in PLAmed (pure PLLA), the higher the solution viscosity [37]. The viscosity of PLAL at 10% and 15% concentration was not high enough to resist fiber deformation without defects at the given electric field and bead formation can be occurred. It could be assumed that the reduced viscosity resulted in an imbalance in viscous solution force and electrostatic force necessary for uniform fiber formation [38].

In electrospun fibers, the bead formation occurs when the surface tension in the charged jet is sufficient to change the jet into droplets to reduce surface area [39]. This is opposed by viscoelastic forces in the jet that resist changes to the fiber shape. In contrast, the increased viscosity of solution created higher viscoelastic forces that resisted the axial stretching during whipping, resulting in larger fiber diameter. This was confirmed by the increasing fiber diameter of PLA with increasing PLA concentration. However, for PLAH−20, the viscosity was too high so it was hardly spun and easily clogged the needle. Pure PLA scaffolds (both PLAH and PLAmed) displayed a wide fiber distribution in diameter when compared with those of the narrow distribution of PLA/SF scaffolds. PLA fibers contained small pores randomly distributed on the fibers owing to solvent evaporation [40]. Furthermore, the PLAmed−6 offers the biggest fiber diameter, which comes from complexity in the course of jet ejection [41].

With the incorporation of SF into the PLA, a gradient in solution viscosity and surface tension appeared during the flow of the emulsion solution. The PLA/SF fibers were drawn with more force, resulting in a comparatively thinner average diameter and distinct fibers [42]. The fiber diameter of PLAH/SF fibers with different ratios (PLAH75:SF25 and

PLAH50:SF50) did not show any obvious difference. For the PLAmed50: SF50 sample, very thin fibers with beads and pores were produced along with nanofiber.

The FITR spectra with characteristic absorption peaks of SF powder, pure PLAH, and PLA/SF scaffolds were presented in Figure 5. Amide I (1626 cm^{-1}) and amide II (1512 cm^{-1}) formed the major bands in the SF protein structure that could be identified with the representative peaks (denoted by hashed lines), thus confirming the presence of SF on the surface of scaffolds [11,43,44].

The mechanical characteristics (Table 5) and structural integrity of the electrospun scaffold were important parameters for the meniscus tissue engineering application. The menisci serve many important biomechanical functions such as load transmission, shock absorption, stability, and joint congruity [45]. Mechanical strength is identified by the tension resistance of electrospun scaffolds in order to maintain their integrity of scaffold during implantation [46]. The mechanical properties of scaffolds were related to the morphology of electrospun fibers [47]. Apparently, the elongation at break of the PLAH/SF scaffold was improved by adding SF solution into the electrospinning solution. With the incorporation of SF content, the Young's modulus and the tensile strength slightly decreased [31]. The mechanical properties of electrospun fibrous scaffolds were involved with their fiber density and junctions [48]. The mechanical properties of pure PLAmed scaffold showed the highest tensile strength and Young's modulus, while the PLAmed/SF scaffold showed lower mechanical properties because of the beads and thin porous fiber. PLAmed (pure PLLA) of high molar mass has sufficient strength for use as load bearing material in medical applications [49].

Moreover, the lower D-Lactide content grades have a greater ability to crystallize [50]. D-lactide induces twists in the regular poly(L-lactide) molecular architecture. Molecular imperfections are responsible for the decrease in both the rate and extent of poly(L-lactide) crystallization [3]. The increase in %crystallinity is usually associated with the formation of bigger or more ordered crystals of the PLA, which can resist the higher tensile strength [51].

The tensile properties of scaffold augmented suture were reported as composed of elastic modulus (3.77 ± 2.81 to 16.90 ± 9.70 MPa), tensile strength (0.60 ± 0.43 to 3.40 ± 1.10 MPa), and %elongation (3.28 ± 1.49 to 20.09 ± 5.89) [52–54]. From our study, the Young's modulus, %elongation, and tensile strength of both PLA and PLA/SF scaffolds were achieved. The %elongation at break of the scaffold obtained in our study can be used to confirm that the scaffold would not be cut through during repair [53]. Thus, our scaffold can be used to help tissue healing by seeding cells on scaffold incorporated suture. The cell seeded scaffold was shown to improve tissue healing and reduce gap formation at the repair site [55].

The effect of SF on thermal properties of PLA/SF scaffolds was shown in TGA thermogram in Figure 6. During the initial heating from room temperature to 250 °C, all samples had a mass loss due to the evaporation of water or solvent molecules. The water content increased significantly when SF was present. This can be ascribed to the better hydrophilicity and hygroscopicity of silk fibroin [56].

With the addition of silk fibroin, the decomposition temperature of the PLA/SF scaffolds tended to be lower. The decomposition rate gradually decreased with the increase of silk fibroin content [56]. From the DSC result, with an increase in SF, %crystallinity of the electrospun fibrous PLA/SF scaffolds decreased because the amorphous phase structure in the silk fibroin gradually increases [43,56,57]. Electrospun PLAmed scaffold had a high %crystallinity and a high melting temperature, which resulted in better mechanical properties than the PLAH scaffold. The cold crystallization peak upon cooling scan was observed in PLAmed and PLAmed/SF scaffolds, indicating that both specimens achieved a semi-crystalline state after the cooling [58]. This may be due to the higher L-lactide content in medical grade PLA [26]. PLAmed has the optical pure PLLA α crystalline form, which has a melting point range of approximately 170–180 °C [26,36]. Lower D-Lactide content meant a higher melting temperature [50]. The T_m and degree of crystallinity are dependent on the purity of the PLA, the crystallization kinetics, and melting behavior of PLA [59].

85

Biodegradability is another important consideration of the scaffold. The scaffold must degrade in a desirable time to ensure proper tissue remodeling or regeneration [60]. The effect of SF content on PLA/SF scaffold degradation was shown in Figure 8. All scaffolds exhibited very low degradation. It can also be observed that the weight loss obtained is a function of the amount of silk fibroin present in the electrospun fibers [14]. PLA contains crystalline and amorphous regions. The long macromolecular chains segments are arranged more regularly and packed more strongly in the crystalline phase than in the amorphous phase. Thus, small molecules of water can attack the polymer chains in the amorphous phase more easily [61]. Adding SF can increase the amourphous region, which can increase the scaffold degradation. The degradation of silk fibroin was related to hydrophilic interaction as well as special nanostructures. In the degradation process, the hydrophilic blocks were firstly degraded [62]. The degradation of the PLA/SF scaffolds prepared in the present study was shown to be controllable by adjusting the PLA/SF ratio [7].

Surface wettability of biomaterials plays a critical role in influencing cell adhesion, cell proliferation, and cell migration [12]. To clarify the effect of SF and its content on the surface wettability of electrospun scaffolds, the water contact angle was measured. Water contact angle results (Figure 9) supported the fact that incorporation of SF into PLA scaffolds decreased the hydrophobicity of pure PLA scaffolds. The reason could be due to the presence of SF with naturally hydrophilic amino groups, carboxylic groups, and other functional groups in the backbone of SF [32,42].

Our results demonstrated that medical grade PLA electrospun scaffolds offered biodegradability and cellular induction for meniscus tissue regeneration. After seeding HCPCs which possess chondrogenic potential on the PLA and PLA/SF scaffolds, initial cell viability and the viability at days 3 and 7 were evaluated (Figure 10). Although higher SF content of PLA/SF scaffolds improved cell viability, the viability was still lower than the control group. Medical grade PLA scaffolds had higher cell viability, but ethanol treatment was mandatory to reduce toxicity of SF during its preparation [63]. Comparing between PLAmed−6 and PLAmed50:SF50, the cell viability was decreased in the PLA/SF composite scaffold. From gene expression analyses, COL1A1 which represented fibrogenicity was higher in PLAmed−6 at days 14 and 28, while COL2A1 was equal on day 7 and day 28 and higher in day 14. These presentations directed that the cells in PLAmed−6 scaffolds functioned toward more fibrogenicity, while the cells in PLAmed50:SF5 offered more chondrogenic properties. Since the HCPC seeded scaffolds were cultured in simple expanded media without any growth factor or mechanical stimulation, the cells could lose chondrogenic phenotype by time [64].

In the meantime, the properties such as smaller fiber diameter, more amino groups, and more hydrophilicity of electrospun PLA/SF fibrous scaffolds also have influenced the interaction between cells and scaffolds [14,32,42,57]. Treatment of scaffolds with 70% ethanol can increase the cell viability [65]. Alcohol treatment can reduce the toxicity of the residued electrospining solvents after fabricating because it effectively eliminates bacteria and viruses, and it can dissolve the chloroform and formic acid easily [66–68].

5. Conclusions

PLA/SF nanofibrous scaffolds were successfully fabricated by electrospinning. In this study, it was found that viscosity played an important role to determine the fiber formation ability, fiber morphology, and size. The average fiber diameter was increased along with an increase in solution viscosity. PLA concentration, structure, and molecular weight were three important parameters that affected the solution viscosity. PLAmed−6 scaffold gave a superior mechanical property, degradability, and cellular induction for meniscus tissue regeneration. However, for commercial non-medical grade PLA used in this study, it was not recommended to be used for medical application because of its toxicity. The addition of SF dominated the nanofiber morphology, diameter distribution, mechanical properties, decomposition temperature, %crystallinity, biodegradability, surface wettability, and cell

86

viability. PLAmed50:SF50 scaffold has the potential to be used as biomimetic meniscus scaffold for scaffold augmented suture based on mechanical properties, cell viability, gene expression, surface wettability, and in vitro degradation.

References

1. Sheng, S.-J.; Hu, X.; Wang, F.; Ma, Q.-Y.; Gu, M.-F. Mechanical and thermal property characterization of poly-L-lactide (PLLA) scaffold developed using pressure-controllable green foaming technology. *Mater. Sci. Eng. C* **2015**, *49*, 612–622. [CrossRef] [PubMed]
2. Castro-Aguirre, E.; Iñiguez-Franco, F.; Samsudin, H.; Fang, X.; Auras, R. Poly(lactic acid)—Mass production, processing, industrial applications, and end of life. *Adv. Drug Deliv. Rev.* **2016**, *107*, 333–366. [CrossRef] [PubMed]
3. Auras, R.; Harte, B.; Selke, S. An overview of polylactides as packaging materials. *Macromol. Biosci.* **2004**, *4*, 835–864. [CrossRef] [PubMed]
4. Cunha, B.L.C.; Bahú, J.O.; Xavier, L.F.; Crivellin, S.; de Souza, S.D.A.; Lodi, L.; Jardini, A.L.; Filho, R.M.; Schiavon, M.I.R.B.; Concha, V.O.C.; et al. Lactide: Production Routes, Properties, and Applications. *Bioengineering* **2022**, *9*, 164. [CrossRef]
5. Masutani, K.; Kimura, Y. Chapter 1. PLA Synthesis. From the Monomer to the Polymer. In *Poly(lactic acid) Science and Technology: Processing, Properties, Additives and Applications*; Royal Society of Chemistry: London, UK, 2014; pp. 1–36. [CrossRef]
6. Sastri, V.R. 2-Regulations for Medical Devices and Application to Plastics Suppliers: History and Overview. In *Plastics in Medical Devices*, 2nd ed.; Sastri, V.R., Ed.; William Andrew Publishing: Oxford, UK, 2014; pp. 9–18. [CrossRef]
7. Liu, W.; Li, Z.; Zheng, L.; Zhang, X.; Liu, P.; Yang, T.; Han, B. Electrospun fibrous silk fibroin/poly(L-lactic acid) scaffold for cartilage tissue engineering. *Tissue Eng. Regen. Med.* **2016**, *13*, 516–526. [CrossRef]
8. Asakura, T.; Suzuki, Y. *Silk Fibroin*; Springer: Berlin/Heidelberg, Germany, 2014; pp. 1–7. [CrossRef]
9. Möller, M.; Popescu, C. 10.16-Natural Fibers. In *Polymer Science: A Comprehensive Reference*; Matyjaszewski, K., Möller, M., Eds.; Elsevier: Amsterdam, The Netherlands, 2012; pp. 267–280. [CrossRef]
10. Lee, H.; Jang, C.H.; Kim, G.H. A polycaprolactone/silk-fibroin nanofibrous composite combined with human umbilical cord serum for subacute tympanic membrane perforation; an in vitro and in vivo study. *J. Mater. Chem. B* **2014**, *2*, 2703–2713. [CrossRef]
11. Wang, F.; Liu, H.; Li, Y.; Li, Y.; Ma, Q.; Zhang, J.; Hu, X. Tunable Biodegradable Polylactide–Silk Fibroin Scaffolds Fabricated by a Solvent-Free Pressure-Controllable Foaming Technology. *ACS Appl. Bio Mater.* **2020**, *3*, 8795–8807. [CrossRef]
12. Yin, G.-B.; Zhang, Y.-Z.; Wang, S.-D.; Shi, D.-B.; Dong, Z.-H.; Fu, W.-G. Study of the electrospun PLA/silk fibroin-gelatin composite nanofibrous scaffold for tissue engineering. *J. Biomed. Mater. Res. A* **2010**, *93*, 158–163. [CrossRef]
13. Wang, S.; Zhang, Y.; Wang, H.; Yin, G.; Dong, Z. Fabrication and Properties of the Electrospun Polylactide/Silk Fibroin-Gelatin Composite Tubular Scaffold. *Biomacromolecules* **2009**, *10*, 2240–2244. [CrossRef]
14. Wang, F.; Wu, H.; Venkataraman, V.; Hu, X. Silk fibroin-poly(lactic acid) biocomposites: Effect of protein-synthetic polymer interactions and miscibility on material properties and biological responses. *Mater. Sci. Eng. C* **2019**, *104*, 109890. [CrossRef]
15. Zhao, Y.; Cheung, H.-Y.; Lau, K.T.; Xu, C.-L.; Zhao, D.-D.; Li, H.-L. Silkworm silk/poly(lactic acid) biocomposites: Dynamic mechanical, thermal and biodegradable properties. *Polym. Degrad. Stab.* **2010**, *95*, 1978–1987. [CrossRef]

16. Sari, A.; Gunaydin, B.; Dinçel, Y. *Meniscus Tears and Review of the Literature*; IntechOpen: London, UK, 2018. [CrossRef]
17. Sun, J.; Vijayavenkataraman, S.; Liu, H. An Overview of Scaffold Design and Fabrication Technology for Engineered Knee Meniscus. *Materials* **2017**, *10*, 29. [CrossRef] [PubMed]
18. De Caro, F.; Perdisa, F.; Dhollander, A.; Verdonk, R.; Verdonk, P. Meniscus Scaffolds for Partial Meniscus Defects. *Clin. Sports Med.* **2020**, *39*, 83–92. [CrossRef] [PubMed]
19. Warnecke, D.; Stein, S.; Haffner-Luntzer, M.; de Roy, L.; Skaer, N.; Walker, R.; Kessler, O.; Ignatius, A.; Dürselen, L. Biomechanical, structural and biological characterisation of a new silk fibroin scaffold for meniscal repair. *J. Mech. Behav. Biomed. Mater.* **2018**, *86*, 314–324. [CrossRef]
20. Kalva, S.N.; Augustine, R.; Al Mamun, A.; Dalvi, Y.B.; Vijay, N.; Hasan, A. Active agents loaded extracellular matrix mimetic electrospun membranes for wound healing applications. *J. Drug Deliv. Sci. Technol.* **2021**, *63*, 102500. [CrossRef]
21. Friné, V.-C.; Hector, A.-P.; Manuel, N.-D.S.; Estrella, N.-D.; Antonio, G.J. Development and Characterization of a Biodegradable PLA Food Packaging Hold Monoterpene-Cyclodextrin Complexes against Alternaria alternata. *Polymers* **2019**, *11*, 1720. [CrossRef]
22. Gil-Castell, O.; Badia, J.D.; Ingles-Mascaros, S.; Teruel-Juanes, R.; Serra, A.; Ribes-Greus, A. Polylactide-based self-reinforced composites biodegradation: Individual and combined influence of temperature, water and compost. *Polym. Degrad. Stab.* **2018**, *158*, 40–51. [CrossRef]
23. Jazrawi, B.; Noroozi, N.; Ansari, M.; Hatzikiriakos, S. Processing aids for biodegradable polymers. *J. Appl. Polym. Sci.* **2013**, *128*, 3592–3600. [CrossRef]
24. Ortenzi, M.A.; Gazzotti, S.; Marcos, B.; Antenucci, S.; Camazzola, S.; Piergiovanni, L.; Farina, H.; Di Silvestro, G.; Verotta, L. Synthesis of Polylactic Acid Initiated through Biobased Antioxidants: Towards Intrinsically Active Food Packaging. *Polymers* **2020**, *12*, 1183. [CrossRef]
25. Meng, X.; Nguyen, N.A.; Tekinalp, H.; Lara-Curzio, E.; Ozcan, S. Supertough PLA-Silane Nanohybrids by in Situ Condensation and Grafting. *ACS Sustain. Chem. Eng.* **2018**, *6*, 1289–1298. [CrossRef]
26. Torino, E.; Aruta, R.; Sibillano, T.; Giannini, C.; Netti, P.A. Synthesis of semicrystalline nanocapsular structures obtained by Thermally Induced Phase Separation in nanoconfinement. *Sci. Rep.* **2016**, *6*, 32727. [CrossRef] [PubMed]
27. Baydemir, T. Investigations on the Properties and Drug Releases of Biodegradable Polymer Coatings on Metal Substrates as Drug Carriers. Ph.D. Thesis, Middle East Technical University, Ankara, Turkey, 2009.
28. Nguyen, T.C.; Ruksakulpiwat, C.; Ruksakulpiwat, Y. The Study on the Grafting of Glycidyl Methacrylate onto Poly(lactic acid) in an Internal Mixer. *Walailak J. Sci. Technol. (WJST)* **2016**, *13*, 1037–1046.
29. Nagarajan, V.; Zhang, K.; Misra, M.; Mohanty, A.K. Overcoming the Fundamental Challenges in Improving the Impact Strength and Crystallinity of PLA Biocomposites: Influence of Nucleating Agent and Mold Temperature. *ACS Appl. Mater. Interfaces* **2015**, *7*, 11203–11214. [CrossRef] [PubMed]
30. Wongnarat, C.; Srihanam, P. Degradation Behaviors of Thai Bombyx mori Silk Fibroins Exposure to Protease Enzymes. *Engineering* **2013**, *5*, 6. [CrossRef]
31. Promnil, S.; Ruksakulpiwat, Y.; Ruksakulpiwat, C.; Numpaisal, P.-O. Effect of Silk Fibroin Content on Physical and Mechanical Properties of Electrospun Poly(lactic acid)/Silk Fibroin Nanofibers for Meniscus Tissue Engineering Scaffold. *J. Phys. Conf. Ser.* **2022**, *2175*, 012016. [CrossRef]
32. Li, L.; Li, H.; Qian, Y.; Li, X.; Singh, G.K.; Zhong, L.; Liu, W.; Lv, Y.; Cai, K.; Yang, L. Electrospun poly (ε-caprolactone)/silk fibroin core-sheath nanofibers and their potential applications in tissue engineering and drug release. *Int. J. Biol. Macromol.* **2011**, *49*, 223–232. [CrossRef]
33. Kim, G.-T.; Lee, J.-S.; Shin, J.-H.; Ahn, Y.-C.; Hwang, Y.-J.; Shin, H.-S.; Lee, J.-K.; Sung, C.-M. Investigation of pore formation for polystyrene electrospun fiber: Effect of relative humidity. *Korean J. Chem. Eng.* **2005**, *22*, 783–788. [CrossRef]
34. Udayakumar, M.; Kollár, M.; Kristály, F.; Leskó, M.; Szabó, T.; Marossy, K.; Tasnádi, I.; Németh, Z. Temperature and Time Dependence of the Solvent-Induced Crystallization of Poly(L-lactide). *Polymers* **2020**, *12*, 1065. [CrossRef]
35. Rissanen, M.; Puolakka, A.; Nousiainen, P.; Kellomäki, M.; Ellä, V. Solubility and Phase Separation of Poly(L,D-Lactide) Copolymers. *J. Appl. Polym. Sci.* **2008**, *110*, 2399–2404. [CrossRef]
36. Burg, K. Chapter 6-Poly(α-ester)s. In *Natural and Synthetic Biomedical Polymers*; Kumbar, S.G., Laurencin, C.T., Deng, M., Eds.; Elsevier: Oxford, UK, 2014; pp. 115–121. [CrossRef]
37. Puchalski, M.; Kwolek, S.; Szparaga, G.; Chrzanowski, M.; Krucińska, I. Investigation of the Influence of PLA Molecular Structure on the Crystalline Forms (α' and α) and Mechanical Properties of Wet Spinning Fibres. *Polymers* **2017**, *9*, 18. [CrossRef]
38. Nezarati, R.M.; Eifert, M.B.; Cosgriff-Hernandez, E. Effects of humidity and solution viscosity on electrospun fiber morphology. *Tissue Eng. Part C Methods* **2013**, *19*, 810–819. [CrossRef] [PubMed]
39. Williams, G.R.; Raimi-Abraham, B.T.; Luo, C.J. Electrospinning fundamentals. In *Nanofibres in Drug Delivery*; UCL Press: London, UK, 2018; pp. 24–59. [CrossRef]
40. Promnil, S.; Numpaisal, P.-O.; Ruksakulpiwat, Y. Effect of molecular weight on mechanical properties of electrospun poly (lactic acid) fibers for meniscus tissue engineering scaffold. *Mater. Today Proc.* **2021**, *47*, 3496–3499. [CrossRef]
41. Mehta, P.P.; Pawar, V.S. 22-Electrospun nanofiber scaffolds: Technology and applications. In *Applications of Nanocomposite Materials in Drug Delivery*; Inamuddin, Asiri, A.M., Mohammad, A., Eds.; Woodhead Publishing: Sawston, UK, 2018; pp. 509–573. [CrossRef]

42. Roy, T.; Maity, P.P.; Rameshbabu, A.P.; Das, B.; John, A.; Dutta, A.; Ghorai, S.K.; Chattopadhyay, S.; Dhara, S. Core-Shell Nanofibrous Scaffold Based on Polycaprolactone-Silk Fibroin Emulsion Electrospinning for Tissue Engineering Applications. *Bioengineering* **2018**, *5*, 68. [CrossRef] [PubMed]
43. Taddei, P.; Tozzi, S.; Zuccheri, G.; Martinotti, S.; Ranzato, E.; Chiono, V.; Carmagnola, I.; Tsukada, M. Intermolecular interactions between B. mori silk fibroin and poly(L-lactic acid) in electrospun composite nanofibrous scaffolds. *Mater. Sci. Eng. C* **2017**, *70*, 777–787. [CrossRef] [PubMed]
44. He, J.; Qin, Y.; Cui, S.; Gao, Y.; Wang, S. Structure and properties of novel electrospun tussah silk fibroin/poly(lactic acid) composite nanofibers. *J. Mater. Sci.* **2011**, *46*, 2938–2946. [CrossRef]
45. Fox, A.J.S.; Bedi, A.; Rodeo, S.A. The basic science of human knee menisci: Structure, composition, and function. *Sports Health* **2012**, *4*, 340–351. [CrossRef]
46. Thanh Tam, T.; Abdul Hamid, Z.; Cheong, K.Y. A Review of Mechanical Properties of Scaffold in Tissue Engineering: Aloe Vera Composites. *J. Phys. Conf. Ser.* **2018**, *1082*, 012080. [CrossRef]
47. Tertyshnaya, Y.; Karpova, S.; Moskovskiy, M.; Dorokhov, A. Electrospun Polylactide/Natural Rubber Fibers: Effect Natural Rubber Content on Fiber Morphology and Properties. *Polymers* **2021**, *13*, 2232. [CrossRef]
48. Wu, J.; Hong, Y. Enhancing cell infiltration of electrospun fibrous scaffolds in tissue regeneration. *Bioact. Mater.* **2016**, *1*, 56–64. [CrossRef]
49. Maharana, T.; Mohanty, B.; Negi, Y.S. Melt–solid polycondensation of lactic acid and its biodegradability. *Prog. Polym. Sci.* **2009**, *34*, 99–124. [CrossRef]
50. Pölöskei, K.; Csézi, G.; Hajba, S.; Tábi, T. Investigation of the thermoformability of various D-Lactide content poly(lactic acid) films by ball burst test. *Polym. Eng. Sci.* **2020**, *60*, 1266–1277. [CrossRef]
51. Oksiuta, Z.; Jalbrzykowski, M.; Mystkowska, J.; Romanczuk, E.; Osiecki, T. Mechanical and Thermal Properties of Polylactide (PLA) Composites Modified with Mg, Fe, and Polyethylene (PE) Additives. *Polymers* **2020**, *12*, 2939. [CrossRef] [PubMed]
52. Rothrauff, B.B.; Numpaisal, P.-O.; Lauro, B.B.; Alexander, P.G.; Debski, R.E.; Musahl, V.; Tuan, R.S. Augmented repair of radial meniscus tear with biomimetic electrospun scaffold: An in vitro mechanical analysis. *J. Exp. Orthop.* **2016**, *3*, 23. [CrossRef]
53. Shimomura, K.; Bean, A.C.; Lin, H.; Nakamura, N.; Tuan, R.S. In Vitro Repair of Meniscal Radial Tear Using Aligned Electrospun Nanofibrous Scaffold. *Tissue Eng. Part A* **2015**, *21*, 2066–2075. [CrossRef]
54. Yan, S.; Ou-Yang, H.-K.; Shan, Y.-L.; Luo, D.-Z.; Wang, H.; Zhang, K. Tensile biomechanical characteristics of human meniscus. *Emerg. Mater. Res.* **2016**, *5*, 44–49. [CrossRef]
55. McCarron, J.A.; Milks, R.A.; Chen, X.; Iannotti, J.P.; Derwin, K.A. Improved time-zero biomechanical properties using poly-L-lactic acid graft augmentation in a cadaveric rotator cuff repair model. *J. Shoulder Elbow Surg.* **2010**, *19*, 688–696. [CrossRef] [PubMed]
56. Wang, F.; Li, Y.; Gough, C.R.; Liu, Q.; Hu, X. Dual-Crystallizable Silk Fibroin/Poly(L-lactic Acid) Biocomposite Films: Effect of Polymer Phases on Protein Structures in Protein-Polymer Blends. *Int. J. Mol. Sci.* **2021**, *22*, 1871. [CrossRef]
57. Holjevac Grgurić, T.; Mijović, B.; Zimić, I.; Dolenec, T.; Kuzmić, S.; Mrkonjić, N.; Tominac-Trcin, M.; Slivac, I.; Zdraveva, E.; Govorcin Bajsic, E. Preparation and Characterization of Electrospun PCL/Silk Fibroin Scaffolds. *Chem. Biochem. Eng. Q.* **2021**, *35*, 31–42. [CrossRef]
58. Yu, W.; Wang, X.; Ferraris, E.; Zhang, J. Melt crystallization of PLA/Talc in fused filament fabrication. *Mater. Des.* **2019**, *182*, 108013. [CrossRef]
59. Farah, S.; Anderson, D.G.; Langer, R. Physical and mechanical properties of PLA, and their functions in widespread applications—A comprehensive review. *Adv. Drug Deliv. Rev.* **2016**, *107*, 367–392. [CrossRef]
60. Bitar, K.N.; Zakhem, E. Design strategies of biodegradable scaffolds for tissue regeneration. *Biomed. Eng. Comput. Biol.* **2014**, *6*, 13–20. [CrossRef] [PubMed]
61. Leonés, A.; Peponi, L.; Lieblich, M.; Benavente, R.; Fiori, S. In Vitro Degradation of Plasticized PLA Electrospun Fiber Mats: Morphological, Thermal and Crystalline Evolution. *Polymers* **2020**, *12*, 2975. [CrossRef] [PubMed]
62. Lu, Q.; Zhang, B.; Li, M.; Zuo, B.; Kaplan, D.L.; Huang, Y.; Zhu, H. Degradation mechanism and control of silk fibroin. *Biomacromolecules* **2011**, *12*, 1080–1086. [CrossRef] [PubMed]
63. Gholipourmalekabadi, M.; Mozafari, M.; Bandehpour, M.; Sameni, M.; Ghanbarian, H. How Ethanol Treatment Affects The Physico-chemical And Biological Characteristics Of Silk Fibroin Nanofibrous Scaffolds. *Adv. Mater. Lett.* **2015**, *6*, 391–394. [CrossRef]
64. Numpaisal, P.-O.; Jiang, C.-C.; Hsieh, C.-H.; Chiang, H.; Chien, C.-L. Prospective Application of Partially Digested Autologous Chondrocyte for Meniscus Tissue Engineering. *Pharmaceutics* **2022**, *14*, 605. [CrossRef]
65. Hirano, N.; Kusuhara, H.; Sueyoshi, Y.; Teramura, T.; Murthy, A.; Asamura, S.; Isogai, N.; Jacquet, R.D.; Landis, W.J. Ethanol treatment of nanoPGA/PCL composite scaffolds enhances human chondrocyte development in the cellular microenvironment of tissue-engineered auricle constructs. *PLoS ONE* **2021**, *16*, e0253149. [CrossRef]
66. D'Amato, A.; Schaub, N.; Cardenas, J.; Franz, E.; Rende, D.; Ziemba, A.; Gilbert, R. Evaluation of procedures to quantify solvent retention in electrospun fibers and facilitate solvent removal. *Fibers Polym.* **2017**, *18*, 483–492. [CrossRef]
67. Kim, S.; Chen, J.; Cheng, T.; Gindulyte, A.; He, J.; He, S.; Li, Q.; Shoemaker, B.A.; Thiessen, P.A.; Yu, B.; et al. PubChem in 2021: New data content and improved web interfaces. *Nucleic Acids Res.* **2021**, *49*, D1388–D1395. [CrossRef]
68. Salvage, R.; Hull, C.M.; Kelly, D.E.; Kelly, S.L. Use of 70% alcohol for the routine removal of microbial hard surface bioburden in life science cleanrooms. *Future Microbiol.* **2014**, *9*, 1123–1130. [CrossRef]

VITAE

Miss Siripanyo Pronil was born on September 17, 1995, in Nakhon Ratchasima Province, Thailand. She finished high school from Suranaree Wittaya School in 2014. She received her Bachelor's Degree in Engineering (Polymer Enigneering) from Suranaree University of Technology in 2018. She continued her Master's degree in Materials Engineering Program at School of Polymer Engineering, Institute of Engineering, Suranaree University of Technology. During her master's degree study, she gave poster and oral presentations in the topic of "Effect of molecular weight on mechanical properties of electrospun poly (lactic acid) fibers for meniscus tissue engineering scaffold" in the 5th International Conference on Smart Materials and Nanotechnology (SmartMat@2020) in Chonburi, Thailand and "Effect of silk fibroin content on physical and mechanical properties of electrospun poly(lactic acid)/silk fibroin nanofibers for meniscus tissue engineering scaffold" in the 21st International Union of Materials Research Societies International Conference in Asia, Chiang Mai, Thailand. The first work was published in Materials Today: Proceedings and the second work was published in Journal of Physics: Conference Series. Her research article in the topic of "Electrospun poly(lactic acid) and silk fibroin based nanofibrous scaffold for meniscus tissue engineering" has been published in Polymers.